Computational Homogenization and Failure Modelling of Masonry

Nitin Kumar

A Thesis Submitted to
Indian Institute of Technology Hyderabad
In Partial Fulfillment of the Requirements for
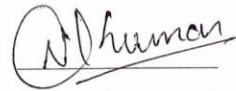The Degree of Master of Technology

भारतीय प्रौद्योगिकी संस्थान हैदराबाद
Indian Institute of Technology Hyderabad
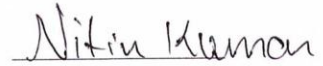
Department of Civil Engineering
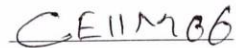
June 2013

Declaration

I declare that this written submission represents my ideas in my own words, and where ideas or words of others have been included, I have adequately cited and referenced the original sources. I also declare that I have adhered to all principles of academic honesty and integrity and have not misrepresented or fabricated or falsified any idea/data/fact/source in my submission. I understand that any violation of the above will be a cause for disciplinary action by the Institute and can also evoke penal action from the sources that have thus not been properly cited, or from whom proper permission has not been taken when needed.

(Signature)

Nitin Kumar

(Nitin Kumar)

CE11M06

(Roll No.)

Approval Sheet

This thesis entitled "**Computational Homogenization and Failure Modelling of Masonry**" by Nitin Kumar is approved for the degree of Master of Technology from IIT Hyderabad

(Dr. Manoj Pandey) Examiner
Dept. of Mech Eng
IITM

(Prof. KVL Subramaniam) Examiner
Dept. of Civil Eng
IITH

(Dr. Amirtham Rajagopal) Adviser and Chairman
Dept. of Civil Eng
IITH

Acknowledgements

Dedication

<div align="right">

Dedicated to
My parents and my Mausi

</div>

Abstract

Masonry is a heterogeneous anisotropic continuum. In particular, the inhomogeneity is due to the different mechanical properties of its constituents. Anisotropy is due to the different masonry patterns, that can be obtained by variation of geometry, nature and arrangement of mortar and brick. The behaviour of masonry is very complex and highly non-linear due to the behaviour of its constituents, which are quasi-brittle in nature and have a large difference in their stiffness. The structural response of such a composite material derives from the complex interaction between its constituents.

Many computational studies have been carried out at various scales to understand and simulate the behaviour of masonry. The modelling of masonry at different scales depends up on the level of accuracy and simplicity desired. This includes micro-modelling and macro-modelling. In micro-modelling, the unit and mortar are represented by continuum elements and unit-mortar interface is represented by a discontinuous interface element. This detailed micro-modelling procedure leads to very accurate results, but requires an intensive computational effort. This drawback can be partially overcome in simplified micro-modelling, by making an assumption that mortar and two unit-mortar interface is lumped into a joint between expended units. The units are expended in order to keep the geometry of structure unchanged. The computational cost of simplified micro-model can be further reduced, by replacing expanded units by the rigid element. Using rigid elements decreases the number of degrees of freedom, which consequently reduces the computational time. In macro-modelling, masonry is considered as a composite, which does not make any distinction between units and mortar. The material is regarded as a fictitious homogeneous anisotropic continuum.

In the present work a micro modelling approach is adopted for the detailed failure analysis of the masonry. This study focuses on plasticity based non-linear analysis of unreinforced masonry structures at micro-level. In particular, the study focuses on analysis of two-dimensional modelling of masonry assumed to have plane stress condition. The main objectives of present study are

- to perform a critical review of masonry and computational modelling of masonry structure;

- to perform a computational homogenization of masonry;

- to propose and develop a constitutive micro-model for unreinforced masonry which includes softening behaviour and incorporates all predominant failure mechanisms;

- to implement the proposed model in commercial software ABAQUS using user defined user subroutine UMAT;

- to perform a numerical study to validate the model by comparing the predicted behaviour with the behaviour observed in experiments on different types of masonry.

Masonry shows the softening behaviour in the post peak region. It is typical due to quasi-brittle in nature of its constituent i.e. brick and mortar. It happened due to the present of progressive internal micro crack. Such mechanical behaviour is commonly attributed to the heterogeneity of the material, due to the presence of different phases and material defects, like flaws and voids. Even prior to loading the structure, brick and mortar contains microcracks. Initially, these microcracks are stable which means that they grow only when the load is increased. But, around peak load an acceleration of crack formation takes place and the formation of macrocracks starts. The macrocracks

are unstable, which means that the load has to decrease to avoid an uncontrolled growth. Thus, Deformation controlled test of masonry results in softening and localization of cracking in a small zone while the rest of masonry remains pristine.

The failure of masonry constituent (unit and mortar) in tension and compression loading is essentially the same and i.e. due to growth of micro level crack in the material. During failure the inelastic strains result from a dissipation of fracture energy. First, due to sliding or mode II, which results in a dry friction process between the components once softening is completed. Second, the split of the head joint and the brick in mode I. Third, the crushing of mortar or brick take place, which release the compressive fracture energy. If the micro-modelling strategy is used for masonry, then all these failure mechanisms should be incorporated in the failure model. On the other hand if the macro-modelling strategy is used, joints are smeared out in an anisotropic homogeneous continuum. Therefore the interaction between the masonry components cannot be incorporated in these types of models. Instead, a relation between average stresses and strains should be established through experiments or homogenization.

As an alternative to difficult experimental tests, continuum parameter are also found in work. In present study, theory of homogenization for periodic media has been applied in a rigorous way for deriving the anisotropic elastic characteristics of masonry. The real geometry has been taken into account (bond pattern and finite thickness of the wall). For the numerical example the two representative volume element having the same ratio of mortar and unit has been considered and their equivalent properties have been found. Moreover, a care full examination for different stiffness ratio between mortar and unit have been done to assess the performance for inelastic behaviour.

Micro-models are best tool to understand the behaviour of masonry. This requires the consideration of the failure mechanisms of the masonry and its constituent. These failure mechanisms are lumped into an interface element, with the assumption that all the inelastic behaviour occurs in interface element, which leads to robust type of modelling, capable of tracing complete load path. The interface element shows the failure mechanism as potential crack, slip and crushing. In this work, a plasticity based composite interface model is proposed for failure analysis of unreinforced masonry. A hyperbolic composite interface model consisting of a single surface yield criterion, which is a direct extension of Mohr-Coulomb criteria with cut in tension region and a cap in compression region. The model is developed by using a fully implicit backward-Euler integration strategy. It is combined with a local/global Newton solver, based on a consistent tangent operator compatible with an adaptive sub stepping strategy. The model is implemented in standard finite element software (ABAQUS) by using user defined subroutine and verification is conducted in all its basic modes. During the verification, it has been found that sub stepping is required to ensure the convergence and accuracy of the final solution at both local and global level.

Finally, the composite interface model is validated by comparing numerical result with experimental results available in the literature. A masonry shear wall is modelled with simplified micro-modelling strategy and behaviour has been studied, particularly post peak behaviour of masonry. At last it has been showed that present model is capable of representing the cyclic shear behaviour of masonry mortar joints.

Nomenclature

$\boldsymbol{\sigma}$	Stress vector
$\boldsymbol{\epsilon}$	Strain vector
σ_{ij}	Second-order stress tensor
ϵ_{ij}	Second-order strain tensor
δ_{ij}	Kronecker delta
E_{ij}	Symmetric second-order tensor for the strain
u_i^p	Periodic displacement field
x_i	Spatial parameters
$\boldsymbol{\Omega}$	Domain
$\hat{\Omega}$	Unit cell
$\boldsymbol{\Sigma}$	Macroscopically homogeneous stress state
$\boldsymbol{E}$	Macroscopically homogeneous strain state
$\boldsymbol{S}$	Fourth order compliance tensor
$\boldsymbol{C}$	Fourth order stiffness tensor
E_b	Youngs modulus of brick unit
E_u	Youngs modulus of mortar
G_b	Shear modulus of brick unit
G_u	Shear modulus of mortar
ν	Poissons ratio
h_m	Actual thickness of mortar joint
σ_{nn}	Normal stress component
σ_{tt}	Tangential stress component
u_{nn}	Normal displacement component
u_{tt}	Tangential displacement component
$\boldsymbol{K}$	Elastic stiffness matrix
k_{nn}, k_{tt}	Component of elastic stiffness matrix
F	Yield function
Q	Potential function
f_c	Compression cap-off function
f_t	Tension-cut function
α_c	Positive integer controls curvature of compression cap
α_t	Positive integer controls curvature of tension-cut
$\boldsymbol{q}$	Hardening Parameter
C, C_q	Apparent cohesion
ϕ	Friction angle
ψ	Dilation angle
ξ	Tension strength
ζ	Compression strength
$\dot{\boldsymbol{W}}^p$	Plastic work hardening per unit of volume
$\dot{w}_1^p, \dot{w}_2^p, \dot{w}_3^p, \dot{w}_4^p$	Work hardening variables

$\sigma_{tt_{r1}}$	Tangential strength at zero tensile strength
$\sigma_{tt_{r2}}$	Minimum tangential strength for zero tensile strength and minimum cohesion and friction angle
C_0, C_{q_0}	Initial apparent cohesion
C_r, C_{q_r}	Residual apparent cohesion
ϕ_0	Initial friction angle
ϕ_r	Residual friction angle
ψ_0	Initial dilation angle
ψ_r	Residual dilation angle
ξ_0	Initial tension strength
ζ_0	Initial compression strength
ζ_p	Peak compression strength
ζ_m	Intermediate compression strength
ζ_r	Residual compression strength
G_f^I	Mode I fracture energy
G_f^{II}	Mode II fracture energy
$\boldsymbol{\epsilon^e}$	Elastic strain
$\boldsymbol{\epsilon^p}$	Plastic strain
$\dot{\lambda}$	Constant slip rate or plastic multiplier
$\boldsymbol{K}^{ep}$	Elasto-plastic tangent modulus
P	Pressure

Contents

Chapter 1

Introduction

1.1 Introduction

Masonry is one of the oldest building material. It have been still in use due to simplicity in construction and other characteristics like aesthetics, solidity, durability and low maintenance, versatility, sound absorption and fire resistance. The technique of masonry constructions was very old and is same as developed thousand year ago. For the example masonry has being used as a Load bearing wall, infill panels to resist the seismic and wind loads for many years. whereas, many new development in material, and advancement in it′s applications have occurred in recent years. The use of masonry as pre-stressed masonry cores and low rise building is presently competitive. However, these innovative application of masonry are hindered by lack of insight and complex behaviour of masonry as a composite material.

Figure 1.1: Photo of Prag Mahal (Bhuj, Gujarat, India) damaged in 2001 Gujarat Earthquake, Photo courtesy: Randolph Langenbach / UNESCO.

Many buildings are masonry construction through out the world, more so in India and many countries of the Europe. These include building of huge architectural and historical values. Many of them are situated in the earthquake prone area, which is one of the main cause of the damage on the buildings and their collapse. For the instance, the Gujarat earthquake (2001) damaged many historical heritage buildings in Gujarat, such as Prag Mahal in Bhuj, which is more then 150 year old, see Figure 1.1, and Umbria-Marche earthquake (1997) damaged many important historical heritage buildings in Italy, such as the Basilica of Saint Francis in Assisi and more than 200 ancient churches, see Figure 1.2.

Figure 1.2: Photo sequence of the transept vault partial collapse occurred in the Basilica of Saint Francis in Assisi, Italy, during the Umbria-Marche earthquake (1997), Photo courtesy: [1].

Therefore, it becomes very important to evaluate the existing building in order to guarantee the safety of people as well as to conserve the architectural heritage. Thus, failure analysis of masonry becomes important to evaluate strength of the existing building and to provide their strengthening solutions. Masonry represents a very particular mechanical behaviour, which is principally due to the lack of homogeneity and standardization. The structural response of such a composite material can be derived from the complex interaction between its constituents i.e. units, mortar and unit-mortar joints.

Numerical approach using powerful techniques such as FEM offers cheap and effective solution for the analysis of masonry in comparison to experimental work, which are expensive and time consuming. Many such methods are available to study the mechanical behaviour of masonry at different level of complexity and cost associated with it. There strategies are still in an experimental phase, hence problem is still open.

1.2 Review of computational modelling for Masonry structures

In the last two decades, the masonry research community has been showing a great interest in sophisticated numerical tools. Because it is opposite to tradition of rules-of-thumb and empirical formulae. Several difficulties arose from adopting existing numerical tools, namely from the mechanics of concrete, rock and composite materials [2–6]. Due very particular nature of masonry [7, 8]. All the aforementioned factors led to the need for developing appropriate and specific tools for the analysis of masonry structures. Several numerical models have been proposed for the structural analysis of masonry constructions. These numerical models could be characterized as

- different theoretical backgrounds and levels of detail, such as information required for serviceability, damage, collapse, failure mechanisms, etc;

- the level of accuracy desired i.e. local or global behaviour of the structure;

- the necessary input data we have (detailed or rough information about material characteristics);

- the costs of numerical simulation (time permissible for the analysis).
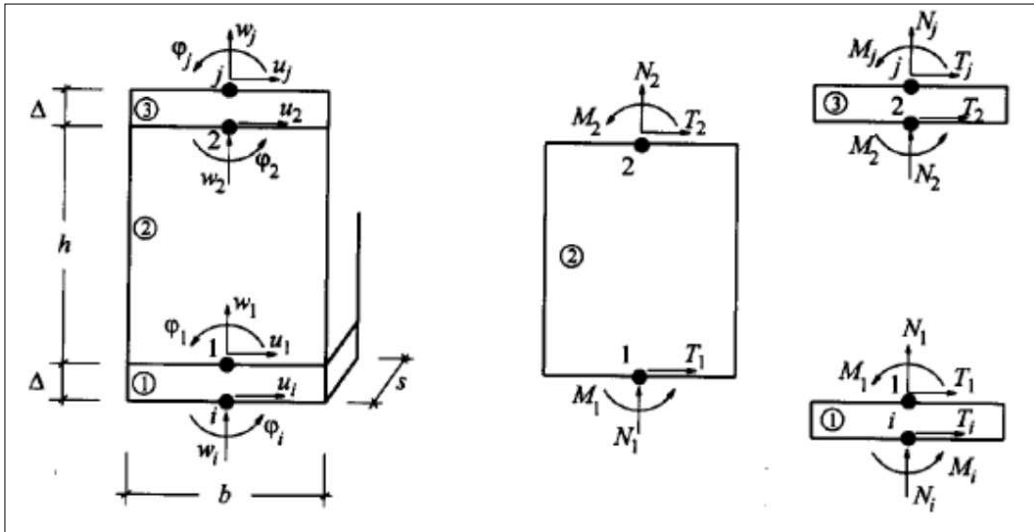
Figure 1.3: Macro-elements proposed by Brencich and Lagomarsino [9].

The simplest approach for modelling of the masonry structure is representing the structure as a combination of structural elements such as truss, beam, plate or shell elements. This is the case of the simplified methods via macro-elements. Brencich and Lagomarsino [9] developed a two-dimensional finite macro-elements model for masonry panel. This model can takes into account the main damage and dissipative mechanism, that has been observed in real and are include by detail theoretical model, see Figure 1.3). Several approaches based on the concept of the equivalent frame method (Magenes and Dalla Fontana [10]; Roca *et al*. [11]) are also being proposed. In which building walls are idealized as equivalent frames made by pier elements, spandrel beam elements and

joint elements, Figure 1.4). All these cited approaches required very less computational effort, since each macro-element represents a structural element (entire wall or masonry panel). Thus, they have very less degrees of freedom. Nevertheless, such approaches provide a coarse description of the real masonry behaviour and are generally used for very huge masonry structure.
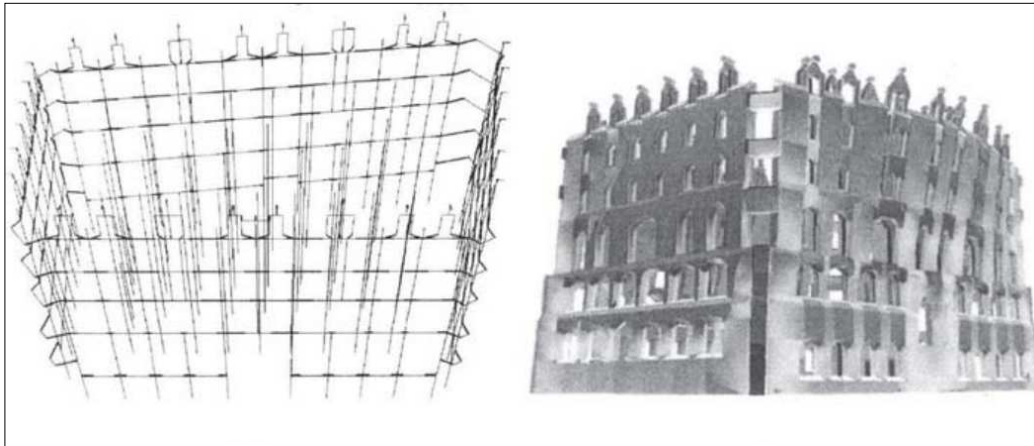
Figure 1.4: Application of the simplified method proposed by Roca *et al.* [11] to the study of the Gauds Casa Botines.

Masonry is an orthotropic composite material that consists of units and mortar joints. In general, numerical representation of masonry can focus on the micro-modelling of the individual components (unit, mortar and unit-mortar interface), or the macro-modelling of masonry as a composite, see Figure 1.5.
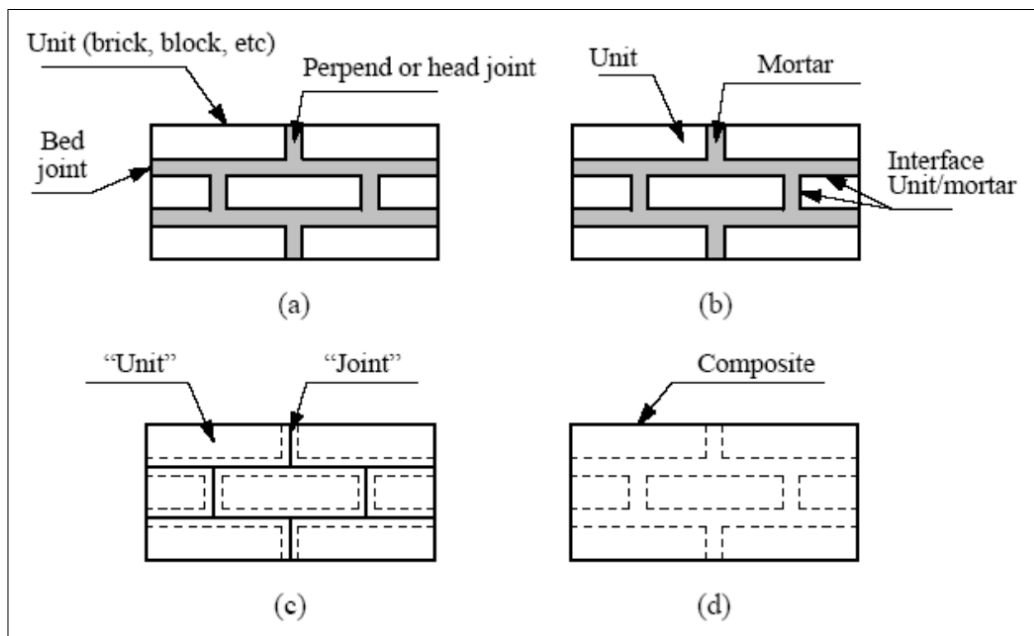
Figure 1.5: Modelling strategies for masonry structures [12]: (a) masonry sample; (b) detailed micro-modelling; (c) simplified micro-modelling; (d) macro-modelling.

1.2.1 Micro-modelling

Micro-modelling is the best tool available to analyse and understand the real and accurate behaviour of masonry. Particularly, when the local response of the structure is important. Such an approach includes distinct representations of units, mortar and the unit-mortar interface. The unit and mortar are represented by continuum elements and unit-mortar interface is represented by discontinuous interface elements. Elastic and inelastic properties of both unit and mortar can be taken into account. The interface represents a potential crack, potential slip and crushing plane. This detailed micro-modelling procedure leads to very accurate results, but requires an intensive computational effort. This drawback is partially overcome by making an assumption that mortar and two unit-mortar interface is lumped into joint between expended units. The units are expended in order to keep the geometry of structure unchanged. Thus in this simplified micro-models (Lofti and Shing [13]; Tzamtzis [14]; Loureno and Rots [15] ; Gambarotta and Lagomarsino [16, 17]) masonry is considered as a set of elastic blocks bonded by potential crack, potential slip and crushing plane at the joints, Figures 1.6 - 1.7.

Figure 1.6: Micro-modelling of masonry shear walls [12]: (a) load-displacement diagrams; (b) deformed mesh at peak load; (c) deformed mesh at collapse.
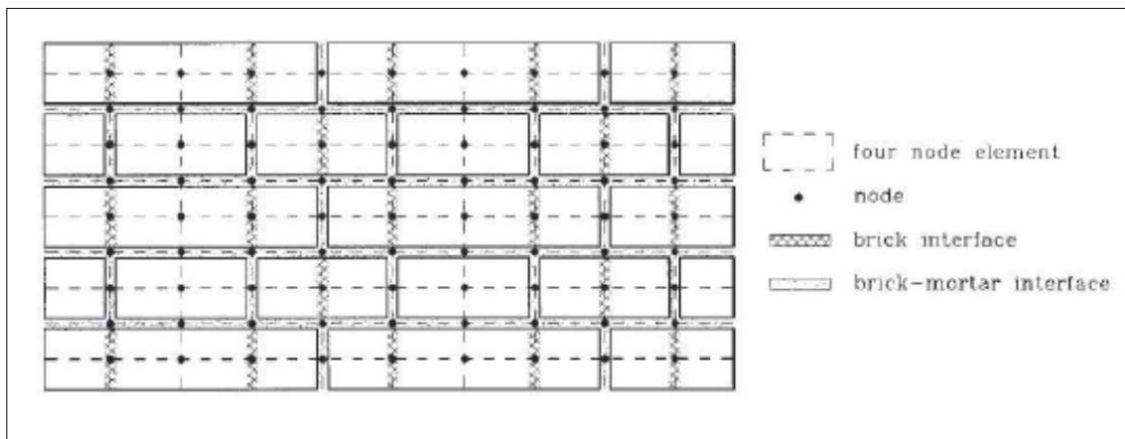
Figure 1.7: Micro-modelling of masonry as per [16, 17].

5

The micro-modelling approaches are suitable for small structural elements, with particular interest in strongly heterogeneous states of stress and strain. The primary aim is to closely represent masonry from the knowledge of the properties of each constituent and the interface. The necessary experimental data must be obtained from laboratory tests of the constituents. Nevertheless, the high level of refinement required to obtain accurate results, means an intensive computational effort (i.e. large number of degrees of freedom in the numerical model), which limits micro-models applicability to the analysis of small elements (e.g. laboratory specimens) or, at least, to small structural details.

A effort has been made by authors (Dolatshahi KM and Aref AJ [18]) to further simplify the micro-modelling by replacing the expended units by rigid element, and it has been shown that using rigid elements along with non-linear line interfaces leads to a reduced number of degrees of freedom, which consequently reduces the computational time (see Figure 1.8). Hence increase the applicability of the micro-models.

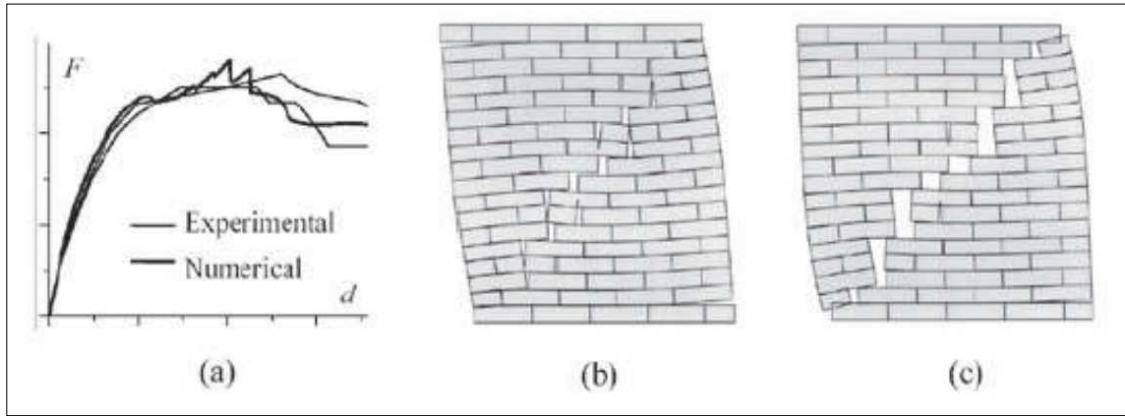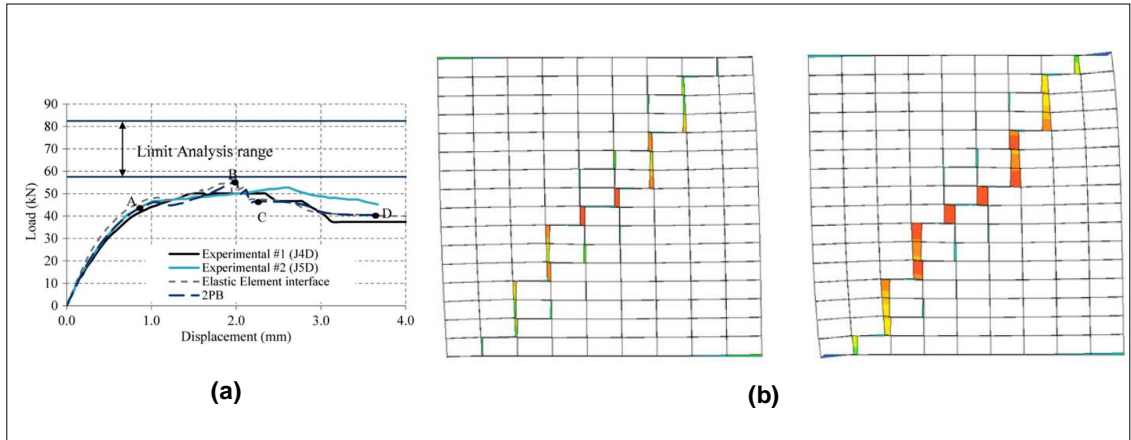Figure 1.8: Micro-modelling of masonry shear walls with rigid elements [18]: (a) load-displacement graph (Based on the model 2PB); (b) crack path in different stages of loading.

1.2.2 Homogenization

On-going to macro-modelling, continuum parameters must be assessed by experiments on specimens of sufficiently large size, under homogeneous states of stress or strain [19–21]. As an alternative to difficult experimental tests, it is possible to assess experimentally the individual components (or simple wallets and cores, see Benedetti *et al.* [22]). This obtained data for individual components are considered as input parameters for the numerical homogenization technique.

The homogenization theory allows the global behaviour (macro-constitutive) to be derived from the behaviour of its constitutive materials or micro-constitutive laws (Anthoine [24], Luciano and Sacco [25]; Gambarotta and Lagomarsino [16, 17]); Zucchini and Lourenco [23, 26]). Such methodologies requires to identifying a basic cell, which generates an entire panel by it′s regular repetition, see Figure 1.9. In this way by exploiting periodicity of the masonry average macro-constitutive law can be obtained from a single basic unit cell. Initially, the homogenization technique had been performed in several successive steps, head joints and bed joints were being introduced successively. In later work homogenization theory for periodic media is rigorously applied to the basic cell to carry out a single step homogenization, with adequate boundary conditions and exact geometry. Finite
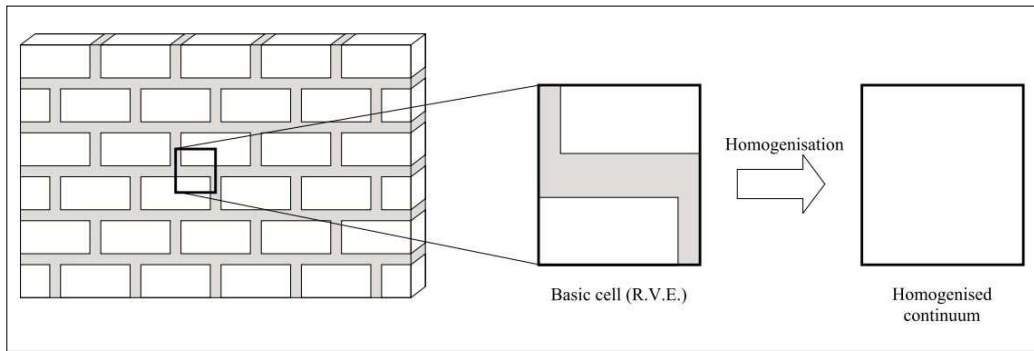
Figure 1.9: Basic cell for masonry and objective of homogenisation [23].

element method was used to obtain numerical solution as exact solutions is not possible [24, 27].

Zucchini and Lourenco [28] proposed an improved micro-mechanical homogenization model for masonry analysis in non-linear domain. The model was coupled with damage and plasticity models, by suitably chosen deformation mechanisms. Moreover, the model was capable of simulating the behaviour of a basic periodic cell up to complete degradation and failure, see Figure 1.10.
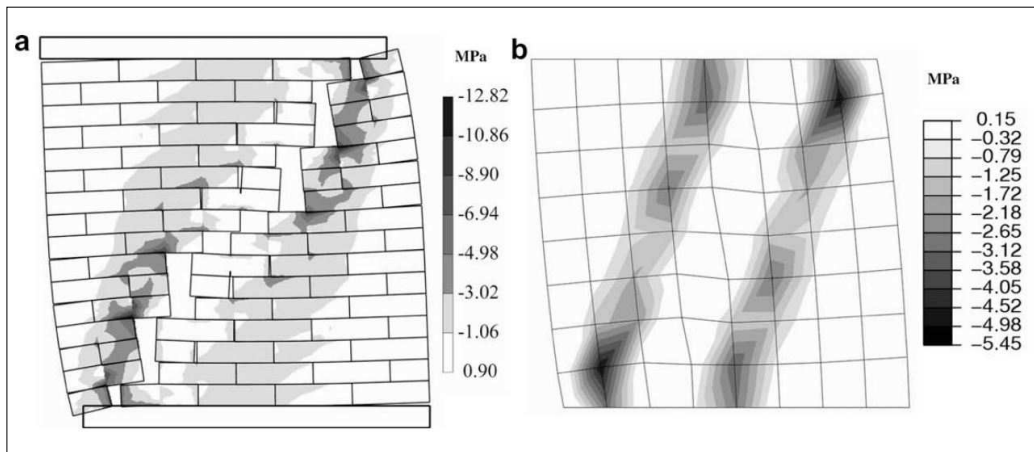
Figure 1.10: Minimum principal stresses for test: (a) interface model at d = 4.1 mm; (b) homogenisation model coupled with damage and plasticity at d = 3.1 mm [28].

1.2.3 Macro-modelling

In large and practical-oriented analyses, the interaction between units and mortar is negligible with respect to the global structural behaviour. Thus in these cases macro-modelling can be used, see Figure 1.5. It does not make any distinction between units and joints and the material is regarded as a fictitious homogeneous anisotropic continuum. A complete macro-model must account for different tensile and compressive strengths along the material axes. It should also account for inelastic behaviour for each material axis. This is clearly a phenomenological approach, and the continuum parameters must be assessed by experiments or homogenization technique. Macro-modelling is more practice oriented due to the reduced time and memory requirements. This type of modelling is most valuable when a compromise between accuracy and efficiency is possible. The macro-models

7

also termed continuum mechanics finite element models. It can be relate to plasticity or damage constitutive laws.

Many research has been conducted on the macro modelling of the masonry through plasticity constitutive laws. In which non-reversibility is govern by internal variables. An example of the former approach is the work of Lourenco [12], see Figure 1.11 - 1.12, which proposed a non-linear constitutive model for in-plane loaded walls based on the plasticity theory (multi surface plasticity). The author proposed an anisotropic plasticity continuum modelling that includes a Rankine type yield surface for tension and Hill type yield surface for the compression. Another example is work of Lofti and Shing [29], the authors used a smeared-crack finite element formulation by adopting the J_2 plasticity model for uncracked masonry and non-linear constitutive models for cracked masonry. The constitutive models admissible field is bounded by a Von-Mises type yield surface in the compression region and the Rankine type yield surface in the tensile region.
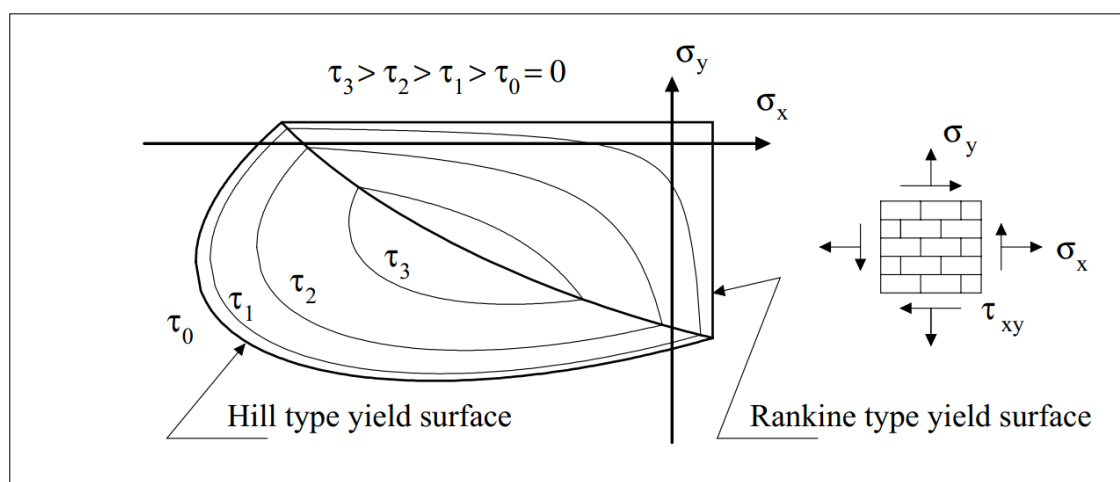
Figure 1.11: Composite yield surface with iso-shear stress lines. Different strength values for tension and compression along each material axis proposed by [12].
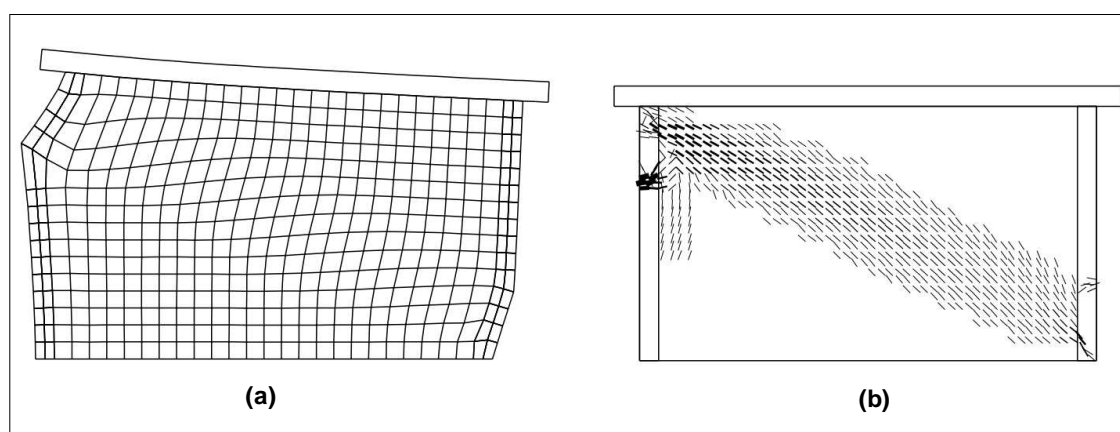
Figure 1.12: Results of the analysis at a displacement of 12.0 [mm]: (a) deformed mesh; (b) cracks [12].

8

Another approach based on Continuum Damage Mechanics. In which damage is control by a scalar or vector or tensor damage variables. Many research has been carried out to developed continuum damage model for masonry. Papa [30] proposed a model based on the introduction of three damage variables, that describes the behaviour of brittle materials subjected to alternating tensile and compressive cyclic loads. It was an extension of a damage model originally developed for isotropic material to the orthotropic case. Berto et al. [31] developed a specific damage model for orthotropic brittle materials with different elastic and inelastic properties along the two material directions, see Figure 1.13.
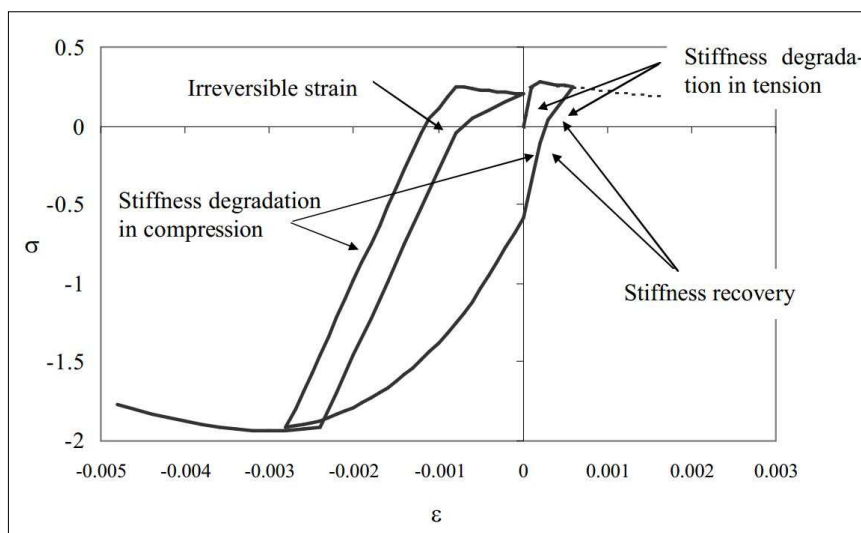
Figure 1.13: Cyclic behavior of plastic-damage model proposed by [31].

The Luca et al. [1, 32] proposed a continuum damage model for orthotropic materials. In which, two stress transformation tensors are used to related tensile and compressive stress states. The transformation relate orthotropic space to fictitious isotropic space, by one-to-one mapping relationships. The constitutive model was adopted in the mapped space, see Figure 1.14. which makes use of two scalar variables which monitor the local damage under tension and compression respectively, see Figure 1.15.
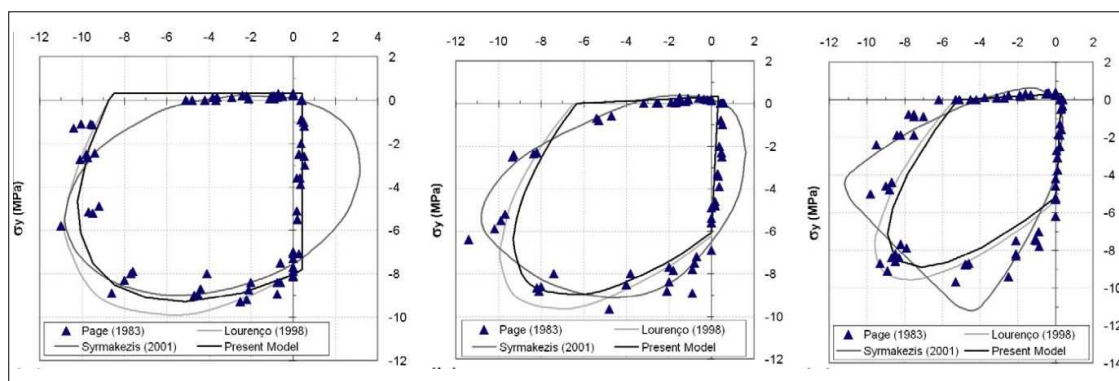
Figure 1.14: Comparison of threshold or yield surfaces available in literature and the one proposed by [32].
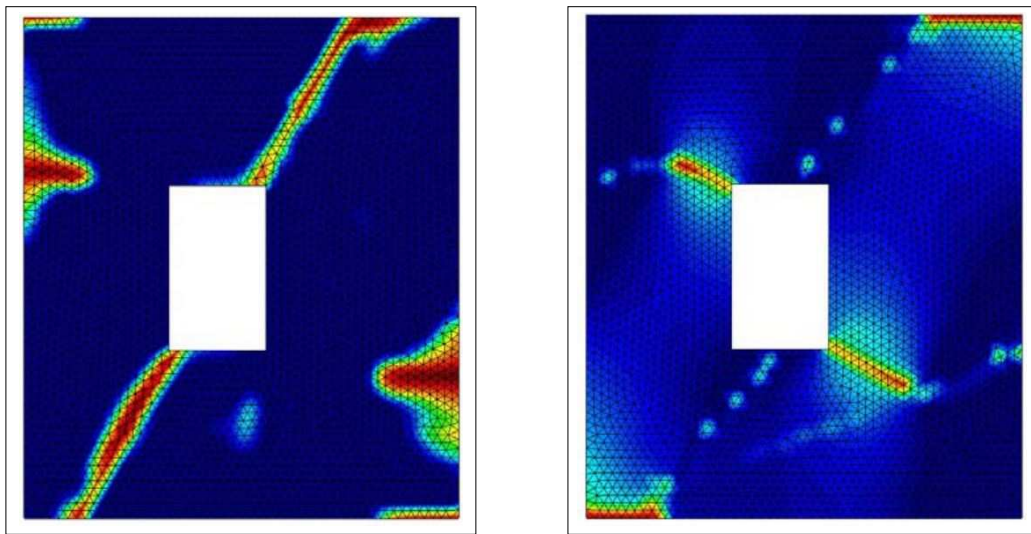
(a) Tensile damage contour   (b) Compressive damage contour

Figure 1.15: Damage contour for a smeared damage model [1].
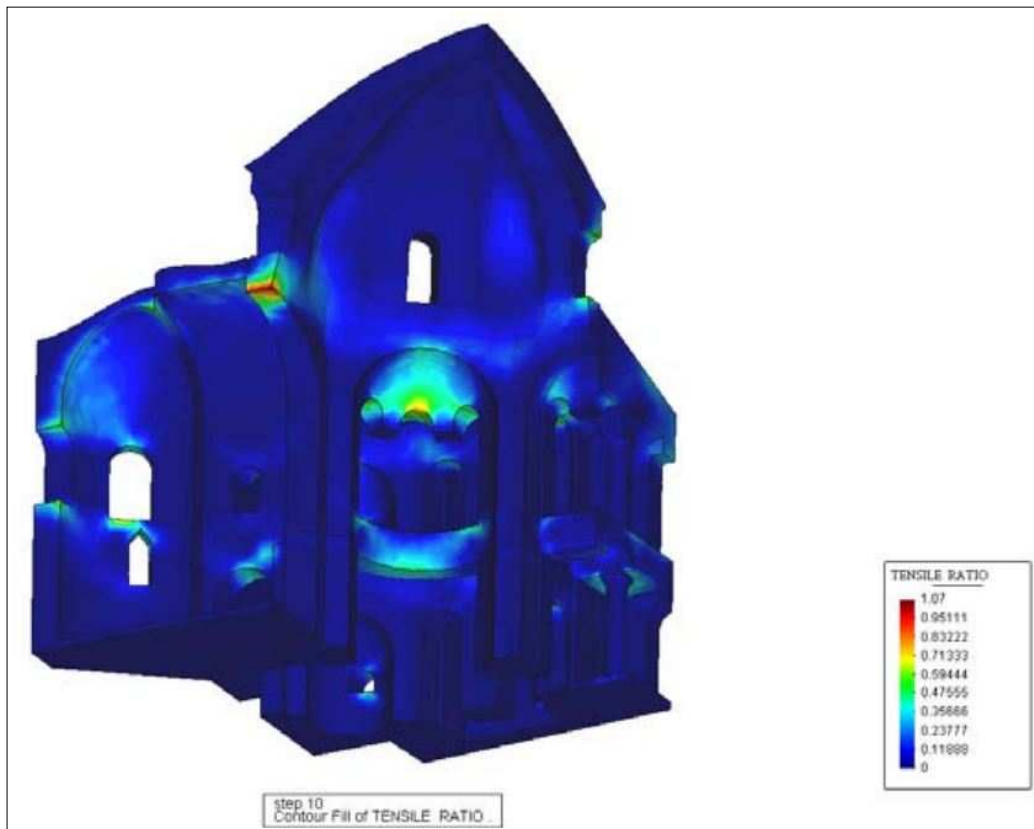
Figure 1.16: Analysis of Kucuk Ayasofya Mosque in Istanbul [33].
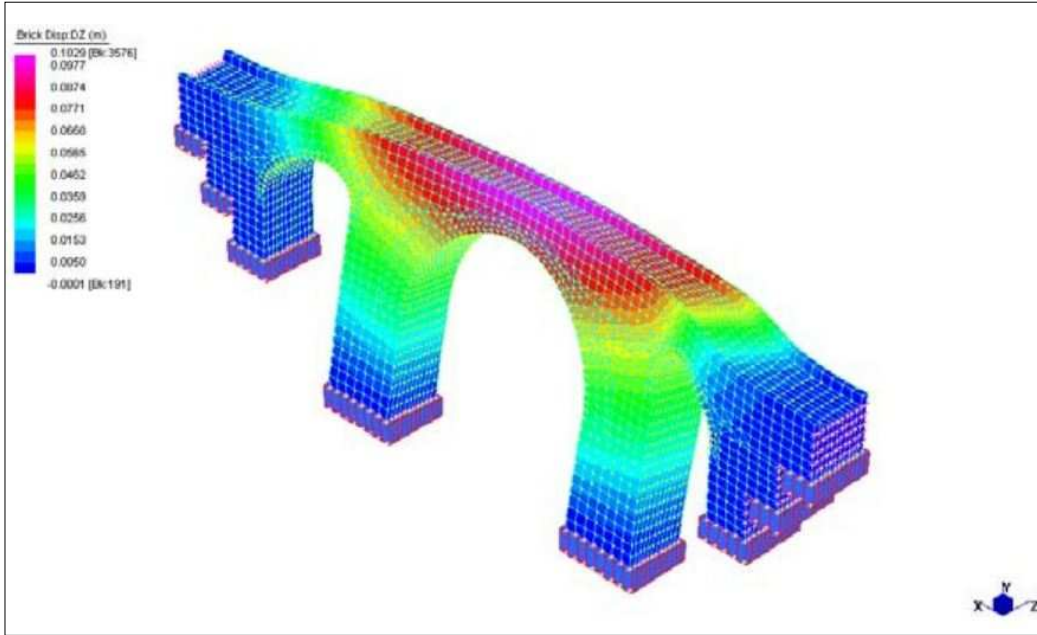
Figure 1.17: Pushover analysis of a masonry arch bridge [34].

Among all the Modelling strategies, the macro-modelling have been extensively used for analysing the seismic response of complex and big masonry structures, such as arch bridges (Pela *et al.* [34]), historical buildings (Mallardo *et al.* [35]), mosques and cathedrals (Massanas *et al.* [33]; Martnez *et al.* [36]; Murcia [37]), see Figures 1.16 and 1.17. However, micro-modelling gives only coarser idea of masonry analysis. whereas, in micro-modelling detail of masonry failure mechanism at local level can be obtained. Thus, in the present work micro modelling is adopted for the detailed failure analysis of the masonry.

1.3 Objectives

In the present work a micro modelling approach is adopted for the detailed failure analysis of the masonry. This study focuses on plasticity based non-linear analysis of unreinforced masonry structures at micro-level. In particular, the study focuses on analysis of two-dimensional modelling of masonry assumed to have plane stress condition. The main objectives of present study are

- to perform a critical review of masonry and computational modelling of masonry structure;

- to perform a computational homogenization of masonry;

- to propose and develop a constitutive micro-model for unreinforced masonry which includes softening behaviour and incorporates all predominant failure mechanisms;

- to implement the proposed model in commercial software ABAQUS using user defined user subroutine UMAT.

- to perform a numerical study to validate the model by comparing the predicted behaviour with the behaviour observed in experiments on different types of masonry.

It is further noted that the model proposed in this study have a much broader applicability than masonry structures. It can be can be used in the micro modelling of the adhesives, joints in rock and stone works etc. The proposed model is applicable to contact in general, all types of interface behaviour where bonding, cohesion and friction between constituents comes form the basic mechanical behaviour.

1.4 Outline of the thesis

This thesis consists of six Chapters

Chapter 1 provides an introduction and the modelling strategies for masonry structures available in literature. Finally, it states the aim and objectives of the research.

Chapter 2 characterizes masonry behaviour. In particular, it addresses the need of a thorough material description in order to develop accurate numerical models.

Chapter 3 presents simple homogenization techniques to derive the global anisotropic behaviour of the masonry. First, the theory of homogenization is presented in a very generic way [3D], by using basic mechanics and mathematics. Then two basic unit cell of the half brick thick masonry wall are considered for numerical application of the theory and compression has been done for the two unit cell. As close form solution is not possible thus FE analysis is done to get the solution.

Chapter 4 introduces an interface failure criterion for the micro-modelling of masonry. A single surface plasticity model is proposed, which is a simple extension of the Mohr-Coulomb criteria with cut-off in tension and cap-off in compression. The inelastic behaviour includes tensile strength softening, cohesion softening, compressive strength hardening and softening, friction softening or hardening, dilatancy softening.

Chapter 5 validates the proposed model in Chapter 4 by means of the FE analysis of an engineering practice case study. Comparison between the calculated numerical results and experimental results have been made in the literature.

Chapter 6 presents an extended summary and the final conclusions which can be derived from this study. Suggestions for future work are also pointed out here.

Chapter 2

Masonry: Material Description

2.1 Introduction

Masonry is the building of structures from individual units laid in and bound together by mortar. The term masonry can also refer to the units themselves. The common materials of masonry construction are brick, stone, marble, granite, travertine, limestone, cast stone, concrete block, glass block, stucco, and tile. Generally, masonry is highly durable form of construction. However, the materials used, the quality of the mortar and workmanship, and the pattern in which the units are assembled can significantly affect the behaviour and durability of the overall masonry construction.
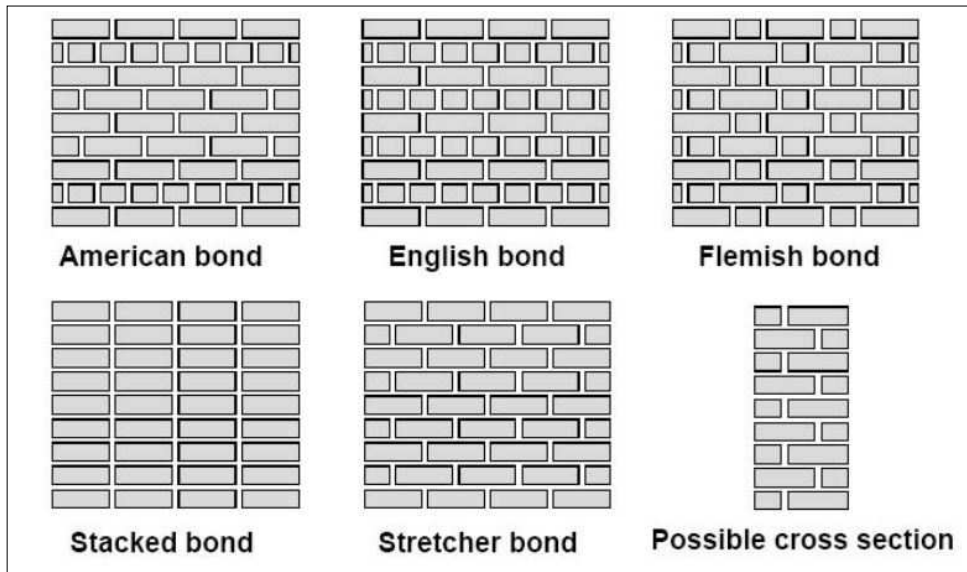
Figure 2.1: Variability of masonry: brick masonry [1].

Masonry is a heterogeneous anisotropic continuum. In particular, the inhomogeneity is due to the different mechanical properties of its constituents. Anisotropy is due to the different masonry patterns, that can be obtained by variation of geometry, nature and arrangement of mortar and brick. Some of the different possible combination of masonry are shown in Figure 2.1. The behaviour of masonry is very complex and highly non-linear due to the behaviour of its constituents, which

are quasi-brittle in nature. Thus for micro-modelling, a material description must be obtained from experimental tests on the masonry constituents. For macro-modelling, a small tests must be performed on masonry specimens of sufficient size under homogeneous states of stress or strain, to obtain average stress-strain relationship (Importance is given to deformation controlled test, because it is capable of capturing the entire load-displacement diagram). As a alternative to experiments, these average stress-strain relationships can be obtained from the homogenization. The complete description of the material is not pursued in this study. The readers are referred to Drysdale *et al.* [7] and Hendry (1990) [8] for more description.

The property of masonry depends up on the large no of factor, such as material properties of the units and mortar; arrangement of units; anisotropy of units; dimension of units; joint thickness; quality of workmanship; degree of curing; environment and age etc. Because of these large number of variable, the masonry research community showing the interest in the sophisticated numerical models from last two decades. Moreover, numerical models required the reliable experimental data. The experimental data are required for test parameters and for the comparisons and conclusions. It is a usual practice to report and measure only strength values. In particular, masonry shows the softening behaviour after peak value. Thus it is very important to retrieve the information of post-peak or softening regime. But very rare information was available in the literature about the softening regime of the masonry and its constituents. Thus, in the following chapter the aspects of softening behaviour is explain before the brief description of masonry and its constituent is given.

2.2   Softening behaviour aspects

Masonry shows the softening behaviour in the post peak region. It is typical due to quasi-brittle in nature of its constituent i.e. brick and mortar. Softening defined as a gradual decrease of mechanical resistance under a continuous increase of deformation. It happened due to the present of progressive internal micro crack. Such mechanical behaviour is commonly attributed to the heterogeneity of the material, due to the presence of different phases and material defects, like flaws and voids. Even prior to loading the structure, mortar contains microcracks due to the shrinkage during curing and the presence of the aggregate. The clay brick contains inclusions and microcracks due to the shrinkage during the burning process. Initially, these microcracks are stable which means that they grow only when the load is increased. During the initial loading the cracks remains stable and number of new crack formation is very less. But, around peak load an acceleration of crack formation takes place and the formation of macrocracks starts. The macrocracks are unstable, which means that the load has to decrease to avoid an uncontrolled growth. In a deformation controlled test the macrocracks growth results in softening and localization of cracking in a small zone while the rest of the specimen unloads. It is assumed that the inelastic behaviour can be described by the integral of the $\sigma - \delta$ diagram. These crack can opened in different mode i.e. fracture energy mode I for tensile loading, fracture energy mode II for shear loading and compressive fracture energy.

2.2.1   Tensile strength softening

The phenomenon of tensile failure has been well identified, see Figure 2.2. The inelastic behaviour of tensile strength degradation is described by the integral of the $\sigma - \delta$ diagram. This quantity is

the tensile fracture energy (G_f), and it is defined as the amount of energy to create a unitary area of a crack opening.

Figure 2.2: Behaviour of quasi-brittle material under uniaxial tensile loading and definition of tensile fracture energy (f_t denotes tensile strength) [12].

2.2.2 Compressive strength softening

In the compressive failure, softening behaviour is highly dependent upon the boundary conditions in the experiments and the size of the specimen. Experimental concrete data provided by Vonk [38] indicated that the behaviour in uniaxial compression is governed by both local and continuum fracturing processes. Similar to tension, the inelastic behaviour of compression strength is described by the integral of the $\sigma - \delta$ diagram, see Figure 2.2. Now, this quantity is the compressive fracture energy (G_c). It has the same notion as the tensile fracture energy (G_f), because the underlying failure mechanisms are identical, viz. continuous crack growth at micro-level.
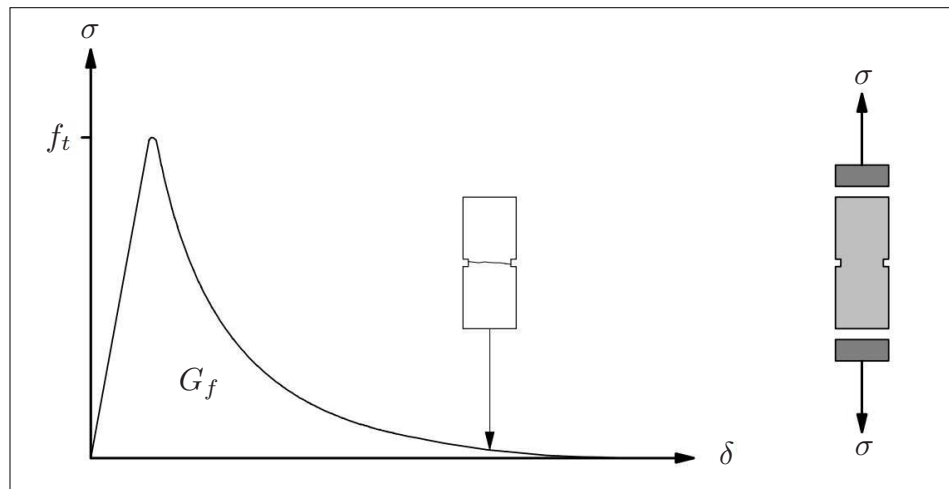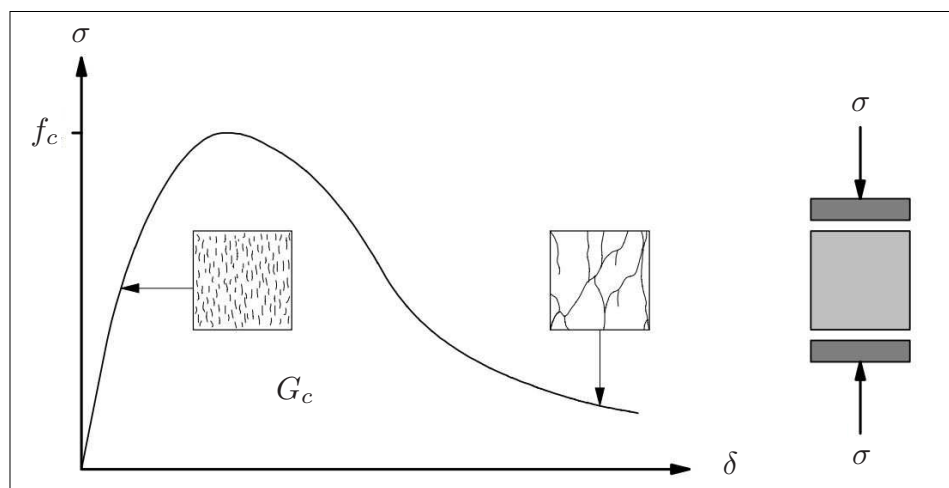

Figure 2.3: Behaviour of quasi-brittle material under uniaxial compressive loading and definition of compressive fracture energy (f_c denotes compressive strength) [12].

2.2.3　Shear strength softening

In the shear failure, a softening behaviour is observed as degradation of the cohesion in Coulomb friction models. it represents the mode II failure mechanism, that consists of slip of the unit-mortar interface under shear loading. Again, it is assumed that the inelastic behaviour is described by the mode II fracture energy G_f^{II}, defined by the integral of the $\tau - \delta$ diagram in the absence of normal confining load, see Figure 2.4.
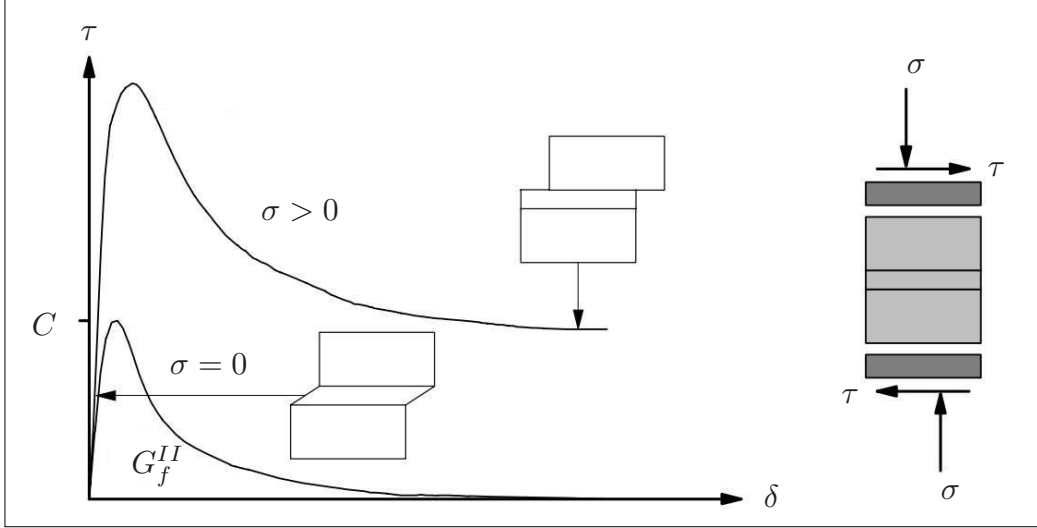
Figure 2.4: Behaviour of masonry under shear and definition of mode II fracture energy (C denotes cohesion) [12].

2.3　Property of masonry constituents

The property of masonry dependants up on the property of its constituents. Thus, it is important to know the property of brick, mortar and unit-mortar interface for studying the masonry. Generally, compression strength test are used for indication the quality of the material.

2.3.1　Masonry units

For the masonry units, a standard tests with solid platens have being done for compressive strength as per IS 3495 part 1. The test results in an artificial compressive strength due to the restraint effect in its lateral direction. The effect can be minimizes by normalizing the compressive strength, by multiplying with appropriate shape/size factor. No experiments in the uni-axial post-peak behaviour of compressed bricks and blocks exists, therefore, no information about the compressive fracture energy G_c can be obtain.

Even though, It is difficult to relate the tensile strength of the masonry unit to its compressive strength due to the different shapes, materials, manufacture processes and volume of perforations. Many researcher conducted extensive testing to obtained a ratio between the tensile and compressive strength. Schubert [39] find ratio ranges from 0.03 to 0.10 for clay, calcium-silicate and concrete units. For the fracture energy G_f of solid clay and calcium-silicate units, both in the longitudinal

and normal directions. Van der Pluijm [40] found fracture energy values ranging from 0.06 to 0.13 $[Nmm/mm^2]$ for tensile strength values ranging from 1.5 to 3.5 $[N/mm^2]$.

2.3.2 Mortar

The compressive strength of is obtained from standard tests carried out on the cube of 75 [mm] as per IS 4031 part-7 1998. Moreover, investigations in mortar disks extracted from the masonry joints has being carried out to fully characterize the mortar behaviour, Bierwirth et al. (1993), Schubert and Hoffman (1994) and Stckl et al.(1994). Nevertheless, there is still a lack of knowledge about the complete mortar uni axial behaviour in tension and compression.

2.3.3 Property of unit-mortar interfaces

The bond between the unit and mortar is most critical part of the masonry and governs most non-linear response of the joints. Moreover, it is the weakest link in masonry assemblages. Predominately two failure phenomena can be considered for unit-mortar interface, one associated with tensile failure (mode I) and the other associated with shear failure (mode II).

Mode I failure

Van der Pluijm [40, 41] carried out deformation controlled tests in series. The test was conducted on small masonry specimens made up of solid clay and calcium-silicate units. These tests resulted in an exponential tension softening curve with a mode I fracture energy G_f^I, see Figure 2.5(a).
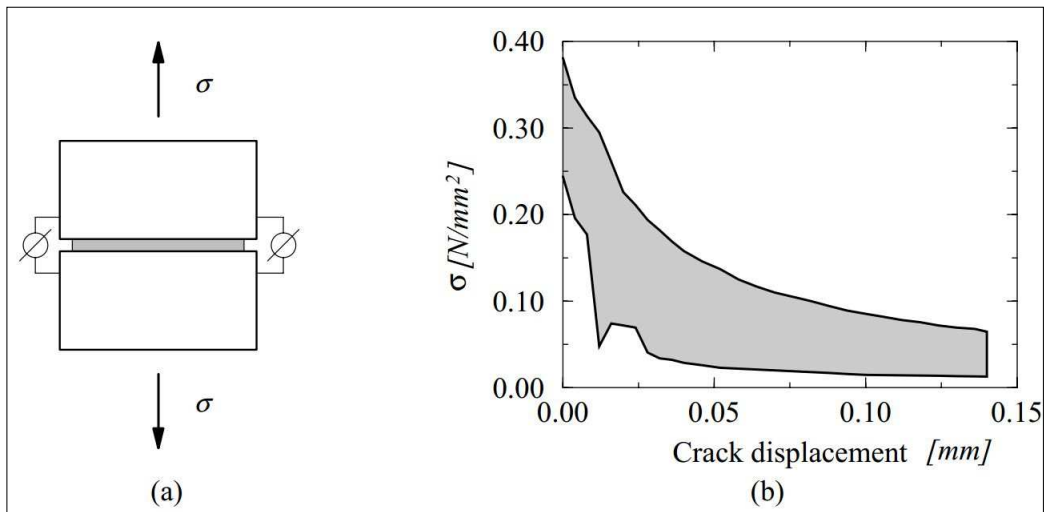
Figure 2.5: Tensile bond behaviour of masonry [40, 41]: (a) test specimen; (b) typical experimental stress-crack displacement results for solid clay brick masonry.

During the first series in 1990, it becomes clear by close observation of the cracked specimens, that the bond area was smaller than the cross sectional area of the specimens. This net bond surface area seems to concentrate in inner part of the specimen. The reduction in bond area is a combined result from shrinkage of the mortar and the process of laying units in the mortar bed joint. In many cases the net bond surfaces area was restricted to central part of the specimen. Therefore, it is

assumed that the reduction of the bond surfaces is caused by the edges of the specimen. With this assumption, it is possible to estimate the fracture energy. Hence, the net bond surface area must be corrected according to the number of edges, see Figure 2.6.
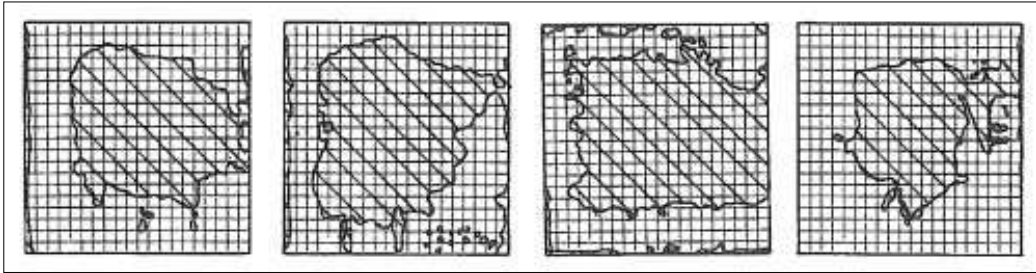
Figure 2.6: Tensile bond surface [40] typical net bond surface area for tensile specimens of solid clay units.

Mode II failure

For capturing the shear response of masonry joints experimentally. It is very important to set-up a uniform state of stress in the joints. But it very is difficult, because the equilibrium constraints introduce non-uniform normal stresses in the joints. For the detailed study readers are referred to Atkinson *et al.* [42] and Van der Pluijm [41].
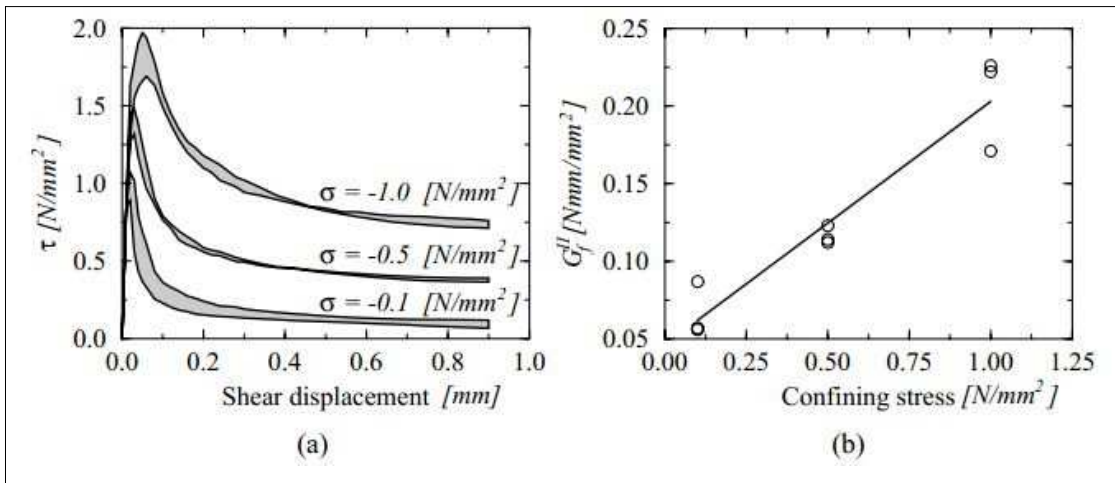
Figure 2.7: Typical shear bond behaviour of the joints for solid clay units, Pluijm [41]: (a) stress-displacement diagram for different normal stress levels; (b) mode II fracture energy G_f^{II} as a function of the normal stress level.

Pluijm [41] presents the most complete characterization of the masonry shear behaviour for solid clay and calcium-silicate units. This involves a direct shear test under different levels of uniform state of stress. This test did not allow for application of tensile stresses and low confining stresses. Because it results in extremely brittle failure, which makes the test set-up potential installable. Where as, for higher confining stresses shearing of the unit-mortar interface is accompanied by diagonal cracking in the units.
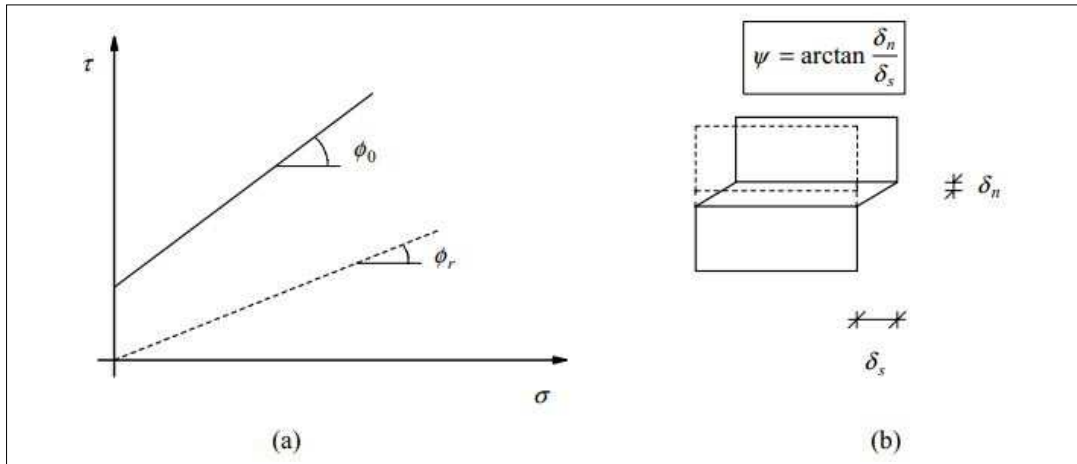
Figure 2.8: Definition of friction and dilatancy angles [12]: (a) Coulomb friction law, with initial and residual friction angle; (b) dilatancy angle as the uplift of neighbouring units upon shearing.

These experimental results yield an exponential shear softening with a residual dry friction, see Figure 2.7(a). The area defined by the stress-displacement diagram and the residual dry friction shear level is called mode II fracture energy G_f^{II}. The value for the fracture energy depends also on the level of the confining stress, see Figure 2.7(b). Evaluation of the net bond surface of the specimens is no longer possible in this case.

Moreover, it has been found that behaviour of masonry is no longer associative i.e. $\delta_{nn} \neq \delta_{tt} \tan \phi$ (δ_{nn} and δ_{tt} is normal and tangential relative displacement). Thus an additional material parameters can be obtained from such an experiment i.e. dilatancy angle, see Figure 2.8. The dilatancy angle ψ measures the uplift of one unit over the other upon shearing. It depends on the level of the confining stress, see Figure 2.9, i.e. for high confining pressures ψ decreases to zero. Further more, dilatancy also decreases with increasing in shear displacement, due to the smoothing of the sheared surfaces.
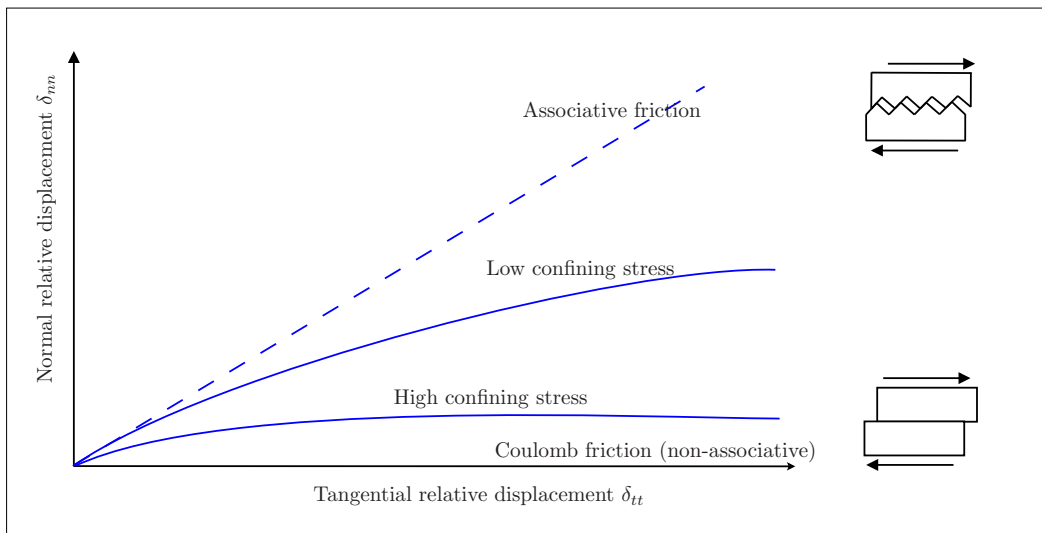
Figure 2.9: Masonry joint behaviour: relation between normal and tangential relative displacement for different confining stress.

19

2.4 Property of masonry as a composite material

The masonry is composite of brick and mortar, thus it is also important to study the masonry behaviour as a composite. In this section uniaxial and biaxial behaviour of masonry as a composite is presented.

2.4.1 Uniaxial behaviour

The uniaxial tests can be applied in two direction to the masonry i.e. one normal to the bed joints and another parallel to the bed joints. The uniaxial tests in the direction normal to the bed joints have received more attention from the masonry community then uniaxial compression test in the direction parallel to the bed joints. This is because of the application and use of masonry as a vertical load bearing structure. However, masonry is an anisotropic material. Thus the resistance to applied loads parallel or perpendicular to the bed joint can have a decisive effect on the load bearing capacity of masonry.

Uniaxial compression behaviour

Hilsdorf [43] presented that the difference in elastic properties of the unit and mortar is the main cause of failure of masonry. In masonry, units are stiffer than mortar and this difference is more pronounced in old masonry.
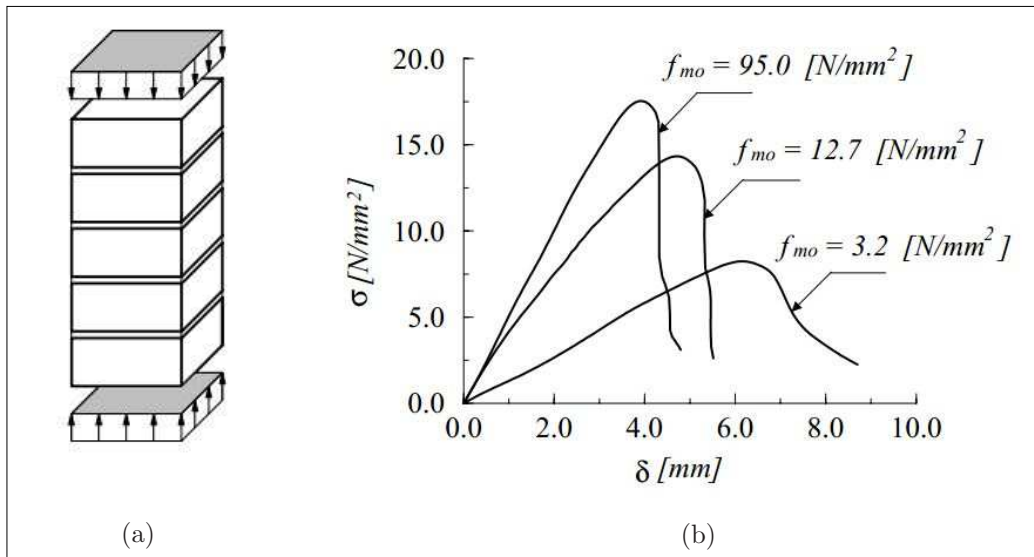
Figure 2.10: Uniaxial behavior of masonry upon loading normal to the bed joints: (a) stacked bond prism; (b) typical experimental stress-displacement diagrams [44].

A test on the stacked bond prism of masonry is frequently used to obtain the uniaxial compressive strength, see Figure 2.10. But, still it is not clear that what are the consequences in the masonry strength of using this type of specimens (see Mann and Betzler [45]). The Uniaxial compression in direction perpendicular to bed joints in masonry leads to a state of triaxial compression in the mortar and of compression/biaxial tension in the unit, see Figure 2.11. Mann and Betzler [45] observed that, initially vertical cracks appear in the units along the middle line of the specimen, and upon

increasing deformation additional cracks appear. Normally vertical cracks at the small side of the specimen lead to failure by splitting of the prism.
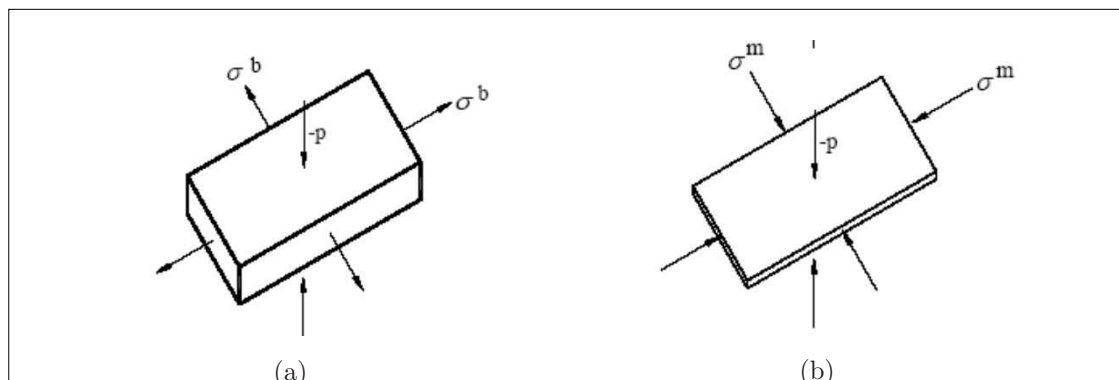
Figure 2.11: Local state of stress in masonry prisms under uniaxial vertical compression [1]: (a) brick; (b) mortar.

The strength and the failure mode of the masonry changes when different inclinations of compression load with respect to bed joints are considered (see [19, 20, 46]). This is because of the anisotropic nature of the material. If loading direction is parallel or perpendicular to bed joints, splitting of the bed joints or head joint in tension occurs, respectively. For intermediate inclinations mixed mechanism was found, which are accomplished by the step diagonal failure of the masonry, see Figure 2.12.
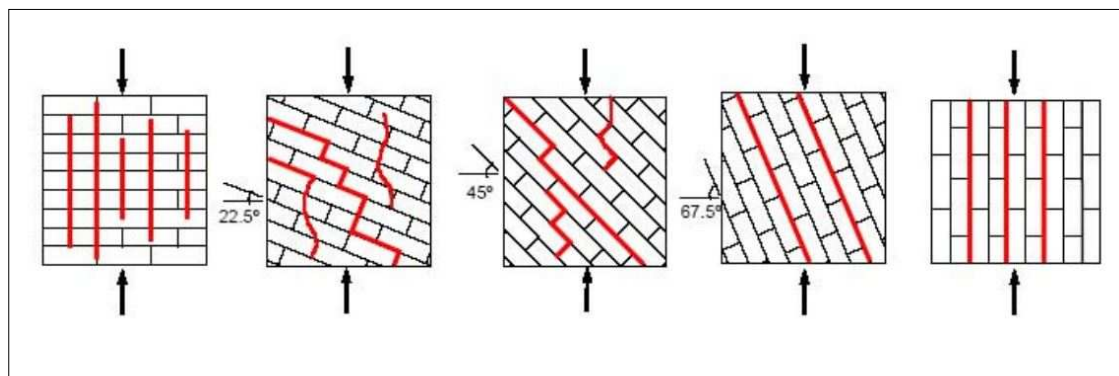
Figure 2.12: Modes of failure of solid clay units masonry under uniaxial compression [19, 20].

Uniaxial tension behaviour

For tensile loading perpendicular to the bed joints, failure is generally caused by failure of unit-mortar bed joint. As a rough approximation, the masonry tensile strength can be equated to the tensile strength of the unit or the joint. In masonry with low strength units and greater tensile bond (or unit-mortar bed joint) strength, for example high-strength mortar and units with numerous small perforations, which produce a dowel effect. The failure may occur as a result of stresses exceeding the unit tensile strength. As a rough approximation, in this case the tensile strength of masonry is equated to the tensile strength of the unit.
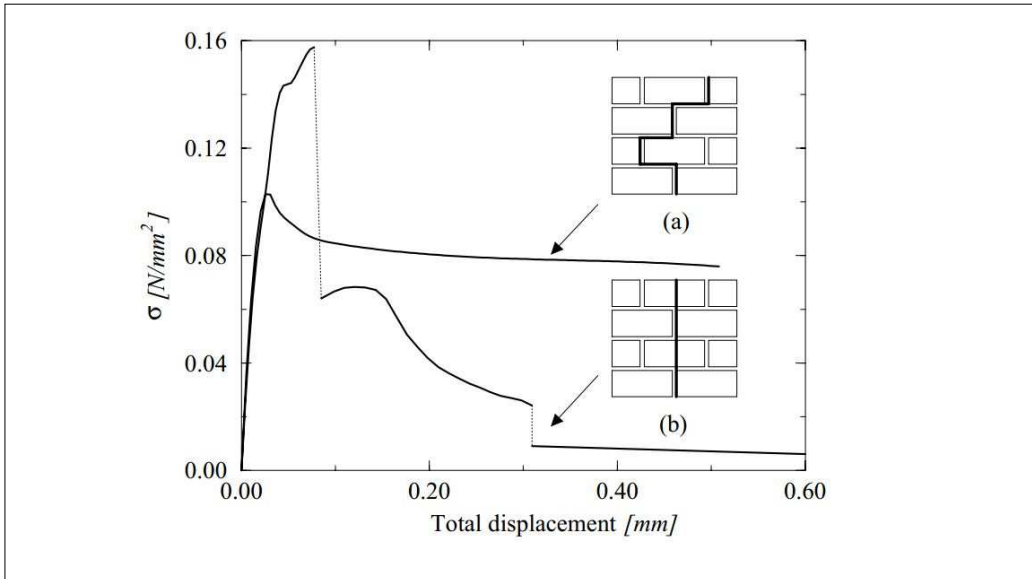
Figure 2.13: Typical experimental stress-displacement diagrams for tension in the direction parallel to the bed joints [47]: (a) failure occurs with a stepped crack through head and bed joints; (b) failure occurs vertically through head joints and units.

For tensile loading parallel to the bed joints situation is diffrent. Thus to find out the tensile strength of masonry, a complete test program was set-up by Backes [47]. The author tested masonry wallets under direct tension. The author found that tension failure was affected by the type of the mortar and the masonry units. For stronger mortar and weaker masonry units, the tension cracks passed along the head mortar joints, and through the centre of the bricks at the intervening courses. For weaker mortar joints and stronger masonry units, the tension crack passed along the head joints of the masonry units and the length of bed joints between staggered head joints, as shown in Figure 2.13.
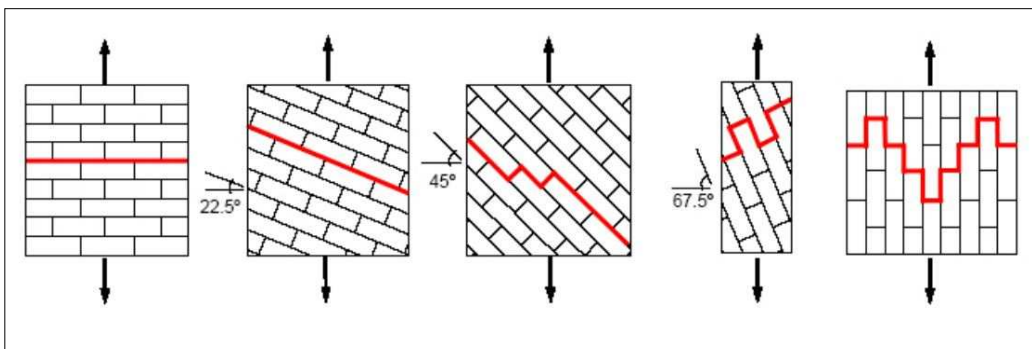
Figure 2.14: Modes of failure of solid clay units masonry under uniaxial tension [19].

The tensile strength and the failure mode change when different inclinations of load with respect to bed joints are considered. Figure 2.14 shows different modes of failure observed by Page [19] on solid clay units masonry walls subjected to uniaxial tension. For intermediate inclinations for the tensile loading, the failure is accomplished by the the sliding and split of the joints diagonally.

22

2.4.2 Bi-axial behaviour

The masonry is anisotropic material. Thus constitutive behaviour of masonry under biaxial stress states can not be completely described from the constitutive behaviour under uniaxial loading conditions. Moreover, The biaxial strength envelope cannot be described in terms of principal stresses. Therefore, the biaxial strength envelope of masonry must be either described in terms of the full stress vector in a fixed set of material axes or, in terms of principal stresses and the rotation angle θ between the principal stresses and the material axes.
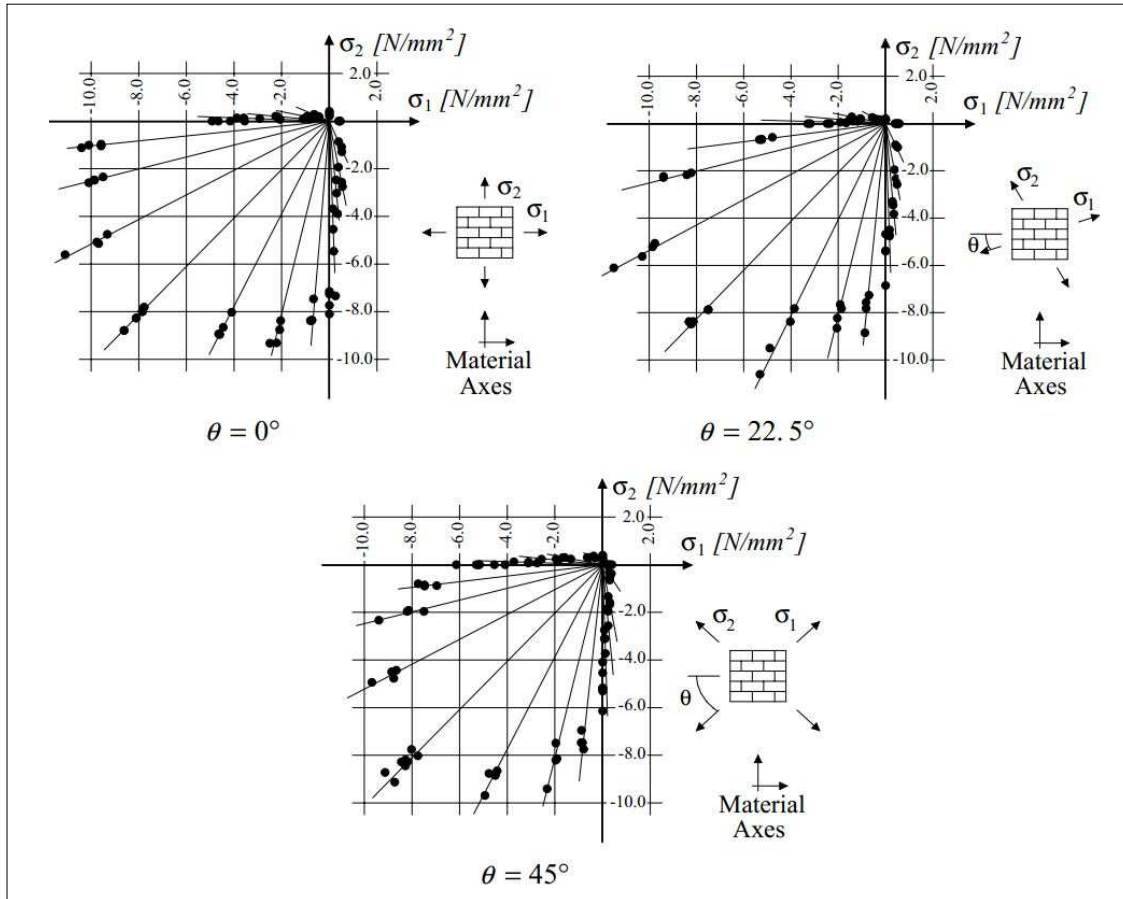
Figure 2.15: Biaxial strength of solid clay units masonry [19, 20].

Page [19, 20] conducted the most complete experiments on the masonry subjected to different proportional biaxial loading, see Figure 2.15. The tests were carried out with half scale solid clay units. The failure mode and strength of the masonry is influences by both the orientation of the principal stresses with regard to the material axes and the principal stress ratio. Noted that the strength envelope shown in Figure 2.15 have a limited applicability for other types of masonry. Different strength envelopes and different failure modes are likely to be found for different materials, unit shapes and geometry. Comprehensive study to characterize the biaxial strength of different masonry types were carried using full scale specimens, see Ganz and Thrlimann [48] for hollow clay units masonry, Guggisberg and Thrlimann [49] for clay and calcium-silicate units masonry and Lurati *et al.* [50] for concrete units masonry.

From the prior knowledge, failure in uniaxial tension occurred by cracking and sliding of the head and bed joints. The influence of the lateral tensile stress on the tensile strength is not known because no experimental results are available. Whereas in the tension-compression loading, lateral compressive stress decreases the tensile strength. The minimum value is achieved when tensile loading direction is perpendicular to the bed joints. Moreover, the failure of the masonry occurs by cracking and sliding of the joints or in a combined mechanism involving both units and joints, see Figure 2.16.
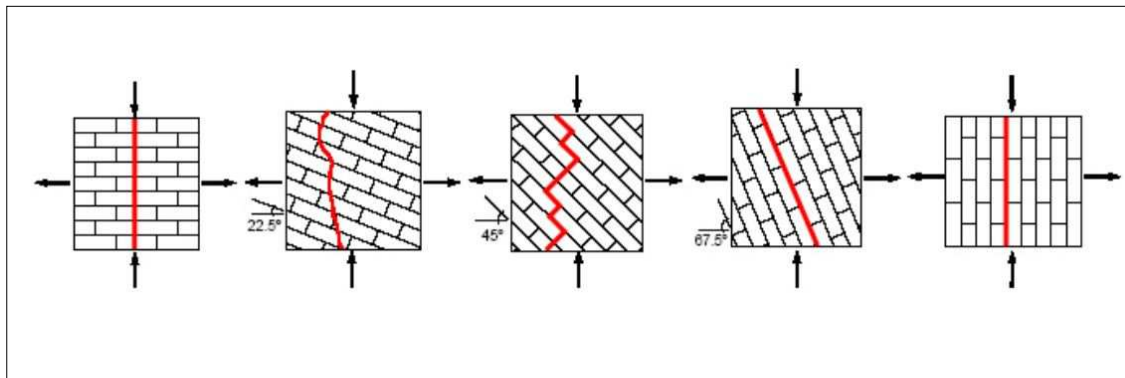
Figure 2.16: Modes of failure of solid clay units masonry under biaxial tension-compression [20].

In biaxial compression, typically failure occurs by splitting of the specimen at mid-thickness and in a plane parallel to its free surface, regardless of the orientation of the principal stresses, see Figure 2.17. The orientation plays a significant role, for principal stress ratios less than and grater than 1 failure occurred in a combined mechanism. It involves both joint failure and lateral splitting. The increase of compressive strength under biaxial compression can be explained by friction in the joints and internal friction in the units and mortar.
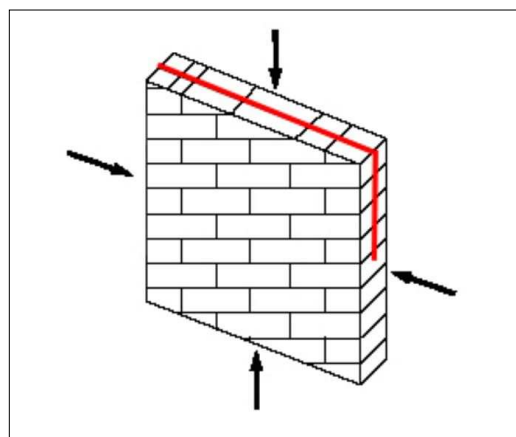
Figure 2.17: Mode of failure of solid clay units masonry under biaxial compression [19].

2.5 Conclusion

Masonry is a heterogeneous anisotropic material that consists of units and mortar. Both the masonry constituents are quasi brittle in nature. Their failure in tension and compression loading is essentially the same and i.e. due to growth of micro level crack in the material. During failure the inelastic strains result from a dissipation of fracture energy. First, due sliding or mode II which results in a dry friction process between the components once softening is completed. Second, the split of the head joint and the brick in mode I. Third, the crushing of mortar or brick take place, which release the compressive fracture energy. If the micro-modelling strategy is used for masonry, then all these failure mechanisms should be incorporated in the failure model.

On the other hand if the macro-modelling strategy is used, joints are smeared out in an anisotropic homogeneous continuum. Therefore, the interaction between the masonry components cannot be incorporated in these types of models. Instead, a relation between average stresses and strains should be established through experiments or homogenization.

Chapter 3

Homogenization of masonry

Masonry is heterogeneous material. Thus, for the macro-modelling of masonry continuum parameters must be assessed by experiments on specimens of sufficiently large size, under homogeneous states of stress or strain. As an alternative to difficult experimental tests. Homogenization technique can be used to determine global behaviour of the masonry. Experimental data of individual components is considered as input for the numerical homogenization technique. Moreover, masonry is periodic material, thus we can exploit its periodicity to simplify homogenization problem.

In this chapter, The homogenization theory for periodic media is implemented in very generic way to derive the anisotropic global behaviour of the masonry. The rigorous application of the homogenization theory in one step and through a full three dimensional behaviour is done. Two basic unit cell of the half brick thick masonry wall are considered for numerical application of the theory and compression has been done for the two unit cell. Moreover, a full examination for different stiffness ratio between mortar and unit has been done to assess the performance for inelastic behaviour. Where the tangent stiffness of one component or the tangent stiffness of the two components tends to zero with increasing inelastic behaviour.

3.1 Overview

The present study is on the composite behaviour of masonry in terms of determining averaged microscopic stress and strains so that the material can be assumed homogeneous. Pande *et al.* [51], Maier *et al.* [52] and Pietruszczak and Niu [53] introduced the homogenization techniques in an approximate manner. In most of these work the homogenization procedure has been performed in several steps, head joints and bed joints being introduced successively. In this case masonry is assumed to be a layered material, which simplifies the problem significantly but such a methodology introduces several errors. The result generally depends on the order of the successive steps (Geymonat *et al.* [54]). The geometrical arrangement is not fully taken into account i.e. different bond patterns may lead to exactly the same result. For example running bond and stack bond result in same results. The thickness of the masonry was not taken in to account, masonry is considered infinitely thin two dimension media under plain stress assumption (Maier *et al.* [52]).

Anthoine [24], Urbanski *et al.* [27] applied the homogenization theory for periodic media rigorously to the basic cell to carry out a single step homogenization, with adequate boundary conditions

and exact geometry. Finite element method was used to obtain numerical solution as exact solutions is not possible. The application of the homogenization theory for the non-linear behaviour of the complex masonry basic cell implies solving the problem for all possible macroscopic loading histories, since the superposition principle does not apply any more. Thus, for the complete determination of the homogenized constitutive law would require an infinite number of computations.

Many studies has been conducted on the homogenization of the masonry in recent years, M Mistler *et al.* [55] focuses on the generalization of the homogenization procedure for out-of-plane behaviour of masonry, in such a way that the in-plane and out-of-plane characteristics of the homogeneous equivalent plate can be derived in one step. Zucchini and Lourenco [28] developed an improved micro-mechanical model for masonry homogenisation for the non-linear domain. The authors coupled the model with damage and plasticity models, that can simulate the behaviour of a basic periodic cell up to complete degradation and failure. IM Gitman *et al.* [56] investigated the representative volume element for different stages of the material response, including pre- and post-peak loading regimes. CK Yan [57] conducted a study on a unified modelling approach for homogenization (forward) and de-homogenization (backward), applicable to unidirectional composite systems. Emphasis is placed on the uniqueness between the forward and the backward modelling processes. Elio Sacco [58] presented a non-linear homogenization procedure for periodic masonry. In this linear elastic constitutive relationship is considered for the blocks, while a new special non-linear constitutive law is proposed for the mortar joints. The Elio Sacco work is extended by Daniela Addessi *et al.* [59] to cosserat model for periodic masonry, which accounts for the absolute size of the constituents, is derived by a rational homogenization procedure based on the transformation field analysis.

3.2   Homogenization theory for periodic media

The theory of homogenization allows global behaviour of the periodic media to be derived from the behaviour of its constituents. In this section theory of homogenization is presented in a very generic way for the [3D] by using basic mechanics and mathematics. Since theory will be applied to the masonry, a half brick thick wall is considered for the analysis.

3.2.1   Description of periodicity

Consider a portion $\boldsymbol{\Omega}$ of a masonry wall, see in Figure 3.1. It is a two dimensional periodic composite continuum, in which brick and mortar are arranged in the running bond. This periodicity can be characterized by a frame of reference $(\alpha_1, \alpha_2, \alpha_3)$. Where α_1, α_2 and α_3 are independent vectors of a basic cell $\hat{\Omega}$, such that property of masonry can be expressed in terms of the these independent variables. The basic cell is considered such that the masonry domain can be generated by repeating the cells in e_1 and e_2 direction. Since finite element calculations are to be performed on the cell, it is preferred to choose cell with least volume and with symmetries. The choice of the cell depends on the arrangement of the brick and mortar for the masonry. For the half brick thick wall, a simplest basic cell is made up of one brick surrounded by half mortar joint. The masonry property in periodic direction can be express as $\alpha_1\beta_1 + \alpha_2\beta_2$, where α_1, α_2 having the zero component of the e_3 and α_3 have only e_3 component i.e. thickness of basic cell $\hat{\Omega}$, β_1 and β_2 are integers. The reference frame for the half brick wall may be written as

$$\alpha_1 = 2le_1 \tag{3.1}$$

$$\alpha_2 = de_1 + 2he_2 \tag{3.2}$$

$$\alpha_2 = 2we_3 \tag{3.3}$$

Where $2l$ is equal to the length of the brick plus the thickness of the head joint, $2w$ is thickness of masonry, $2h$ is equal to the height of the brick plus the thickness of the bed joint and d is the overlapping. $d = 0$ gives stack bond, $d = 1$ gives running bond. For the more complex geometry, masonry would require larger basic cell, i.e. cell involving more than one brick.

In the boundary surface of the three-dimensional basic cell. Two different regions may be separated, Figure 3.1, $\partial\hat{\Omega}_i$ which is internal to the wall (interfaces with adjacent cells) and $\partial\hat{\Omega}_e$ which is external (lateral faces). $\partial\hat{\Omega}_i$ can be divided into three pairs of identical sides (due to periodicity in e_1 and e_2) corresponding to each other through a translation along α_1, α_2 or $\alpha_1 - \alpha_2$ (opposite sides). Where two pairs (only α_1, α_2) are of identical sides in the case of stack bond pattern. As there is no periodicity in e_3 direction, thus the two lateral faces of $\partial\hat{\Omega}_e$ are just opposite sides of the cell.
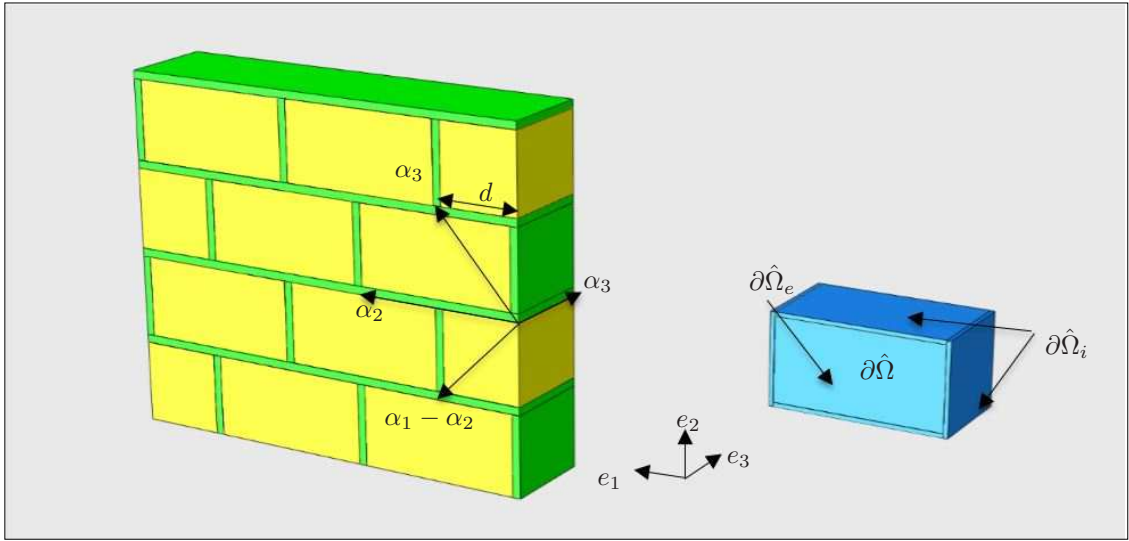
Figure 3.1: Half brick thick masonry wall in running bond with frame of reference (left) and corresponding three dimension basic cell (right).

Now, suppose the portion $\hat{\Omega}$ of masonry is subjected to a globally (macroscopically) homogeneous stress state, see Figure 3.2. A stress state is said to be globally or macroscopically homogeneous over a domain $\hat{\Omega}$ if all basic cells within $\hat{\Omega}$ undergo the same loading conditions. This can be achieved by apply biaxial principal stress state to the domain. A cell lying nears the boundary $\partial\hat{\Omega}$ of the specimen is not subjected to the same loading as one lying in the centre. However, on account of the Saint-Venant principle, all cells lying far enough from the boundary are subjected to the same loading conditions and therefore deform in the same way. In particular, two joined cells must

still fit together in their common deformed state. Means that, condition (i) stress compatibility and condition (ii) strain compatibility must be satisfy on the internal boundary $\partial\hat{\Omega}_i$. The external boundary $\partial\hat{\Omega}_e$ remain stress free.

If we are passing from a cell to the next cell, which is identical to first one. This means that, passing from a side to the opposite one in the same cell $\hat{\Omega}$. Then the condition (i) becomes stress vectors $\boldsymbol{\sigma}.\boldsymbol{n}$ are opposite on opposite sides of $\partial\hat{\Omega}_i$ because external normal $\boldsymbol{n}$ are also opposite. Such a stress field $\boldsymbol{\sigma}$ is said to be periodic on $\partial\hat{\Omega}_i$, whereas the external normal n and the stress vector $\boldsymbol{\sigma}.\boldsymbol{n}$ are said to be anti-periodic on $\partial\hat{\Omega}_i$. For the condition (ii), it is necessary that opposite sides can be superimposed in their deformed states without separation or overlapping. The displacement fields on two opposite sides must be a rigid displacement. Any strain periodic displacement field u can be written in the following way

$$u_i(x_1, x_2, x_3) = \delta_{ij}E_{jk}\delta_{kl}x_l + u_i^p(x_1, x_2, x_3) \tag{3.4}$$
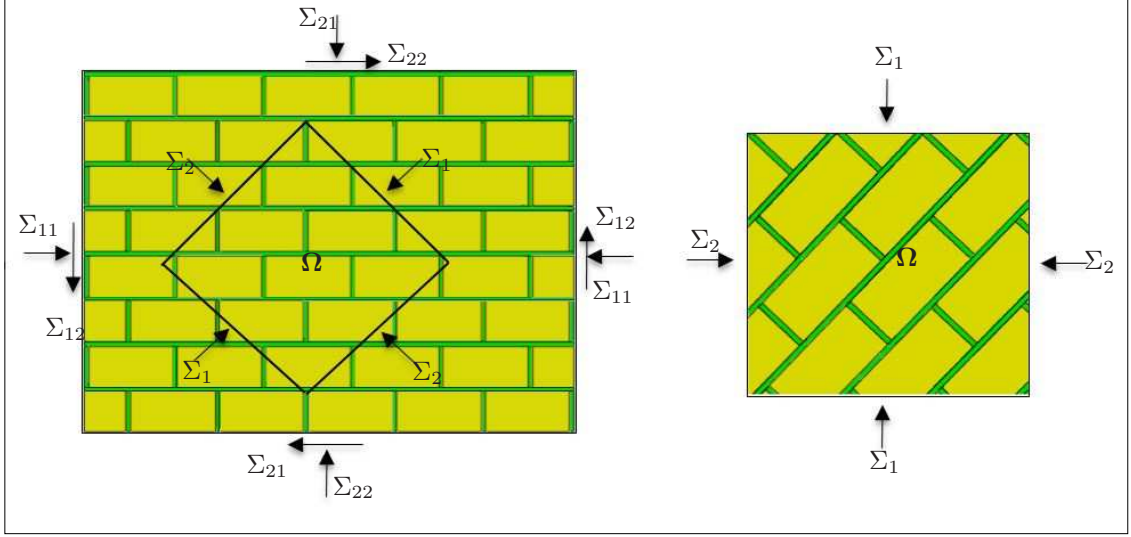
Figure 3.2: Half brick thick masonry wall subjected to macroscopically homogeneous stress state $\boldsymbol{\Sigma}$.

Where E is a symmetric second-order tensor for the strain; δ_{ij} is the Kronecker delta; u_i^p is a periodic displacement field and x_1, x_2, x_3 are the spatial parameters. In particular, the anti-symmetric part of E corresponds to a rigid rotation of the cell. Only the symmetric part of E is considered (rigid displacements are disregarded) with the intuitive definition of the average of a quantity on the cell. The average of strain can be written as

$$\bar{\epsilon}_{ij} = \frac{1}{|\hat{\Omega}|} \int \epsilon_{ij}(u) \, d\hat{\Omega} \tag{3.5}$$

Where $|\hat{\Omega}|$ stands for the volume of the basic cell. Similarly, for consistency of the equation- with the stress. The average of the stress on the cell should be given by

$$\bar{\sigma}_{ij} = \frac{1}{|\hat{\Omega}|} \int \sigma_{ij} \, d\hat{\Omega} \tag{3.6}$$

29

3.2.2 Homogenization

Let us consider the problem of a masonry specimen subjected to a macroscopically homogeneous stress state $\mathbf{\Sigma}$. The above conditions (conditions (i) and (ii) in the previous section) make it possible to study the problem within a single cell (unit cell) of the domain rather than on the whole domain. In order to find out $\boldsymbol{\sigma}$ and $\boldsymbol{u}$ everywhere in a cell, equilibrium conditions and constitutive relationships must be added, so that the problem can be solved. The required equation can be written as

$$div\boldsymbol{\sigma} = 0 \;\; on \; \hat{\Omega} \; (No \; body \; force) \tag{3.7}$$

$$\boldsymbol{\sigma} = F(\boldsymbol{\epsilon}(u)) \; (complete \; constitutive \; law) \tag{3.8}$$

$$\boldsymbol{\sigma}.\boldsymbol{n} = 0 \;\; on \; \partial\hat{\Omega}_e \tag{3.9}$$

$$\boldsymbol{\sigma} \; periodic \; on \; \partial\hat{\Omega}_i \; (\boldsymbol{\sigma}.\boldsymbol{n} \; anti \; periodic \; on \; \partial\hat{\Omega}_i) \tag{3.10}$$

$$\boldsymbol{u} - \bar{\boldsymbol{\epsilon}}.\boldsymbol{x} \; periodic \; on \; \partial\hat{\Omega}_i \tag{3.11}$$

$$\bar{\boldsymbol{\sigma}} = \mathbf{\Sigma} \;\; where \; \mathbf{\Sigma} \; is \; given, \; for \; stress \; contralled \; laoding \tag{3.12}$$

Where the constitutive law $F(\boldsymbol{\epsilon}(u))$ is a periodic function of the spatial variable x. Since it describes the behaviour of the different materials in the composite cell. A problem similar to Equation 3.12 is obtained when replacing the stress controlled loading by a strain controlled loading

$$\bar{\boldsymbol{\epsilon}} = \boldsymbol{E} \;\; where \; \boldsymbol{E} \; is \; given, \; for \; displacement \; contralled \; laoding \tag{3.13}$$

In both cases, the resolution of Equations 3.12 and 3.13 is sometimes termed localization because the local (microscopic) fields $\boldsymbol{\sigma}$ and $\boldsymbol{\epsilon}$ are determined from the global (macroscopic) quantity $\mathbf{\Sigma}$ or $\boldsymbol{E}$. The average procedure can be written in the more rigorous form as

$$\overline{\boldsymbol{\sigma} : \boldsymbol{\epsilon}(u)} = \bar{\boldsymbol{\sigma}} : \bar{\boldsymbol{\epsilon}}(u) = \mathbf{\Sigma} : \boldsymbol{E} \tag{3.14}$$

Where $[^-]$ defines the average of the quantity over the unit cell. Ones we get $\boldsymbol{\sigma}$ and $\boldsymbol{\epsilon}$, then the missing macroscopic quantity $\mathbf{\Sigma}$ or $\boldsymbol{E}$ can be determine through the average relation (Equation 3.14). Homogenization theory can only be applied when the load are homogeneous in nature or the variation of the load from a unit cell to another is very small. In practice, this is satisfied if the size of the unit cell is very small as compared to the structure and thus two adjacent cells have almost the same position there for undergo almost the same loading.

If the both the constituent of the masonry wall are considered to be linear elastic and perfectly bonded then the relations can be written as

For stress controlled loading

$$div\boldsymbol{\sigma} = 0 \;\; on \; \hat{\Omega} \; (No \; body \; force) \tag{3.15}$$

$$\epsilon(u) = \boldsymbol{S} : \boldsymbol{\sigma} \tag{3.16}$$

$$\boldsymbol{\sigma}.\boldsymbol{n} = 0 \quad on \ \partial\hat{\Omega}_e \tag{3.17}$$

$$\boldsymbol{\sigma} \ periodic \ on \ \partial\hat{\Omega}_i \ (\boldsymbol{\sigma}.\boldsymbol{n} \ anti \ periodic \ on \ \partial\hat{\Omega}_i) \tag{3.18}$$

$$\boldsymbol{u} - \boldsymbol{S} : \boldsymbol{\sigma}.\boldsymbol{x} \ periodic \ on \ \partial\hat{\Omega}_i \tag{3.19}$$

For displacement controlled loading

$$div\boldsymbol{\sigma} = 0 \quad on \ \hat{\Omega} \ (No \ body \ force) \tag{3.20}$$

$$\boldsymbol{\sigma} = \boldsymbol{C} : \epsilon(u) \tag{3.21}$$

$$\boldsymbol{\sigma}.\boldsymbol{n} = 0 \quad on \ \partial\hat{\Omega}_e \tag{3.22}$$

$$\boldsymbol{\sigma} \ periodic \ on \ \partial\hat{\Omega}_i \ (\boldsymbol{\sigma}.\boldsymbol{n} \ anti \ periodic \ on \ \partial\hat{\Omega}_i) \tag{3.23}$$

$$\boldsymbol{u} - \boldsymbol{E}.\boldsymbol{x} \ periodic \ on \ \partial\hat{\Omega}_i \tag{3.24}$$

Where S fourth order compliance tensor and C fourth order stiffness tensor.

3.3 Finite element Analysis for determining the homogenizes properties

To illustrate the aforementioned method of homogenization, the two unit cell of masonry wall are considered, to determine anisotropic characteristics of the masonry. As close form solution is not possible thus, the homogenization is done through the finite element analyses using commercial software package. In particular, the two basic unit cell are taken from a single leaf masonry wall in running bond, as shown in the Figure 3.3. The assigned dimensions to both the unit cell is such that volume fraction of the mortar and brick remains same. Brick and mortar are assumed to be isotropic: the Young′s moduli and Poisson′s ratios are $2X10^5 \ MPa$ and 0.15 for the brick, $2X10^4 \ MPa$ and 0.15 for the mortar respectively. The brick dimensions are 210 X 50 X 100 mm^3. Head and bed mortar joints is 10 mm thick.

In the present work, the study of elastic response of the model is done, for a generic loading condition as linear combination of the elastic responses for six elementary loading conditions. Both stress-prescribed and displacement-prescribed analyses have been carried out in the present work. The finite element model which has been used in numerical analysis is given in Figure 3.4. 8 nodded linear brick element with reduced integration is used for the simulation. The structured mesh was
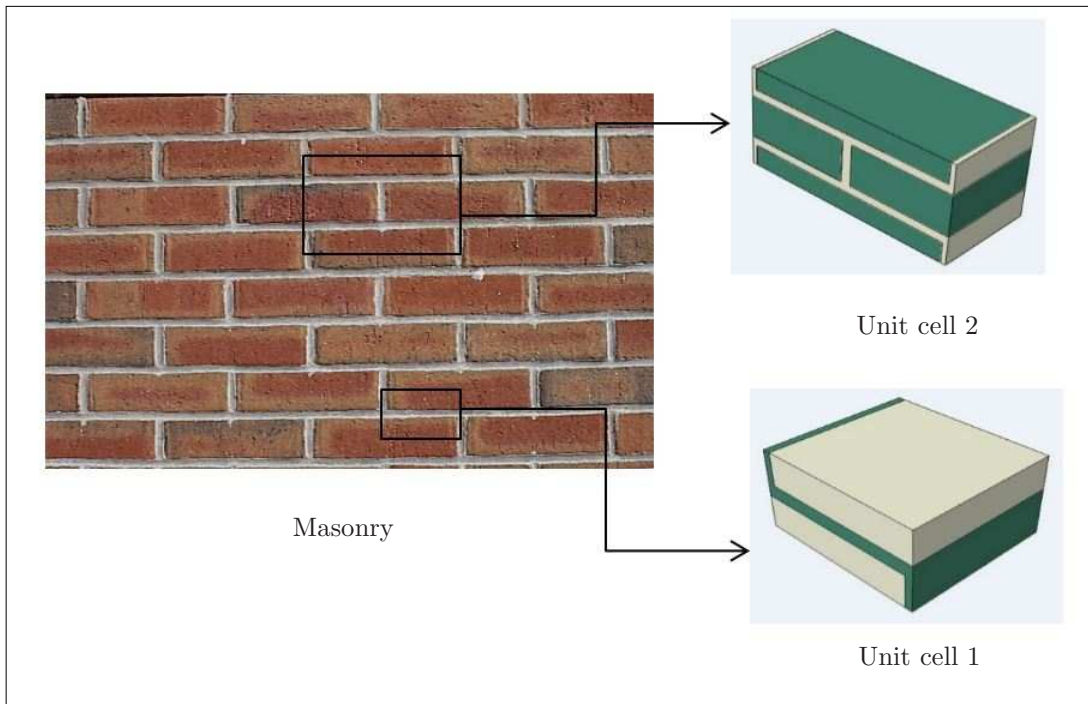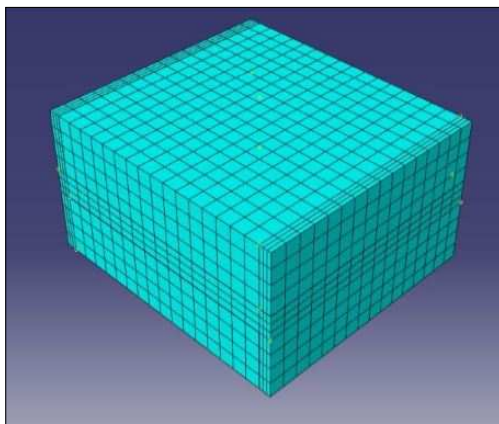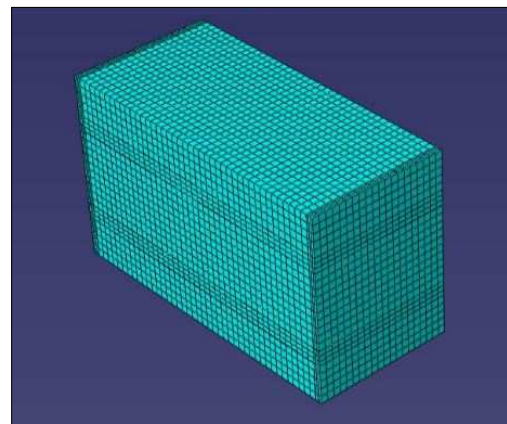
Figure 3.3: Chosen micro mechanical model.

obtained by taking into account a uniform element size of 0.5 cm. Thus the unit *cell* 1 and unit *cell* 2 have 5280 and 21120 elements respectively.

(a) Unit cell 1

(b) Unit cell 2

Figure 3.4: Finite element model

3.3.1 Stress prescribed analysis

In the stress-prescribed analysis, the overall compliance tensor is to be obtained by means of six numerical analysis i.e. XX-compression, YY-compression, ZZ-compression, XY-shear, XZ-shear, and YZ-shear. The boundary conditions for all the six numerical analysis are applied as per the Section 3.2.2 and are listed in Table 3.1. An anisotropic mechanical behaviour is considered, thus stress strain relationship can be written in the following form

$$
\left\{ \begin{array}{c} \bar{\epsilon}_1 \\ \bar{\epsilon}_2 \\ \bar{\epsilon}_3 \\ \bar{\epsilon}_4 \\ \bar{\epsilon}_5 \\ \bar{\epsilon}_6 \end{array} \right\} = \left[\begin{array}{cccccc} \bar{S}_{11} & \bar{S}_{12} & \bar{S}_{13} & \bar{S}_{14} & \bar{S}_{15} & \bar{S}_{16} \\ \bar{S}_{21} & \bar{S}_{22} & \bar{S}_{23} & \bar{S}_{24} & \bar{S}_{25} & \bar{S}_{26} \\ \bar{S}_{31} & \bar{S}_{32} & \bar{S}_{33} & \bar{S}_{34} & \bar{S}_{35} & \bar{S}_{36} \\ \bar{S}_{41} & \bar{S}_{42} & \bar{S}_{43} & \bar{S}_{44} & \bar{S}_{45} & \bar{S}_{46} \\ \bar{S}_{51} & \bar{S}_{52} & \bar{S}_{53} & \bar{S}_{54} & \bar{S}_{55} & \bar{S}_{56} \\ \bar{S}_{61} & \bar{S}_{62} & \bar{S}_{63} & \bar{S}_{64} & \bar{S}_{65} & \bar{S}_{66} \end{array} \right] \left\{ \begin{array}{c} \bar{\sigma}_1 \\ \bar{\sigma}_2 \\ \bar{\sigma}_3 \\ \bar{\sigma}_4 \\ \bar{\sigma}_5 \\ \bar{\sigma}_6 \end{array} \right\} \tag{3.25}
$$

Where the superscript $[^-]$ means that the above written quantities refer to the average values within the considered unit cell.

Compliance tensor is obtain by applying the six loading conditions one at a time, only a single column of the compliance tensor is obtain by applying one loading condition out of the six. By applying the average theorem to the unit cell and using the Equations 3.5-3.6, the following relation are obtained for the compliance tensor and the average stress value in the unit cell

$$
\bar{S}_{ij} = \frac{\bar{\epsilon}_i}{\bar{\sigma}_j} \tag{3.26}
$$

$$
\bar{\sigma}_j = \frac{1}{|\hat{\Omega}|} \int \sigma_j \, d\hat{\Omega} = \mathbf{\Sigma} \tag{3.27}
$$

Where i, j =1, 2, 3, 4, 5, 6; and $|\hat{\Omega}|$ stands for the volume of the unit cell and is the generic stress-prescribed component. The average value of strain within the unit cell is obtained as

$$
\bar{\epsilon}_i = \sum \frac{\epsilon_i^{(e)}}{n} \tag{3.28}
$$

Where n = number of elements in the uniformly discretized unit cell; $\epsilon_i^{(e)}$ = the average value of ith strain component for generic element. The average value of stress within the unit cell is obtained as

$$
\bar{\sigma}_j = \sum \frac{\sigma_j^{(e)}}{n} \tag{3.29}
$$

Where $\sigma_j^{(e)}$ = the average value of jth strain component for generic element. Hence, all six stress states are applied one by one to both the unit cell and the single columns of compliance tensor is obtained by using the Equation 3.26 and the corresponding coefficient of compliance tensor are given below

33

Table 3.1: Boundary conditions - stress prescribed

	XX-direction		YY-direction		ZZ-direction	
	Side face (Left)	Side face (Right)	Top Face	Bottom face	Front faces	Back faces
Normal Stress in XX-direction	Pressure = constant	Pressure = -constant	All d.o.f. free	All d.o.f. free	All d.o.f. free	All d.o.f. free
Normal Stress in YY-direction	All d.o.f. free	All d.o.f. free	Pressure = constant	Pressure = -constant	All d.o.f. free	All d.o.f. free
Normal Stress in ZZ-direction	All d.o.f. free	All d.o.f. free	All d.o.f. free	All d.o.f. free	Pressure = constant	Pressure = -constant
Shear Stress in XY-Plane	Z-SYMM	Z-SYMM	Surface traction = constant	Surface traction = -constant	Z-SYMM	Z-SYMM
Shear Stress in XY-Plane	Surface traction = constant	Surface traction = -constant	Y-SYMM	Y-SYMM	Y-SYMM	Y-SYMM
Shear Stress in XY-Plane	X-SYMM	X-SYMM	X-SYMM	X-SYMM	Surface traction = constant	Surface traction = -constant

∗ Unit cell 1

$$\bar{S}_{ij} = 10^{-6} \begin{bmatrix} 8.37 & -1.17 & -0.99 & 0 & 0 & 0 \\ -1.17 & 13.01 & -1.08 & 0 & 0 & 0 \\ -0.99 & -1.08 & 7.16 & 0 & 0 & 0 \\ 0 & 0 & 0 & 15.88 & 0 & 0 \\ 0 & 0 & 0 & 0 & 8.17 & 0 \\ 0 & 0 & 0 & 0 & 0 & 15.9 \end{bmatrix} \tag{3.30}$$

∗ Unit cell 2

$$\bar{S}_{ij} = 10^{-6} \begin{bmatrix} 7.97 & -1.11 & -0.96 & 0 & 0 & 0 \\ -1.11 & 12.76 & -1.06 & 0 & 0 & 0 \\ -0.96 & -1.06 & 7.11 & 0 & 0 & 0 \\ 0 & 0 & 0 & 15.82 & 0 & 0 \\ 0 & 0 & 0 & 0 & 8.65 & 0 \\ 0 & 0 & 0 & 0 & 0 & 14.82 \end{bmatrix} \tag{3.31}$$

3.3.2 Displacement prescribed analysis

In the displacement-prescribed analysis, the aim is to find out stiffness tensor by means of six numerical analysis i.e. XX-compression, YY-compression, ZZ-compression, XY-shear, XZ-shear, and YZ-shear. The boundary conditions for the six numerical analysis are applied as per the Section 3.2.2 and are listed in Table 3.2. An anisotropic mechanical behaviour is considered, thus stress strain relationship can be written in the following form

$$\begin{Bmatrix} \bar{\sigma}_1 \\ \bar{\sigma}_2 \\ \bar{\sigma}_3 \\ \bar{\sigma}_4 \\ \bar{\sigma}_5 \\ \bar{\sigma}_6 \end{Bmatrix} = \begin{bmatrix} \bar{C}_{11} & \bar{C}_{12} & \bar{C}_{13} & \bar{C}_{14} & \bar{C}_{15} & \bar{C}_{16} \\ \bar{C}_{21} & \bar{C}_{22} & \bar{C}_{23} & \bar{C}_{24} & \bar{C}_{25} & \bar{C}_{26} \\ \bar{C}_{31} & \bar{C}_{32} & \bar{C}_{33} & \bar{C}_{34} & \bar{C}_{35} & \bar{C}_{36} \\ \bar{C}_{41} & \bar{C}_{42} & \bar{C}_{43} & \bar{C}_{44} & \bar{C}_{45} & \bar{C}_{46} \\ \bar{C}_{51} & \bar{C}_{52} & \bar{C}_{53} & \bar{C}_{54} & \bar{C}_{55} & \bar{C}_{56} \\ \bar{C}_{61} & \bar{C}_{62} & \bar{C}_{63} & \bar{C}_{64} & \bar{C}_{65} & \bar{C}_{66} \end{bmatrix} \begin{Bmatrix} \bar{\epsilon}_1 \\ \bar{\epsilon}_2 \\ \bar{\epsilon}_3 \\ \bar{\epsilon}_4 \\ \bar{\epsilon}_5 \\ \bar{\epsilon}_6 \end{Bmatrix} \tag{3.32}$$

Where the superscript $[^-]$ means that the above written quantities refer to the average values within the considered unit cell.

Stiffness tensor is obtain by applying the six loading conditions one at a time, only a single column of the stiffness tensor is obtain by applying one loading condition out of the six. By applying the average theorem to the unit cell and using the Equations 3.5-3.6, the following relation are obtained for the average strain value in the unit cell

$$\bar{\epsilon}_i = \frac{1}{|\hat{\Omega}|} \int \epsilon_i(u) \, d\hat{\Omega} = \boldsymbol{E} \tag{3.33}$$

Table 3.2: Boundary conditions - displacement prescribed

	XX-direction		YY-direction		ZZ-direction	
	Side face (Left)	Side face (Right)	Top Face	Bottom face	Front faces	Back faces
Normal Displacement in XX-direction	X-SYMM	Displacement = -constant	Y-SYMM	All d.o.f. free	All d.o.f. free	All d.o.f. free
Normal Displacement in YY-direction	X-SYMM	X-SYMM	Y-SYMM	Displacement = -constant	All d.o.f. free	All d.o.f. free
Normal Displacement in ZZ-direction	X-SYMM	X-SYMM	Y-SYMM	Y-SYMM	All d.o.f. free	Displacement = -constant
Shear Displacement in XY-Plane	Z-SYMM	Z-SYMM	Displacement = constant	Displacement = -constant	Z-SYMM	Z-SYMM
Shear Displacement in XY-Plane	Displacement = constant	Displacement = -constant	Y-SYMM	Y-SYMM	Y-SYMM	Y-SYMM
Shear Displacement in XY-Plane	X-SYMM	X-SYMM	X-SYMM	X-SYMM	Displacement = constant	Displacement = -constant

Where i, j =1, 2, 3, 4, 5, 6; and $|\hat{\Omega}|$ stands for the volume of the unit cell and $\boldsymbol{E}$ is the generic strain component, such that $\bar{\epsilon}_i.\boldsymbol{x} = u_i^0$, Where u_i^0 is a prescribed displacement on the boundary of the unit cell. The average theorem yields the following relation to obtain the stiffness tensor

$$\bar{C}_{ij} = \frac{\bar{\sigma}_j}{\bar{\epsilon}_i} \tag{3.34}$$

Where i, j =1, 2, 3, 4, 5, 6. The average value of stress within the unit cell is obtained as

$$\bar{\sigma}_i = \sum \frac{\sigma_i^{(e)}}{n} \tag{3.35}$$

Where n = number of elements in the uniformly discretized unit cell; $\sigma_i^{(e)}$ = the average value of ith strain component for generic element. The average value of stress within the unit cell is obtained as

$$\bar{\epsilon}_j = \sum \frac{\epsilon_j^{(e)}}{n} \tag{3.36}$$

Where $\epsilon_j^{(e)}$ = the average value of jth strain component for generic element. Hence, all six stress states are applied one by one to both the unit cell and the single columns of stiffness tensor is obtained by using the Equation 3.34 and the corresponding coefficient of stiffness tensor are given below

* Unit cell 1

$$\bar{C}_{ij} = 10^6 \begin{bmatrix} 0.14 & 0.01 & 0.02 & 0 & 0 & 0 \\ 0.01 & 0.08 & 0.01 & 0 & 0 & 0 \\ 0.02 & 0.01 & 0.17 & 0 & 0 & 0 \\ 0 & 0 & 0 & 0.07 & 0 & 0 \\ 0 & 0 & 0 & 0 & 0.14 & 0 \\ 0 & 0 & 0 & 0 & 0 & 0.07 \end{bmatrix} \tag{3.37}$$
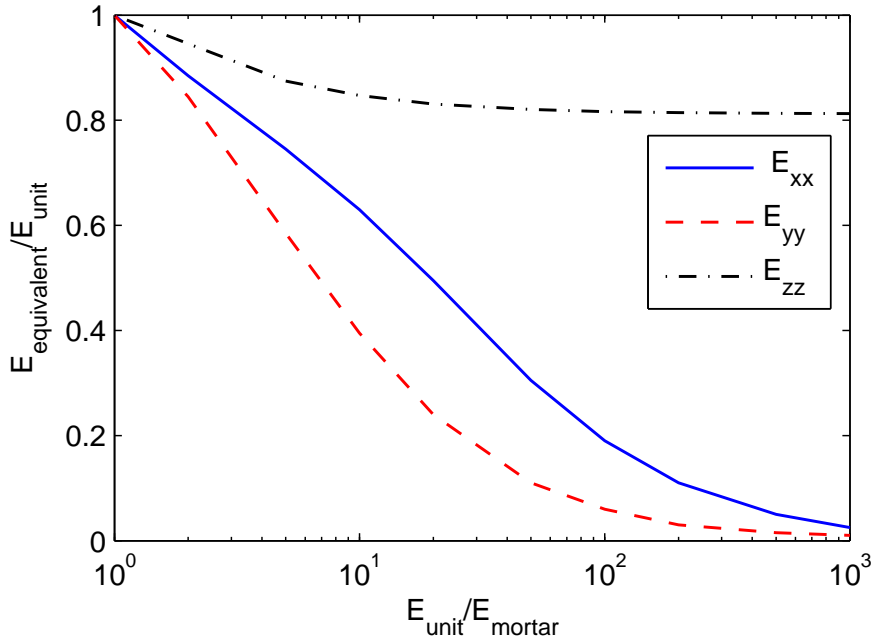
* Unit cell 2

$$\bar{C}_{ij} = 10^6 \begin{bmatrix} 0.14 & 0.01 & 0.02 & 0 & 0 & 0 \\ 0.01 & 0.08 & 0.01 & 0 & 0 & 0 \\ 0.02 & 0.01 & 0.17 & 0 & 0 & 0 \\ 0 & 0 & 0 & 0.07 & 0 & 0 \\ 0 & 0 & 0 & 0 & 0.13 & 0 \\ 0 & 0 & 0 & 0 & 0 & 0.07 \end{bmatrix} \tag{3.38}$$

3.4 Result

The different stiffness ratios allows us to assess the performance of the model for inelastic behaviour. In fact, non-linear behaviour is associated with (tangent) stiffness degradation and homogenization of non-linear processes will result in large stiffness differences between the components. In the limit, the ratio between the stiffness of the different components is zero or infinity. The material properties of the unit are kept constant, whereas the properties of the mortar are varied. In particular, for the unit, the Young's modulus E_b is 20 GPa and the Poisson's ratio is 0.15. For the mortar, the Young's modulus is varied to yield a ratio E_b/E_m ranging from 1 to 1000. In this section, a graphs has been plot for different stiffness ratios between mortar and unit, to study the effects of mortar moduli on the homogenized equivalent material properties of the unit cells see Figure 3.5-3.7 for stress prescribed analysis, and Figure 3.8-3.9 for displacement prescribed analysis.

The two different basic cells of same masonry having the same volume of its constituent has been to analysis the effect of basic cell. One can fairly concludes from the previous section, by comparing the stiffness and compliances matrices of two basic cells that the values are all most similar. Moreover, the plot for stress and displacement prescribed analysis are also same. In detail, the equivalent material property i.e. Young's modulus, shear modulus and Poisson's ratio decreases with increase in the ratio of Young's modules of unit and mortar (i.e. with decrease in Young's modules of mortar).


(a) Unit cell 1: Young's modulus

First of all, equivalent Young's modules E_{xx}[1], E_{yy} of masonry decreases with increase in the ratio of young's modules of unit and mortar up to its constant residual, as both unit and mortar interdependently contributes to equivalent Young's modules. Whereas, the equivalent Young's modules E_{zz} (for out of plane direction) reduces rapidly till the stiffness ratio of 10, after that E_{zz} became almost
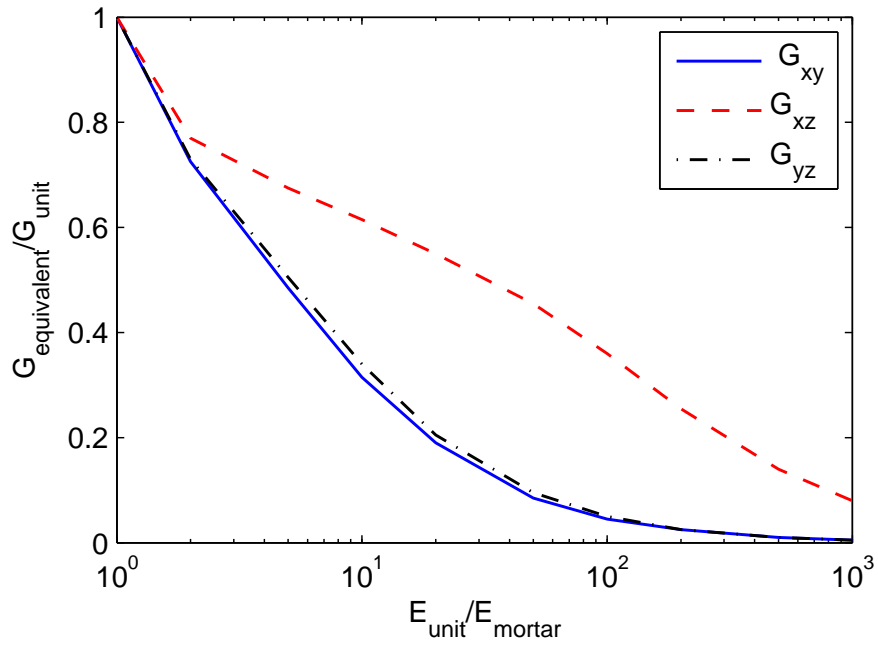
---

[1] $E_{ii} = C_{ii}$
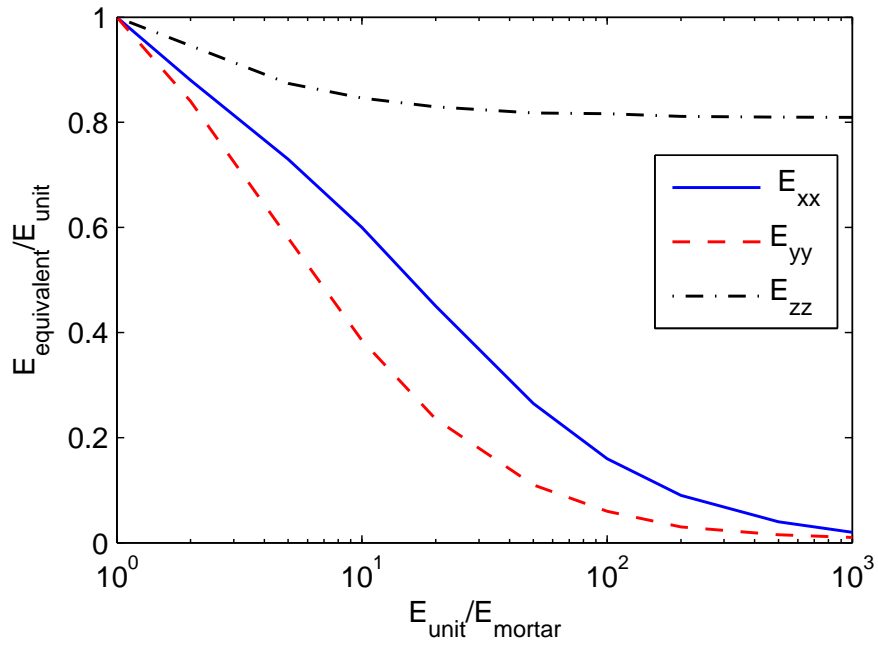
(b) Unit cell 2: Young's modulus

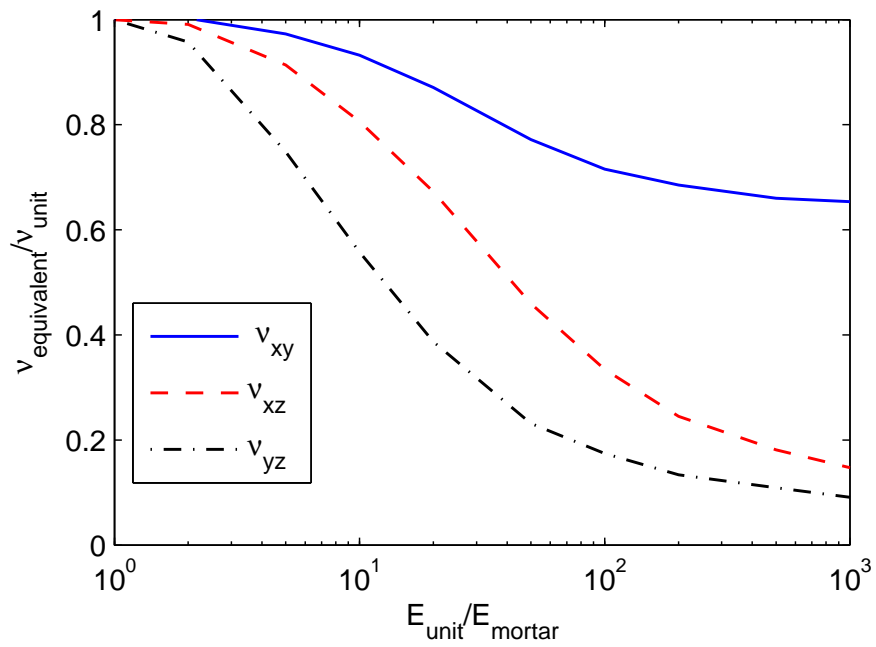Figure 3.5: Variation of stress prescribed homogenized value for different stiffness ratio.
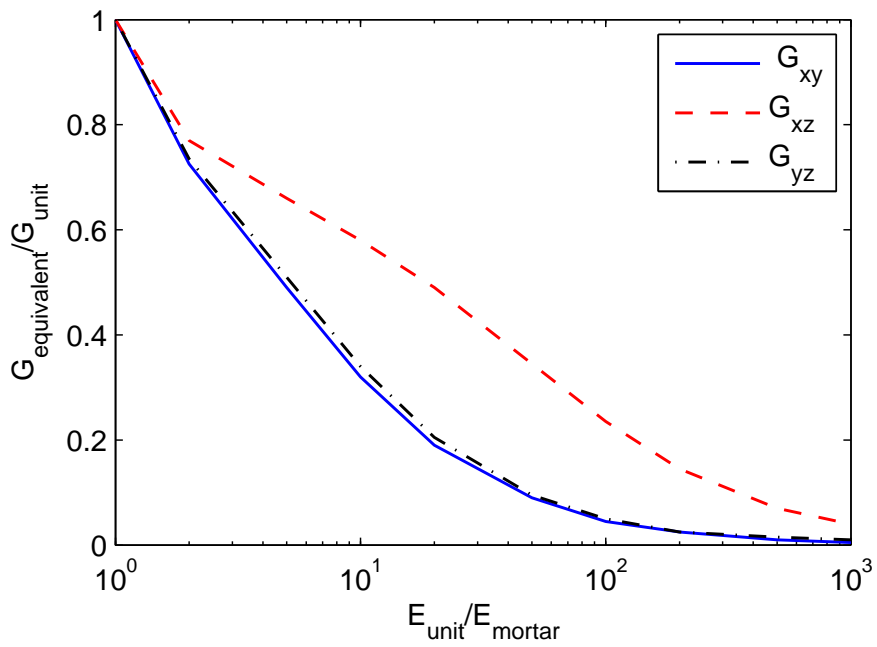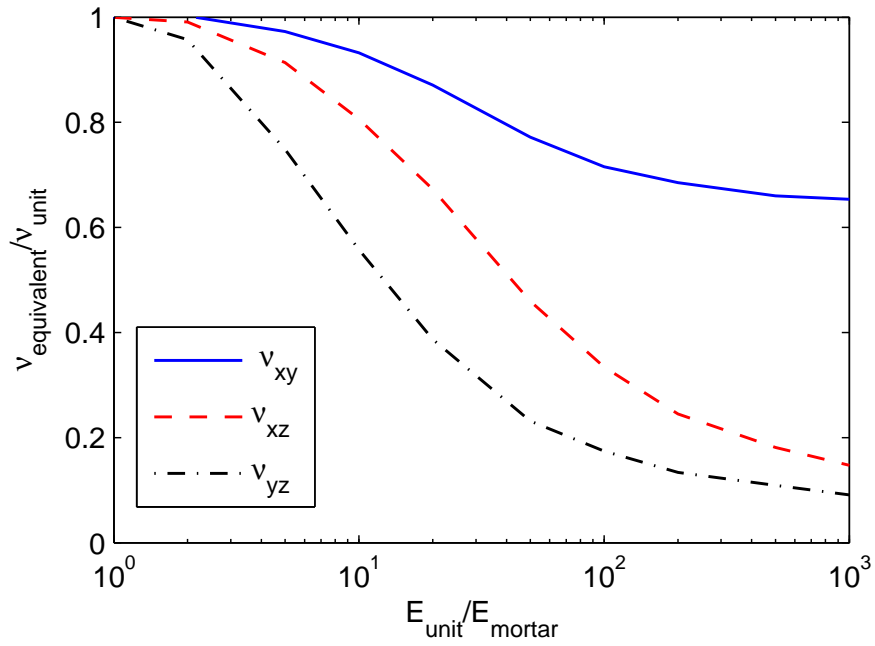

(a) Unit cell 1: Shear modulus

(b) Unit cell 2: Shear modulus

Figure 3.6: Variation of stress prescribed homogenized value for different stiffness ratio.
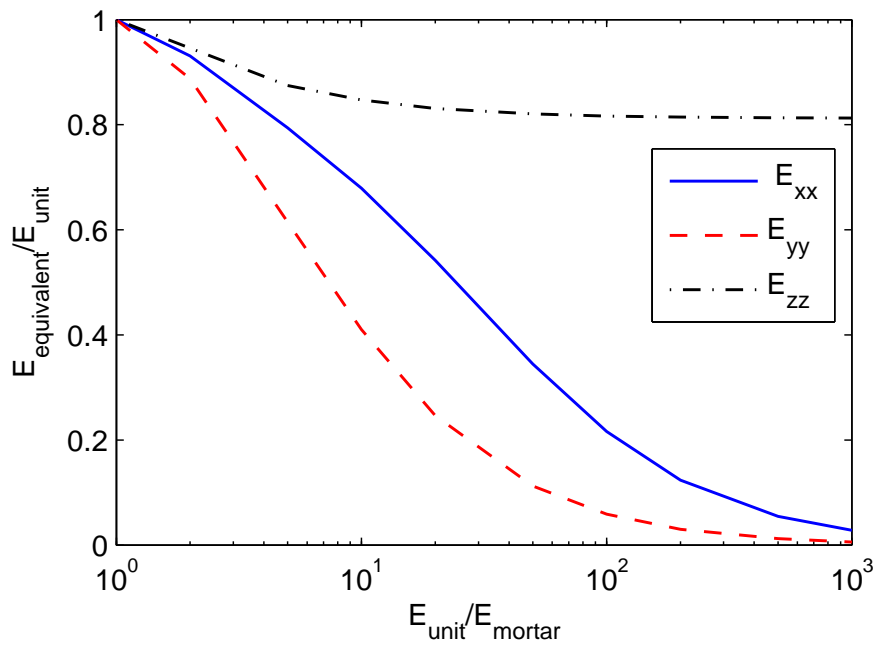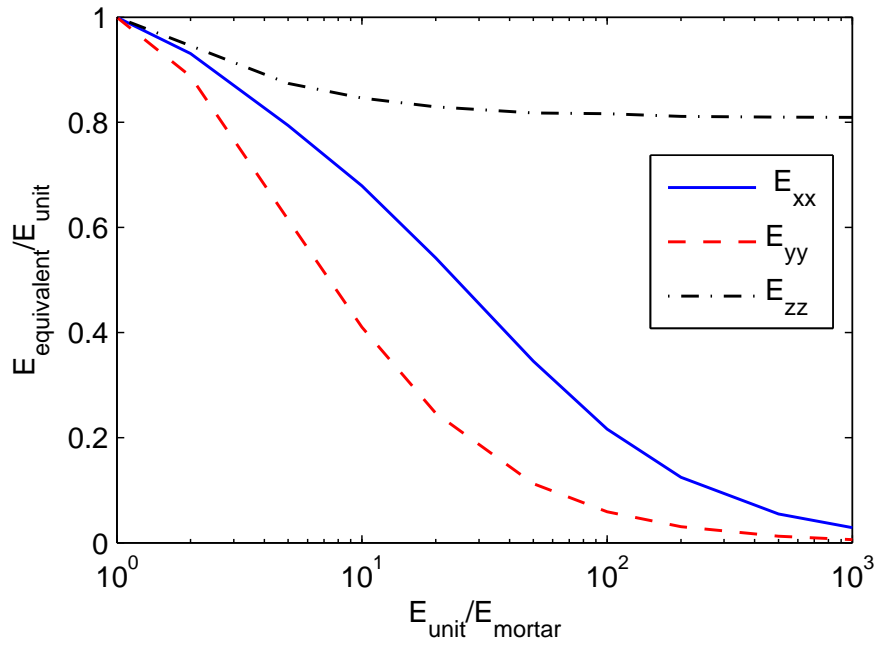

(a) Unit cell 1: Poisson's ratio

(b) Unit cell 2: Poisson's ratio

Figure 3.7: Variation of stress prescribed homogenized value for different stiffness ratio.
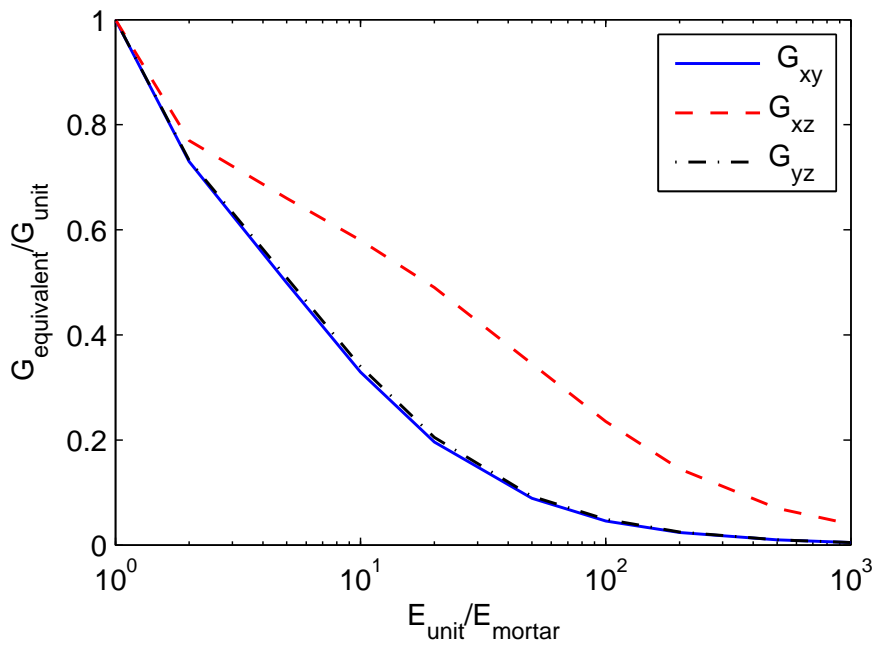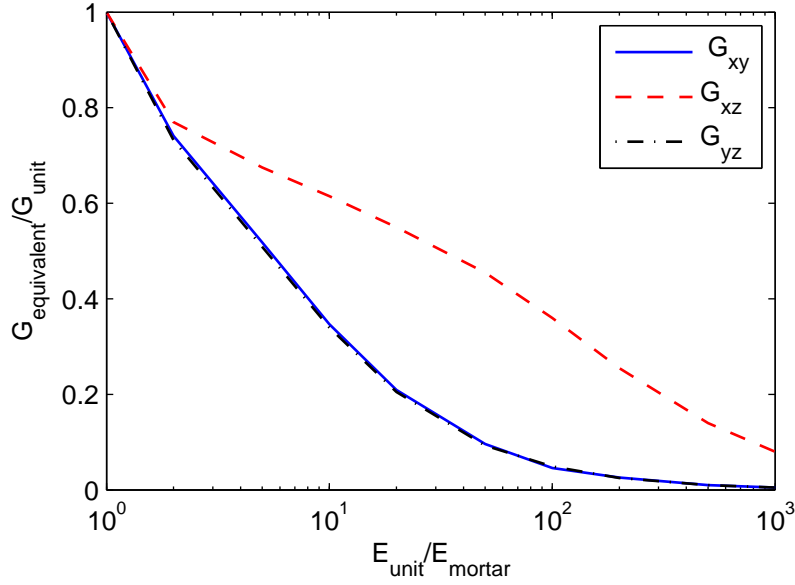

(a) Unit cell 1: Young's modulus

(b) Unit cell 2: Young's modulus

Figure 3.8: Variation of displacement prescribed homogenized value for different stiffness ratio.

(a) Unit cell 1: Shear modulus

(b) Unit cell 2: Shear modulus

Figure 3.9: Variation of displacement prescribed homogenized value for different stiffness ratio.

constant as in out of plane unit and mortar independently contribute to equivalent Young's modules and after the stiffness ratio of 10 the contribution of contribution of mortar become negligibly small. Second, the shear modulus of the masonry also decreases with increase in the ratio of shear moduli, but the rate of shear module $G_{xy}{}^2$ and G_{xz} is almost constant till it reaches its constant residual value whereas softening rate of shear module G_{yz} deceases when mortar strength get exhausted and the softening rate of equivalent shear module G_{yz} is govern by softening of shear module unit only. Finally, the similar behaviour can be observed for the Poisson's ratio that equivalent passion ratio also decrease with increase in the ratio of moduli of brick and mortar.

3.5   Conclusions

The homogenization theory for periodic media has been applied in a rigorous way for deriving the anisotropic elastic characteristics of masonry that is in one step. In particular, the real geometry has been taken into account (bond pattern and finite thickness of the wall). The theory has been numerically applied to the two representative volume element having the same ratio of mortar and unit for the same masonry wall (running bond) and their equivalent property has been found. As the matter of fact, numerical application showed that the masonry behaviour is anisotropic in nature, and that varying the basic cell for the same masonry will not effect the result. Moreover, a care full examination for different stiffness ratio between mortar and unit has been done to assess the performance for inelastic behaviour.

The average stress-strain relationship derived from the homogenization can be used in the damage or plasticity based macro-modelling of the masonry.

$^2G_{ij} = C_{ij}$

Chapter 4

The Composite Interface Model

4.1   Introduction

Micro-models is best tool to understand the behaviour of masonry. This requires the consideration of the failure mechanisms of the masonry and its constituent. These failure mechanisms are lumped into a interface element, with the assumption that all the inelastic behaviour occurs in interface element. Which leads to robust type of modelling, capable to tracing complete load path. The interface element shows the failure mechanism as potential crack, slip and crushing. In this chapter, a Composite Interface Model is developed in the plasticity concepts and its implementation and numerical performance is assessed. The Composite Interface Model includes Coulomb fiction envelope for mode II failure, with tension cut for mode I failure and compression cap for compression failure. A single surface yield function is used for the model, to remove the singularity that occurs in the conner region in multi surface plasticity.

4.2   Overview

Many attempts were made to use interface element for micro modelling of the masonry. Aryan and Hegemier [60], Page [61] made early attempts to study the masonry failure using micro modelling. Stankowski *et al.* [62, 63] proposed a plasticity based constitutive model to describe the fracture and slip of the interface in cementitious materials, the model uses a curvilinear Mohr-Coulomb yield function with a tension cut-off and the yield function has a smooth transition between shear and tension region. They considered the tensile strength softening without changing shape of yield function (i.e. degradation of tensile strength is considered whereas cohesion and friction angle are considered to be unchanged). Lotfi *et al.* [13, 64] have developed an interface model that incorporates additional softening mechanisms i.e. the degradation of cohesion and friction angle and additional attention has been paid to include the dilatancy. The models presented here can simulate initiation and propagation of crack under combined normal and shear stresses in tension-shear and compression-shear region, but however failure to simulate masonry under high compression stress. Lourenço [12, 15, 65] introduced multi-surface interface model for analysis of masonry structures. The constitutive model is based on multi-surface plasticity, which can be illustrated by three yield function: a tension cut-off for mode-I failure, a Mohr-Coulomb failure envelope for mode-II failure

and a cap model for compressive failure. The model is capable of simulating masonry under tension-shear, compression-shear and even under high compression stress. Due to presence of three yield criteria, singularity problem arises at the non-smooth corner in transition zone from tension to shear and shear to compression.

Many other plasticity based constitutive model have also been proposed in recent years, Giambanco *et al.* [66] presented an interface model suitable to simulate the behaviour of mortar joint in the masonry, using the Mohr-Coulomb bilinear limit surface with tension-cut off. The model considers the softening response that occurs along with decohesion process in the presence of shear and tension. Oliveira and Lourenco [67, 68] extended the Lourenco and Rots model to damage formulation for simulating the cyclic behaviour of interface element. Dolatshahi *et al.* [18] used the Lourenco and Rots model and have shown that in a computational scheme, the use of rigid elements along with non-linear line interfaces leads to a reduced number of degrees-of-freedom, which consequently reduces the computational time.

4.3   Masonry failure mechanism

Many failure mechanism are possible, most prominent masonry failure mechanisms [12, 15, 19, 20, 69] are (a) cracking of unit in direct tension, (b) cracking of mortar joint, (c) bed or head joint failure at low value of normal stress, (d) diagonal tension cracking of the unit, (e) masonry crushing. The failure mechanism are shown in Figure 4.1. Where (a) is unit mechanism, (b) and (c) are the joint mechanism and (d) and (e) are the combine mechanism. An accurate masonry model must include all these failure mechanisms.
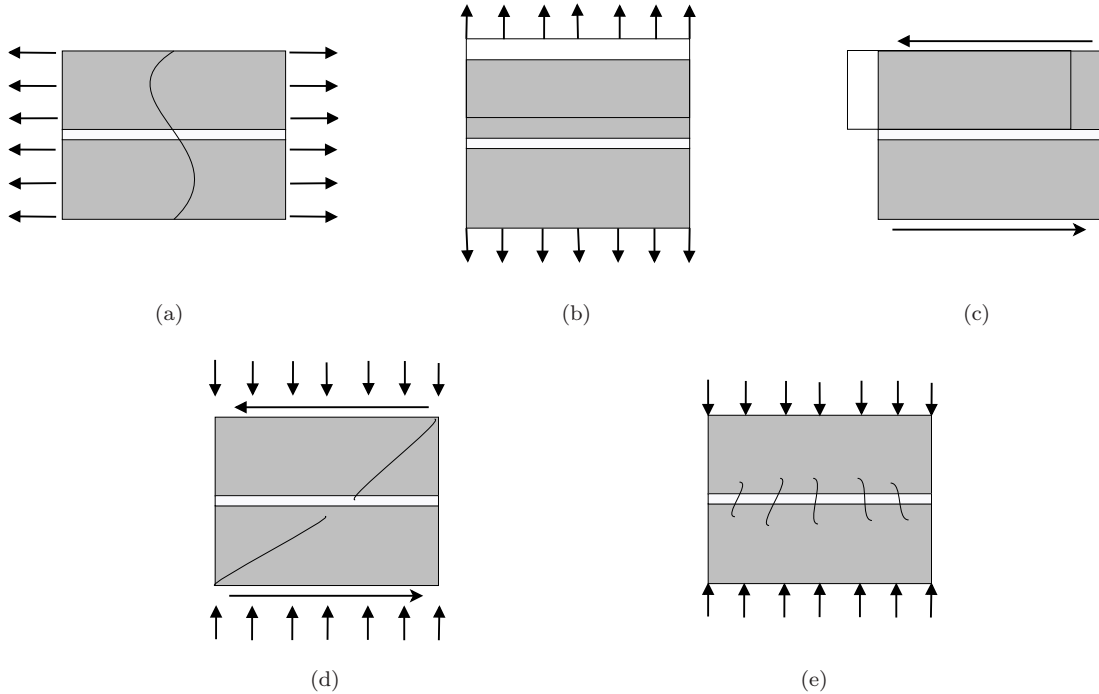

Figure 4.1: Prominent masonry failure mechanisms: (a) unit direct tensile cracking; (b) joint tensile cracking; (c) joint slipping; (d) unit diagonal tensile cracking; (e) masonry crushing.

4.4   The Composite Interface Model

The composite interface model is used to represent the mechanical behaviour of discontinuous inter-face element for joint interface in the masonry modelling, which includes potential crack, slip, and crushing planes. In the following section, a complete description of numerical implementation of a plasticity based composite interface model is explained.

4.4.1   Elastic behaviour

The interface elements allows the discontinuity in the displacement field and their behaviour is described by relation between traction force and relative displacement of the interface element. The generalised stress-strain relation can be written in standard form as

$$\boldsymbol{\sigma} = \boldsymbol{K}\boldsymbol{\epsilon} \tag{4.1}$$

In a 2D framework, $\boldsymbol{\sigma} = \{\sigma_{nn}, \sigma_{tt}\}^T$, $\boldsymbol{\epsilon} = \{\epsilon_{nn}, \epsilon_{tt}\}^T$ and $\boldsymbol{K} = diag\{k_{nn}, k_{tt}\}^T$ where nn and tt designate normal and tangential components. For simplifying the model, the effect of Poisson′s ratio is assumed to be negligible. The Poisson′s ratio of the brick is considerably lower than mortar, and most of the behaviour of the masonry is governed by joint mechanics, mortar mechanism and splitting of the brick, thus this assumption seems to be valid. Due to lager difference in the thickness of the mortar and unit, the units are assumed to be linear-elastic. The component of elastic stiffness matrix $\boldsymbol{K}$ can be written as

$$\frac{1}{k_{nn}} = \frac{1}{h_m}\left(\frac{1}{E_b} + \frac{1}{E_m}\right) \tag{4.2}$$

$$\frac{1}{k_{tt}} = \frac{1}{h_m}\left(\frac{1}{G_b} + \frac{1}{G_m}\right) \tag{4.3}$$

Where E_b, E_m, G_b and G_m are the elastic Young′s moduli and the elastic shear moduli for brick unit and mortar. h_m is the actual thickness of mortar joint.

4.4.2   Plastic behaviour

In the present study a rate independent composite interface model, defined by hyperbolic function (Equation 4.4) has been proposed (see Figure 4.2). The proposed model is a simple extension of the Mohr-Coulomb criteria with cut-off in tension and cap-off in compression, which result in the single surface yield criteria capable of representing pressure-dependent friction shear failure and cracking by cut-off in-tension and crushing by cap-off in compression under combined normal and tangential stresses. The model includes all the mechanisms of the masonry failure and also overcomes the problem of the singularity that occurs in multi-surfaces yield criteria.

$$F(\boldsymbol{\sigma}, \boldsymbol{q}) := -[(C - \sigma_{nn}\tan(\phi))]^2 f_c(\boldsymbol{\sigma}, \boldsymbol{q}) f_t(\boldsymbol{\sigma}, \boldsymbol{q}) + \sigma_{tt}^2 \tag{4.4}$$

$$f_c(\boldsymbol{\sigma}, \boldsymbol{q}) := \frac{2}{\pi}\arctan\left(\frac{\sigma_{nn} - \zeta}{\alpha_c}\right) \tag{4.5}$$

$$f_t(\boldsymbol{\sigma}, \boldsymbol{q}) := \frac{2}{\pi} \arctan\left(\frac{\xi - \sigma_{nn}}{\alpha_t}\right) \tag{4.6}$$
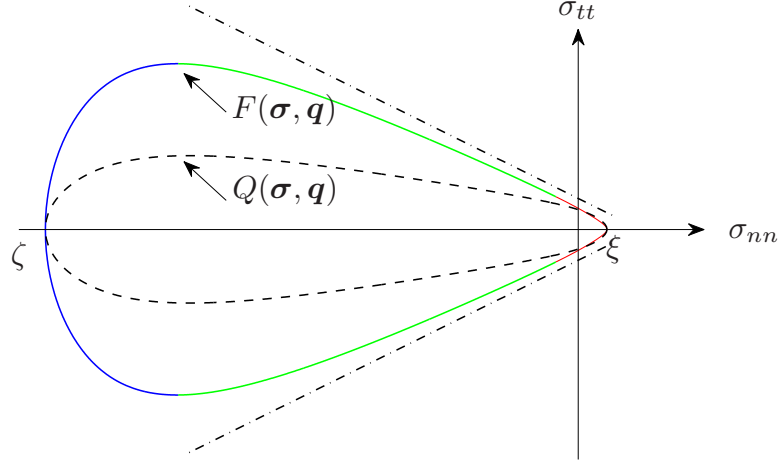

Figure 4.2: Trace of yield function $F(\boldsymbol{\sigma}, \boldsymbol{q})$ and potential function $Q(\boldsymbol{\sigma}, \boldsymbol{q})$; red, green, blue lines represents the tension-cut, shear and compression-cap region respectively.

Where the vector $\boldsymbol{q} = \boldsymbol{q}(C, C_q, \phi, \psi, \xi, \zeta)$ is a function of six internal hardening parameters, which implicate the apparent cohesion (C, C_Q), friction angle (ϕ), dilation angle (ψ), tensile strength (ξ) and compression strength (ζ). In the yield function, ξ denotes tension cut-off and ζ denotes compression cap. The function $f_c(\boldsymbol{\sigma}, \boldsymbol{q})$ and $f_t(\boldsymbol{\sigma}, \boldsymbol{q})$ are the compression cap and tension cut-off functions respectively. The function $f_c(\boldsymbol{\sigma}, \boldsymbol{q})$ has the zero value at the cap and the function $f_t(\boldsymbol{\sigma}, \boldsymbol{q})$ has zero value at tension-cut. For all other stress-states both the function have value approximately equal to one. The parameters α_c and α_t control the curvature of the compression cap and tension cut-off at transition region.

A non-associated formulation is used because friction and dilatency angles are considerably different [42, 70]. Therefore, the plastic potential is described in terms of another hyperbolic function with different values of apparent cohesion (C_Q) and frictional angle (dilation angle (ψ)), with same tensile (ξ) and compressive strength (ζ). The expression of potential function reads

$$Q(\boldsymbol{\sigma}, \boldsymbol{q}) := -[C_Q - \sigma_{nn} \tan(\psi)]^2 f_c(\boldsymbol{\sigma}, \boldsymbol{q}) f_t(\boldsymbol{\sigma}, \boldsymbol{q}) + \sigma_{tt}^2 \tag{4.7}$$

4.4.3 Evolution laws

Evolution laws for hardening or softening behaviour for the composite interface model is defined by the rate of plastic work per unit of volume. During plastic loading internal variables can be express as

$$\dot{\boldsymbol{W}}^p := \boldsymbol{\sigma}^T \boldsymbol{\epsilon}^p \tag{4.8}$$

Where $\dot{\boldsymbol{W}}^p$ is the rate of plastic work hardening per unit of volume. In the present study, evolution of yield surface in tension-shear and compression-shear region has been assumed such that during plastic loading in tension-shear region, tensile strength (ξ) decreases exponentially while friction angle (ϕ) remain unchanged, and in compression-shear region both friction and tensile strength both degrades exponentially. In addition, the compression strength changes when plastic loading path intersects with the compression cap. The above assumptions can be expressed by four internal variables i.e. $\dot{\boldsymbol{W}}^p := \dot{\boldsymbol{W}}^p(\dot{w}_1^p, \dot{w}_2^p, \dot{w}_3^p, \dot{w}_4^p)$ where $\dot{w}_1^p$ and $\dot{w}_2^p$ represent degradation in tensile strength, $\dot{w}_2^p$ and $\dot{w}_3^p$ govern the frictional strength degradation and $\dot{w}_4^p$ gives change in the compression strength.

$$\dot{w}_1^p := \langle \sigma_{nn} \rangle \dot{u}_{nn}^p \tag{4.9}$$

$$\dot{w}_2^p := (\sigma_{tt} - \sigma_{tt_{r1}} sign(\sigma_{tt})) \dot{u}_{tt}^p \tag{4.10}$$

$$\dot{w}_3^p := (\sigma_{tt_{r1}} - \sigma_{tt_{r2}}) sign(\sigma_{tt}) \dot{u}_{tt}^p \tag{4.11}$$

$$\dot{w}_4^p := \langle\langle \sigma_{nn} \rangle\rangle \dot{u}_{nn}^p \quad for \ \sigma_{nn} < \zeta_c \tag{4.12}$$

Where the symbol $\langle \rangle$ denotes for Macaulay bracket and $\langle x \rangle = (x + |x|)/2$ and $\langle\langle x \rangle\rangle = (x - |x|)/2$. ζ_c denotes the transient point from compression cap to Mohr-Coulomb friction envelope. $\sigma_{tt_{r1}}$ is the tangential strength when tensile strength is completely exhausted; $\sigma_{tt_{r2}}$ is minimum tangential strength for the final contracted yield surface. In tension-shear region, $\sigma_{tt_{r1}}$ and $\sigma_{tt_{r2}}$ are assumed to be zero and in compression-shear region they can be express as

$$\sigma_{tt_{r1}}^2 = -2C_r \tan\phi \ f_c f_t \tag{4.13}$$

$$\sigma_{tt_{r2}}^2 = -2C_r \tan\psi_r \ f_c f_t \tag{4.14}$$

In tension-shear region, during plastic loading the yield surface will contract until the tensile strength is exhausted and cohesion reaches a minimum value, see Figure 4.3(a), i.e. yield surface contracts from F_0 to F_1. While in compression-shear region, plastic loading reduces the tensile strength, cohesion as well as friction angle to its residual value (i.e. yield surface contracts to F_2). If the plastic loading path intersects the compression cap region, yield surface will evolve due to hardening in compression, see Figure 4.3(b), i.e. yield surface evolves from F_0 to F_1. After the compression-strength reaches its maximum value, there is a subsequent softening and compression strength reduces to minimum value due to contraction of yield surface i.e. yield surface contracts from F_1 to F_2.
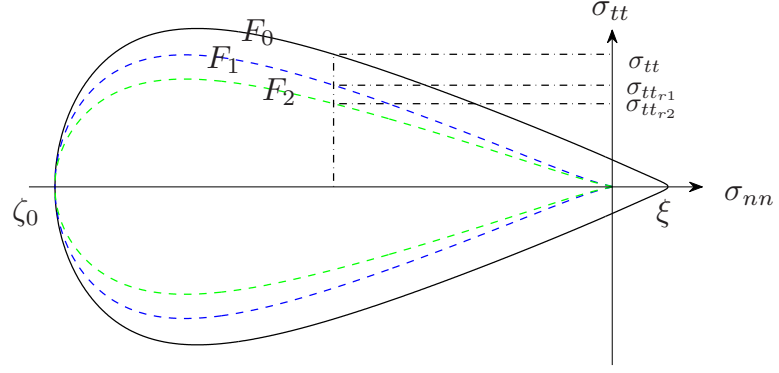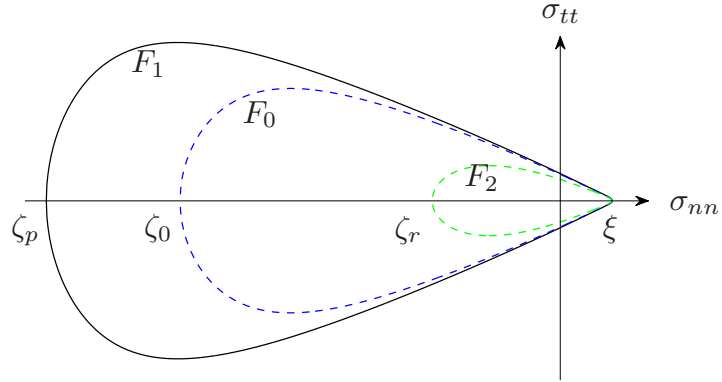
Figure 4.3: Evolution of yield surfaces (a) Tension and shear region; (b) Compression region.

The hardening parameter $\boldsymbol{q}$ can be related to the internal variables as follows

$$C := C_r + (C_0 - C_r) \exp^{-\beta_C \left(\dfrac{w_1^p}{G_f^I} + \dfrac{w_2^p}{G_f^{II}} \right)} \tag{4.15}$$

$$C_Q := C_{Q_r} + (C_{Q_0} - C_{Q_r}) \exp^{-\beta_{C_Q} \left(\dfrac{w_1^p}{G_f^I} + \dfrac{w_2^p}{G_f^{II}} \right)} \tag{4.16}$$

$$\phi := \phi_r + (\phi_0 - \phi_r) \exp^{-\beta_\phi w_3^p} \tag{4.17}$$

$$\psi := \psi_r + (\psi_0 - \psi_r) \exp^{-\beta_\psi w_3^p} \tag{4.18}$$

$$\xi := \xi_0 \exp^{-\beta_\xi \left(\dfrac{w_1^p}{G_f^I} + \dfrac{w_2^p}{G_f^{II}} \right)} \tag{4.19}$$

49

$$
\zeta = \begin{cases}
\zeta_0 + (\zeta_p - \zeta_0)\sqrt{\left(\dfrac{2w_4^p}{w_p}\right) - \left(\dfrac{w_4^p}{w_p}\right)^2} & \text{if} \quad w_4^p \le w_p \\[2ex]
\zeta_0 + (\zeta_p - \zeta_p)\left(\dfrac{w_4^p - w_p}{w_m - w_p}\right)^2 & \text{if} \quad w_p \le w_4^p \le w_m \\[2ex]
\zeta_r + (\zeta_m - \zeta_r)\exp^{\beta_\zeta \left(\dfrac{w_4^p - w_p}{\zeta_m - \zeta_r}\right)} & \text{if} \quad w_4^p > w_m
\end{cases}
\tag{4.20}
$$

Where G_f^I and G_f^{II} are the mode I and mode II fracture energy and β_i is a parameter that controls the softening of the internal variable. The subscript 0 stands for initial value and r for residual value whereas subscript p and m indicate intermediate values. The preceding hardening equation can be written in a compact form as follows

$$
\dot{\boldsymbol{W}}^p = \boldsymbol{H}\dot{\boldsymbol{\epsilon}}^p
\tag{4.21}
$$

4.4.4 Elastic-plastic tangent modulus

The total strain ϵ can be decomposed into sum of elastic strain and plastic strain i.e.

$$
\boldsymbol{\epsilon} = \boldsymbol{\epsilon}^e + \boldsymbol{\epsilon}^p
\tag{4.22}
$$

Where $\boldsymbol{\epsilon}^e$ and $\boldsymbol{\epsilon}^p$ are the elastic strain and plastic strain or irreversible strain respectively and the notion of irreversibility of plastic flow can be introduced by non-associated flow rule. It can be written in rate form as

$$
\dot{\boldsymbol{\epsilon}}^p = \dot{\lambda}\boldsymbol{m}
\tag{4.23}
$$

Where $\dot{\lambda}$ is the constant slip rate or plastic multiplier. The plastic multiplier can be found by checking the consistency condition (persistency condition) together with Kuhn-Tucker condition ($F \le 0, \dot{\lambda} \ge 0, \dot{\lambda}F = 0$). The consistency condition can be written as $\dot{\lambda}\dot{F} = 0$ for yield condition $\dot{\lambda} > 0$ and $\dot{F} = 0$ and we can be written it as

$$
\dot{F} = \frac{\partial F}{\partial \boldsymbol{\sigma}}\dot{\boldsymbol{\sigma}} + \frac{\partial F}{\partial \boldsymbol{q}}\dot{\boldsymbol{q}} = 0
\tag{4.24}
$$

$$
\dot{\lambda} = \frac{\boldsymbol{n}\boldsymbol{K}\boldsymbol{\epsilon}}{\boldsymbol{n}^T\boldsymbol{K}\boldsymbol{m} + \boldsymbol{p}^T\boldsymbol{\varpi}}
\tag{4.25}
$$

In which $\boldsymbol{m} := \partial Q/\partial \boldsymbol{\sigma}$, $\boldsymbol{n} := \partial F/\partial \boldsymbol{\sigma}$, $\boldsymbol{p} := \partial Q/\partial \lambda$, $\boldsymbol{\varpi} := (\partial \boldsymbol{q}/\partial \boldsymbol{W}^p)(\partial \boldsymbol{W}^p/\partial \boldsymbol{\epsilon}^p)(\partial \boldsymbol{\epsilon}^p/\partial \lambda) = (\partial \boldsymbol{q}/\partial \boldsymbol{W}^p)\boldsymbol{H}\boldsymbol{m}$. Now we can define hardening parameter in its rate form as $\boldsymbol{q} = \dot{\lambda}\boldsymbol{\varpi}$. Putting the plastic multiplier ($\dot{\lambda}$) in the rate form of stress-strain relationship to get elasto-plastic tangent modulus $\boldsymbol{K}^{ep}$, i.e.

$$
\dot{\boldsymbol{\sigma}} = \boldsymbol{K}(\dot{\boldsymbol{\epsilon}} - \dot{\lambda}\boldsymbol{m}) = \boldsymbol{K}^{ep}\dot{\boldsymbol{\epsilon}}
\tag{4.26}
$$

$$
\boldsymbol{K}^{ep} = \boldsymbol{K} - \frac{\boldsymbol{K}\boldsymbol{m} \otimes \boldsymbol{n}\boldsymbol{K}}{\boldsymbol{n}^T\boldsymbol{K}\boldsymbol{m} + \boldsymbol{p}^T\boldsymbol{\varpi}}
\tag{4.27}
$$

4.4.5 Algorithmic aspect of local and global solver

In the present section, the composite interface model is implemented into a finite element framework with elastic-plastic continuum elements, which gives rise to a set of non-linear algebraic-differential equations, and are to be solved. The Newton-Raphson scheme is used to solve non-linear system of equations, which leads to combined local and global approach. Local solver provides the new internal state variable for a given relative displacement, subsequently global solver provides the solution for the unbalanced force to accommodate stress distribution within the finite load increments. In this section, numerical strategy is presented at both local (Constitutive level) and global level (Structural level).

Elastic predictor-plastic correct strategy

The implicit backward Euler integration method is used to integrate the differential constitutive equations. The backward Euler method is a first order (i.e. local truncation error is $O(h^2)$ for a single step) method and is unconditionally stable. The integration procedure leads to a set of algebraic-incremental equations, which can be split in to elastic predictor, followed by plastic corrector if and only if the trial stress-state violates the current trail yield condition.

The time discretization of an interval of interest as $[0,\ T] = \bigcup_{n=1}^{N}[t_n, t_{n+1}]$. The relevant problem can be seen with in time interval $[t_n, t_{n+1}]$. It is assumed that the stress-state $(\boldsymbol{\sigma}_n, \boldsymbol{q}_n)$ at current time $t = t_n$ should satisfy the equilibrium conditions and be admissible. For prescribed increment in strain $\dot{\boldsymbol{\epsilon}}$, at the next time step $t_{n+1} = t_n + \Delta t$ the strain is given by $\boldsymbol{\epsilon}_{n+1} = \boldsymbol{\epsilon}_n + \Delta\boldsymbol{\epsilon}$, and this can be split into two part i.e. $\Delta\boldsymbol{\epsilon} = \Delta\boldsymbol{\epsilon}^e + \Delta\boldsymbol{\epsilon}^p$. According to the elastic predictor-plastic correct strategy, the stress and internal variables can be written in their incremental form as

$$\boldsymbol{\sigma}_{n+1} = \boldsymbol{\sigma}_n + \boldsymbol{K}\Delta\boldsymbol{\epsilon}^e = \boldsymbol{\sigma}_n + \boldsymbol{K}(\Delta\boldsymbol{\epsilon} - \Delta\boldsymbol{\epsilon}^p) \tag{4.28}$$

$$\boldsymbol{\sigma}_{n+1} = \boldsymbol{\sigma}_{n+1}^{trial} + \Delta\lambda_{n+1}\boldsymbol{K}\boldsymbol{m}_{n+1} \tag{4.29}$$

$$\boldsymbol{q}_{n+1} = \boldsymbol{q}_n + \Delta\lambda_{n+1}\boldsymbol{\varpi}_{n+1} \tag{4.30}$$

Where $\boldsymbol{\sigma}_{n+1}^{trial} = \boldsymbol{\sigma}_n + \boldsymbol{K}\Delta\boldsymbol{\epsilon}$ is the trial stress. During the elastic predictor step (say point A), if the trial stress goes outside the yield surfaces at the point B, see Figure 4.4) after cutting the yield surface at the contact point o; $F(\boldsymbol{\sigma}_{n+1}^{trial}, \boldsymbol{q}_{n+1}) > 0$, then plastic corrector step projects the stress-state at the point D after the evolution or contraction of the yield surface due to the change in internal variable. In the Figure 4.4 point C represents the final converged stress-state for an elastic-perfectly plastic model. In the present study plastic step mobilizes the plastic work which changes the internal hardening parameter $(\boldsymbol{q})$ that expands or contracts the yield surface. It should be noted that the solution of the plastic corrector step must satisfy the full consistency at point D, rather than differential consistency $(\dot{F} = 0)$.

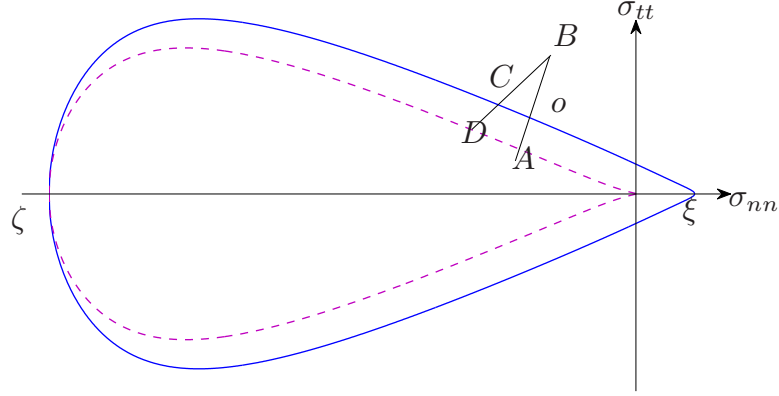$$F(\boldsymbol{\sigma}_{n+1}, \boldsymbol{q}_{n+1}) = 0 \tag{4.31}$$

Figure 4.4: Plot of the integration process, initial converged stress at point $A(\boldsymbol{\sigma}_n)$, contact point at o $(\boldsymbol{\sigma}_{n+1}^0)$, trial stress B $(\boldsymbol{\sigma}_{n+1}^{trial})$, final stress for elastic-perfectly plastic Model at point C, final converged stress for evolved or shrunk yield surface at point D $(\boldsymbol{\sigma}_{n+1})$.

Contact point

The plastic corrector step only produces the change in the stress and internal variable $(\boldsymbol{\sigma}_n, \boldsymbol{q}_n)$. Therefore, it is very important to find the contact point for the present elastic predictor step. Mathematically, it can be express as

$$F(\boldsymbol{\sigma}_n + \gamma \Delta \boldsymbol{\sigma}, \boldsymbol{q}_n) = 0 \tag{4.32}$$

Where $\boldsymbol{\sigma}_n, \boldsymbol{q}_n$ are the variables from the last converged elastic or plastic step, and γ is unknown integer within the range [0 1], which converges the stress to the contact point.

Local iteration strategy

The backward Euler method gives rise to non-linear system of equations, which has to be solved to get actual stress state. In the present study full Newton-Raphson method is used to solve non-linear system of equations. It provides quadratic convergence with initial root sufficiently close, and also ensures the asymptotic quadratic convergence at the global level for structural equilibrium. Newton-Raphson strategy is used for the solution of non-linear equation in monolithic format, as illustrated in the [71–73] for the J_2 plasticity. The strategy is highly influenced by the choice of the independent variables and sequence of the numerical operations. It requires the determination of residual for the set non-linear Equations 4.29, 4.30 and 4.31. It can be written as

$$\boldsymbol{r}(\boldsymbol{\sigma}_{n+1}, \boldsymbol{q}_{n+1}, \Delta\lambda_{n+1}) = \begin{cases} \boldsymbol{\sigma}_{n+1} - \boldsymbol{\sigma}_{n+1}^{trial} + \Delta\lambda_{n+1}\boldsymbol{K}\boldsymbol{m}_{n+1} = 0 \\ \boldsymbol{q}_{n+1} - \boldsymbol{q}_n + \Delta\lambda_{n+1}\boldsymbol{\varpi}_{n+1} = 0 \\ F(\boldsymbol{\sigma}_{n+1}, \boldsymbol{q}_{n+1}) = 0 \end{cases} \tag{4.33}$$

Linearization of the residual, and expanding the residual. we can write

$$r(\boldsymbol{\sigma} + \delta\boldsymbol{\sigma}, \boldsymbol{q} + \delta\boldsymbol{q}, \Delta\lambda + \delta\lambda) = r(\boldsymbol{\sigma}, \boldsymbol{q}, \Delta\lambda) + \frac{r(\boldsymbol{\sigma}, \boldsymbol{q}, \Delta\lambda)}{\partial(\boldsymbol{\sigma}, \boldsymbol{q}, \lambda)} \begin{bmatrix} \delta\boldsymbol{\sigma} \\ \delta\boldsymbol{q} \\ \delta\lambda \end{bmatrix} + O(\delta^2) \qquad (4.34)$$

Where the truncation after first order term is zero $(O(\delta^2) \cong 0)$ and $\dfrac{r(\boldsymbol{\sigma}, \boldsymbol{q}, \Delta\lambda)}{\partial(\boldsymbol{\sigma}, \boldsymbol{q}, \lambda)}$ is the gradient of residual with respect to its dependent variable i.e. $\boldsymbol{\sigma}$, $\boldsymbol{q}$, λ commonly known as Jacobian. The Jacobian for residual at time step n+1 can be express as

$$\boldsymbol{J}(\boldsymbol{\sigma}_{n+1}, \boldsymbol{q}_{n+1}, \Delta\lambda_{n+1}) = \begin{bmatrix} \boldsymbol{I} + \Delta\lambda\boldsymbol{K}\dfrac{\partial\boldsymbol{m}}{\partial\boldsymbol{\sigma}} & \Delta\lambda\boldsymbol{K}\dfrac{\partial\boldsymbol{m}}{\partial\boldsymbol{q}} & \boldsymbol{K}\boldsymbol{m} \\ -\Delta\lambda\boldsymbol{K}\dfrac{\partial\boldsymbol{\varpi}}{\partial\boldsymbol{\sigma}} & -\Delta\lambda\boldsymbol{K}\dfrac{\partial\boldsymbol{\varpi}}{\partial\boldsymbol{q}} & -\boldsymbol{\varpi} \\ \dfrac{\partial\boldsymbol{F}}{\partial\boldsymbol{\sigma}} & \dfrac{\partial\boldsymbol{F}}{\partial\boldsymbol{q}} & 0 \end{bmatrix} \qquad (4.35)$$

The actual solution is achieved by letting the residual go to zero for that current time step during plastic loading. This can be achieved by performing iterations cycles. The iteration will end when residual will become smaller then prescribed tolerance value.

$$0 = r(\boldsymbol{\sigma}_{n+1}^k, \boldsymbol{q}_{n+1}^k, \Delta\lambda_{n+1}^k) + \boldsymbol{J}^{-1}(\boldsymbol{\sigma}_{n+1}^k, \boldsymbol{q}_{n+1}^k, \Delta\lambda_{n+1}^k) \begin{bmatrix} \delta\boldsymbol{\sigma}_{n+1}^{k+1} \\ \delta\boldsymbol{q}_{n+1}^{k+1} \\ \delta\lambda_{n+1}^{k+1} \end{bmatrix} \qquad (4.36)$$

$$\begin{bmatrix} \delta\boldsymbol{\sigma}_{n+1}^{k+1} \\ \delta\boldsymbol{q}_{n+1}^{k+1} \\ \delta\lambda_{n+1}^{k+1} \end{bmatrix} = -\boldsymbol{J}^{-1}(\boldsymbol{\sigma}_{n+1}^k, \boldsymbol{q}_{n+1}^k, \Delta\lambda_{n+1}^k) \, r(\boldsymbol{\sigma}_{n+1}^k, \boldsymbol{q}_{n+1}^k, \Delta\lambda_{n+1}^k) \qquad (4.37)$$

$$\begin{bmatrix} \boldsymbol{\sigma}_{n+1}^{k+1} \\ \boldsymbol{q}_{n+1}^{k+1} \\ \lambda_{n+1}^{k+1} \end{bmatrix} = \begin{bmatrix} \boldsymbol{\sigma}_{n+1}^k \\ \boldsymbol{q}_{n+1}^k \\ \lambda_{n+1}^k \end{bmatrix} + \begin{bmatrix} \delta\boldsymbol{\sigma}_{n+1}^{k+1} \\ \delta\boldsymbol{q}_{n+1}^{k+1} \\ \delta\lambda_{n+1}^{k+1} \end{bmatrix} \qquad (4.38)$$

For starting the iteration a sufficiently close initial solution is required, as the convergence of local iteration cycle depends up on the initial root. Thus initial solution is chosen to be the elastic solution at the contact point.

$$\boldsymbol{\sigma}_{n+1}^0 = \boldsymbol{\sigma}_{n+1}^{trial} + (1 - \gamma)\Delta\boldsymbol{\sigma}; \quad \boldsymbol{q}_{n+1}^0 = \boldsymbol{q}_n; \quad \Delta\lambda_{n+1}^0 = 0 \qquad (4.39)$$

Note that the variable $\Delta\lambda_{n+1}^0$ is taken equal to zero at first iteration of every new load step, as plastic multiplier captures the plastic process incrementally. The initial hardening parameter values $\boldsymbol{q}_{n+1}^0$ are the last converge hardening parameter values.

Global iteration strategy

The converged solution form local iteration strategy can be used for the determination of consistent tangent operator $\dfrac{\Delta\boldsymbol{\sigma}}{\Delta\boldsymbol{\epsilon}}$ for the current time step. Thus, in order to compute the tangent operator using the Jacobian, we have to differentiate the residual with respect to the strain and then using the chain rule we will get

$$\frac{\partial}{\partial\boldsymbol{\epsilon}}\left[\begin{array}{c}\boldsymbol{\sigma}_{n+1}-\boldsymbol{\sigma}_{n+1}^{trial}+\Delta\lambda_{n+1}\boldsymbol{K}\boldsymbol{m}_{n+1}\\ \boldsymbol{q}_{n+1}-\boldsymbol{q}_n+\Delta\lambda_{n+1}\boldsymbol{\varpi}_{n+1}\\ F(\boldsymbol{\sigma}_{n+1},\boldsymbol{q}_{n+1})\end{array}\right]=0 \tag{4.40}$$

$$\frac{\partial}{\partial\boldsymbol{\epsilon}}\left[\begin{array}{c}\boldsymbol{\sigma}+\Delta\lambda\boldsymbol{K}\boldsymbol{m}\\ \boldsymbol{q}-\Delta\lambda\boldsymbol{\varpi}\\ F(\boldsymbol{\sigma},\boldsymbol{q})\end{array}\right]_{n+1}=\frac{\partial}{\partial\boldsymbol{\epsilon}}\left[\begin{array}{c}\boldsymbol{\sigma}+\boldsymbol{K}\Delta\boldsymbol{\epsilon}\\ \boldsymbol{q}\\ 0\end{array}\right]_n \tag{4.41}$$

$$\left[\begin{array}{ccc}\dfrac{\partial}{\partial\boldsymbol{\sigma}}&\dfrac{\partial}{\partial\boldsymbol{q}}&\dfrac{\partial}{\partial\lambda}\end{array}\right]_{n+1}\left[\begin{array}{c}\boldsymbol{\sigma}+\Delta\lambda\boldsymbol{K}\boldsymbol{m}\\ \boldsymbol{q}-\Delta\lambda\boldsymbol{\varpi}\\ F(\boldsymbol{\sigma},\boldsymbol{q})\end{array}\right]_{n+1}\left[\begin{array}{ccc}\dfrac{\partial\boldsymbol{\sigma}}{\partial\boldsymbol{\epsilon}}&\dfrac{\partial\boldsymbol{q}}{\partial\boldsymbol{\epsilon}}&\dfrac{\partial\lambda}{\partial\boldsymbol{\epsilon}}\end{array}\right]^T_{n+1}=\frac{\partial}{\partial\boldsymbol{\epsilon}}\left[\begin{array}{c}\boldsymbol{\sigma}+\boldsymbol{K}\Delta\boldsymbol{\epsilon}\\ \boldsymbol{q}\\ 0\end{array}\right]_n \tag{4.42}$$

$$\boldsymbol{J}(\boldsymbol{\sigma}_{n+1},\boldsymbol{q}_{n+1},\Delta\lambda_{n+1})\cdot\left[\begin{array}{ccc}\dfrac{\partial\boldsymbol{\sigma}}{\partial\boldsymbol{\epsilon}}&\dfrac{\partial\boldsymbol{q}}{\partial\boldsymbol{\epsilon}}&\dfrac{\partial\lambda}{\partial\boldsymbol{\epsilon}}\end{array}\right]^T_{n+1}=\left[\begin{array}{c}\boldsymbol{K}\\ 0\\ 0\end{array}\right] \tag{4.43}$$

$$\left[\begin{array}{c}\left[\dfrac{\partial\boldsymbol{\sigma}}{\partial\boldsymbol{\epsilon}}\right]_{2x2}\\ \left[\dfrac{\partial\boldsymbol{q}}{\partial\boldsymbol{\epsilon}}\right]_{6x2}\\ \left[\dfrac{\partial\lambda}{\partial\boldsymbol{\epsilon}}\right]_{1x2}\end{array}\right]_{9x2}=\boldsymbol{J}^{-1}(\boldsymbol{\sigma}_{n+1},\boldsymbol{q}_{n+1},\Delta\lambda_{n+1})_{9x9}\left[\begin{array}{c}\boldsymbol{K}\\ 0\\ 0\end{array}\right]_{9x2} \tag{4.44}$$

The consistent tangent operator can extracted from the preceding expression,and we can defined the consistent tangent operator as:

$$\left[\frac{\partial\boldsymbol{\sigma}}{\partial\boldsymbol{\epsilon}}\right]_{2x2}=O_{2x2}\left\{\boldsymbol{J}^{-1}(\boldsymbol{\sigma}_{n+1},\boldsymbol{q}_{n+1},\Delta\lambda_{n+1})_{9x9}\left[\begin{array}{c}\boldsymbol{K}\\ 0\\ 0\end{array}\right]_{9x2}\right\} \tag{4.45}$$

54

4.4.6 Algorithmic Implementation

The plasticity based composite interface model is implemented in commercial finite element software ABAQUS [74] by writing the user defined subroutine UMAT, which allows to define a user defined mechanical constitutive model for a material. During the analysis, the UMAT is called at the all integration points of the elements. At end of the increment UMAT updates the stress, internal state variables and elasto-plastic tangent operator. The proposed numerical integration algorithm implemented in the UMAT is presented in Algorithm 1.

Steps
1. Recover Solution Dependent Variables from the last converged iteration cycle
$$\boldsymbol{\sigma}_{n+1}, \boldsymbol{q}_n, \boldsymbol{W}_n^p, \boldsymbol{\epsilon}_n^p$$
2. Compute trial elastic stress
$$\boldsymbol{\sigma}_{n+1}^{trial} = \boldsymbol{\sigma}_n + \boldsymbol{K}\Delta\boldsymbol{\epsilon}$$
3. Compute the yield function $F^{trial}(\boldsymbol{\sigma}_{n+1}^{trial}, \boldsymbol{q}_n)$
4. Check for the yield condition
if $F^{trial}(\boldsymbol{\sigma}_{n+1}^{trial}, \boldsymbol{q}_n) < 0$ **then**
    Elastic State
    update $\boldsymbol{\sigma}_{n+1} = \boldsymbol{\sigma}_{n+1}^{trial}$;
    update $\boldsymbol{q}_{n+1} = \boldsymbol{q}_n$;
    update $\boldsymbol{W}_n^p = \boldsymbol{W}_n^p$;
    update $\boldsymbol{\epsilon}_n^p = \boldsymbol{\epsilon}_n^p$;
else
    Plastic State
    Compute the contact point $F(\boldsymbol{\sigma}_n + \gamma\Delta\boldsymbol{\sigma}, \boldsymbol{q}_n)$;
    while $||\boldsymbol{r}(\boldsymbol{\sigma}_n, \boldsymbol{q}_n, \Delta\lambda_n)|| < tol$ **do**
        Compute $\boldsymbol{n}_n^k, \boldsymbol{m}_n^k, \boldsymbol{\varpi}_n^k$;
        Compute $\boldsymbol{J}_n^k(\boldsymbol{\sigma}_n^k, \boldsymbol{q}_n^k, \Delta\lambda_n^k) = \dfrac{\boldsymbol{r}(\boldsymbol{\sigma}_n^k, \boldsymbol{q}_n^k, \Delta\lambda_n^k)}{\partial(\boldsymbol{\sigma}_n^k, \boldsymbol{q}_n^k, \lambda_n^k)}$;
        Compute $\delta(\boldsymbol{\sigma}_n, \boldsymbol{q}_n, \lambda_n)^{k+1} = -\boldsymbol{J}^{-1}(\boldsymbol{\sigma}_n^k, \boldsymbol{q}_n^k, \Delta\lambda_n^k)\boldsymbol{r}(\boldsymbol{\sigma}_n^k, \boldsymbol{q}_n^k, \Delta\lambda_n^k)$;
        Compute $[\boldsymbol{\sigma}_n, \boldsymbol{q}_n, \lambda_n]^{k+1} = [\boldsymbol{\sigma}_n, \boldsymbol{q}_n, \lambda_n]^k + \delta(\boldsymbol{\sigma}_n, \boldsymbol{q}_n, \lambda_n)^{k+1}$;
    end
    update $\boldsymbol{\sigma}_{n+1} = \boldsymbol{\sigma}_n^{k+1}$;
    update $\boldsymbol{q}_{n+1} = \boldsymbol{q}_n^{k+1}$;
    update $\boldsymbol{W}_{n+1}^p = (\boldsymbol{W}_n^p)^{k+1}$;
    update $\boldsymbol{\epsilon}_n^p = (\boldsymbol{\epsilon}_n^p)^{k+1}$;
    Compute $\boldsymbol{K}^{ep}$
end

Algorithm 1: Monolithic numerical integration algorithm.

4.4.7 Verification Examples

In order to verify the proposed composite interface model various verification examples have been considered in this section. The formulated constitutive model is verified by implementing a single zero-thickness interface, which is a 4-node two dimensional cohesive element with two integration point. The material parameter used for verification are tabulated in Table 4.1 and 4.2 obtained from the calibration process. Specifically, to find the values of mode I and mode II fracture energy, it is assumed that $G_f^I = 5G_{f,min}^I$ and $G_f^{II} = 10G_f^I$, where $G_{f,min}^I = \xi_0^2/2k_{nn}$ corresponding to the perfectly brittle tensile fracture. The verification examples include interface in tension, compression

and shear mode condition. The implementation is done in ABAQUS, by using the user defined subroutine (UMAT).

Table 4.1: Elastic material property for the Brick and joints

Brick		Joint	
E	ν	k_{nn}	k_{tt}
N/mm^2		N/mm^3	N/mm^3
2000	0.15	1000	1000

Table 4.2: Inelastic material property for the joints

Tension		Shear					Cap
ξ_0	G_f^I	$C_0\backslash C_r$	$C_{Q0}\backslash C_{Qr}$	$\phi_0\backslash\phi_r$	ψ	G_f^{II}	ζ_p
N/mm^2	Nmm/mm^2	N/mm^2	N/mm^2	$radian$	$radian$	Nmm/mm^2	N/mm^2
2.0	$5\xi_0^2/2K_{nn}$	$1.4\xi_0\backslash0.1C_Q$	$1.1\xi_0\backslash0.1C_Q$	$0.65\backslash0.50$	$0.30\backslash0.20$	$10G_f^I$	30

Direct tension test

In this test the interface is subjected to direct tension. A normal relative displacement is applied to the nodes on the top face of the interface element while all the degrees of freedom on the bottom face are fixed. Figure 4.5 shows the variation of tensile strength ξ with mix mode fracture energy $\frac{w_1^p}{G_f^I} + \frac{w_2^p}{G_f^{II}}$. The response exhibits a exponential degradation of the tensile strength and matches well with the analytical values.
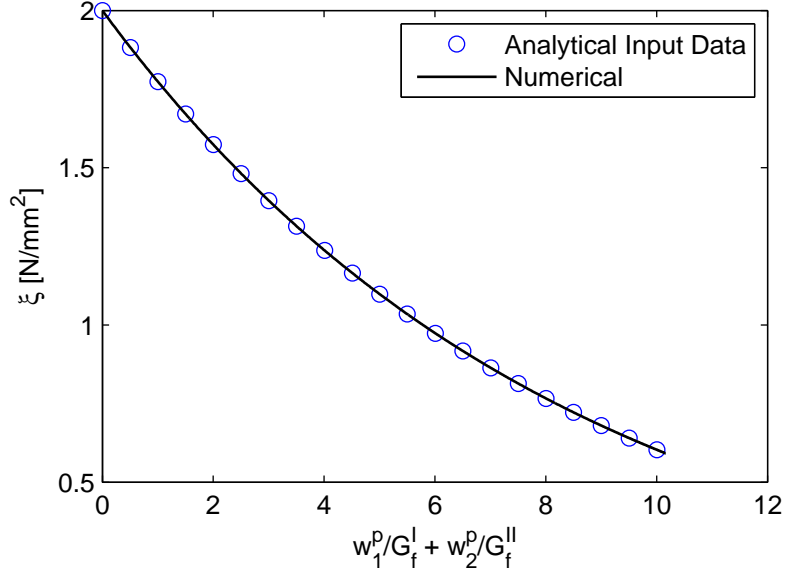
Figure 4.5: Plot of distribution of tensile strength ξ with $\left(\dfrac{w_1^p}{G_f^I} + \dfrac{w_2^p}{G_f^{II}}\right)$.

Direct compression test

In this test the interface is subjected to direct compression. The test is performed to check the functionality of the compression cap. A normal relative displacement is applied to produce the pure compression state in the interface and variation of compression strength (ζ) with work hardening parameter w_4^p is traced and compared with the analytical values by solving Equation 4.20. It can be observed from Figure 4.6, that the internal hardening variable (ζ) coincides well with the analytical values.
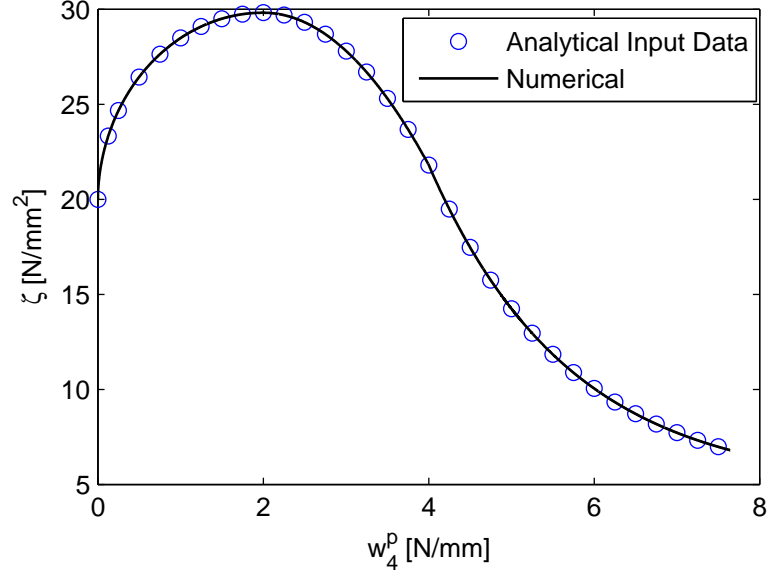
Figure 4.6: Plot of distribution of compression strength ζ with w_4^p.

Direct shear test under compressive stress

In this test the interface is subjected to direct shear test under different normal compressive stress. The interface element is loaded with normal compressive stress. Then, a relative shear displacement is applied at the top surface, while all degrees of freedom on the bottom face are kept fixed. This load sequence is repeated for various levels of constant normal compressive stress. The results of this test are shown in Figure 4.7(a). A plot of distribution of tangential stress with relative tangential displacement are plotted for different compressive stress (0.1, 1, 10 Mpa). A shear softening behaviour is observed. The result shows that the shear capacity of the interface increases with increase in compressive stress. After the initial elastic response, all response curves show a similar post-peak behaviour, with a steeper part given by the decrease of all softening parameters ($\boldsymbol{q}$). After that, ξ remains zero, and the shear traction diminishes. Finally, all softening curves tend to the residual shear value that corresponds to the residual cohesion (C_r) and friction angle (ϕ_r).

In Figure 4.7(b), the distribution of normal displacements with relative tangential displacements is plotted. It can be observed that the dilatancy decreases with increase in compressive stress, and approaches a limiting value when the interface degrades to the residual dilation angle (ψ_r).
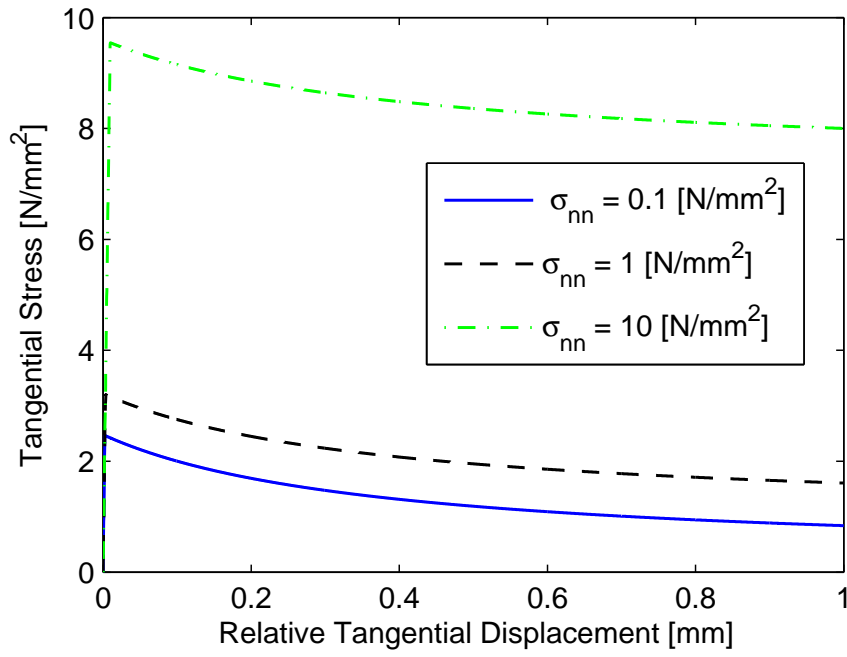
(a)
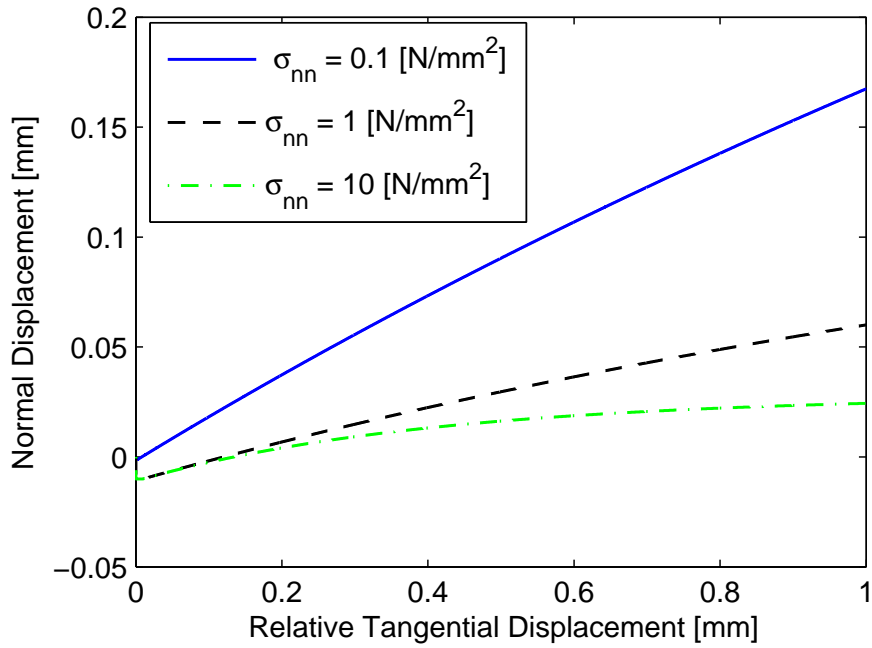
(b)

Figure 4.7: Plot for direct shear test under different constant compressive stress (a) distribution of tangential stress with relative tangential displacement; (b) distribution of normal displacements with relative tangential displacements.

4.4.8 Sub stepping

There are three critical aspects on which the success of numerical algorithm depends: first, Robustness, it ensures that for reasonable choices of initial conditions and input data, the algorithm will not fail and it will provide a solution. Second, Accuracy ensures that the solution is within a tolerance threshold. Third, Non-associativity, it ensures that numerical algorithm will work for the dilatancy angle, for return mapping. All these aspects becomes very importance because the entire global solution depends on the solution of the constitutive equations at the Gauss point level. To check these aspects on the proposed Composite Interface Model, implementation of different examples are presented below.

Robustness

To check the robustness of proposed algorithm, campaign of different load paths, and different load increment is applied to 2D interface model. Seven load path are considered for tension shear and compression region each. Load is applied in all cases from $\sigma = 0$ up to a certain value of the trial stress state, σ^{trail}. In particular, four load increment are considered N := 5, 25, 125, 625. The material parameter used in these example are given in Table 4.1 and 4.2. The result of these numerical example are summarized in Table 4.3, in term of no of iteration required for the convergence of algorithm with the tolerance of 1^{-10}.

Table 4.3: Convergence of algorithm without sub-stepping for different load path, at a Gauss point level

	Tension-shear region						
	$\theta = 0$	$\theta = 15$	$\theta = 30$	$\theta = 45$	$\theta = 60$	$\theta = 75$	$\theta = 90$
$N = 5$	4	8	7	6	7	6	6
$N = 25$	5	16	14	12	14	8	8
$N = 125$	5	$Fail$	14	15	16	8	10
$N = 625$	6	$Fail$	$Fail$	$Fail$	$Fail$	$Fail$	12
	Compression-shear region						
	$\theta = 90$	$\theta = 105$	$\theta = 120$	$\theta = 135$	$\theta = 150$	$\theta = 175$	$\theta = 180$
$N = 5$	6	6	8	8	11	25	E
$N = 25$	8	16	12	13	12	12	4
$N = 125$	10	20	13	$Fail$	13	12	7
$N = 625$	12	22	17	$Fail$	17	16	9

The result shows that for load paths whose directions are different from $\theta = 0$ and $\theta = 90$, the algorithm does not converge if the loading step size is large then 125. It demonstrates need for sub stepping to achieve optimal performance. The sub stepping procedure will only take place, when the algorithm does not reach convergence within a prescribed number of iterations. To check the results of this new procedure the same campaign of numerical test is repeated, and its results

are summarized in Table 4.4. The number of iterations is augmented by the total number of sub increments (between parentheses) which are needed for convergence.

Table 4.4: Convergence of algorithm with sub-stepping for different load path, at a Gauss point level

	Tension-shear region						
	$\theta = 0$	$\theta = 15$	$\theta = 30$	$\theta = 45$	$\theta = 60$	$\theta = 75$	$\theta = 90$
$N = 5$	4	8	7	6	7	6	6
$N = 25$	5	16	14	12	14	8	8
$N = 125$	5	39(2)	14	15	16	8	10
$N = 625$	6	198(8)	113(8)	101(8)	117(8)	64(8)	12
	Compression-shear region						
	$\theta = 90$	$\theta = 105$	$\theta = 120$	$\theta = 135$	$\theta = 150$	$\theta = 175$	$\theta = 180$
$N = 5$	6	6	8	8	11	25	E
$N = 25$	8	16	12	13	12	12	4
$N = 125$	10	20	13	97(8)	13	12	7
$N = 625$	12	22	17	481(40)	17	16	9

Accuracy

It has also been observed that number of iterations increases as the load step size increases. However, there are special situations in which do not follow this trend i.e. uniaxial tension ($\theta = 0$), pure shear ($\theta = 90$) and uniaxial compression ($\theta = 180$). If the convergence for some special situations does not depend of the loading step size, the issue remains whether the accuracy of the solution depends strongly on the load step size. To find out this, three different load steps are considered where u equals 1×10^{-4}, 5×10^{-4}, 1×10^{-3}. A fourth loading size step is computed, u equals 1×10^{-5}, to compare the accuracy of those results. The latter step size is considered sufficiently small to serve as an accurate reference solution to compare with.

(a)
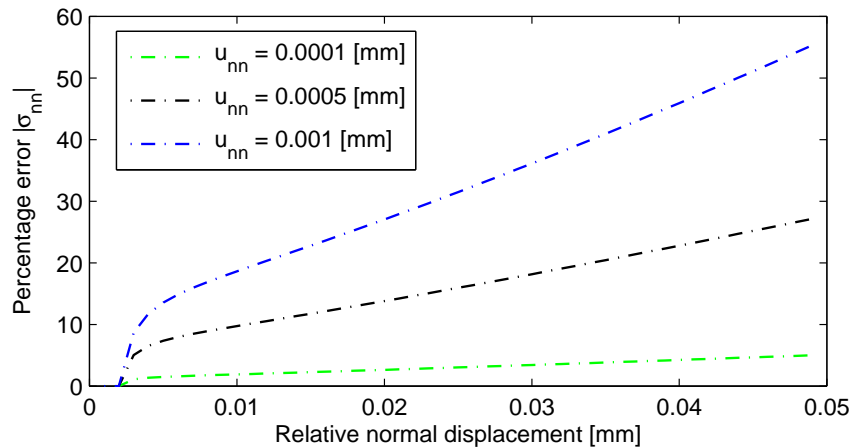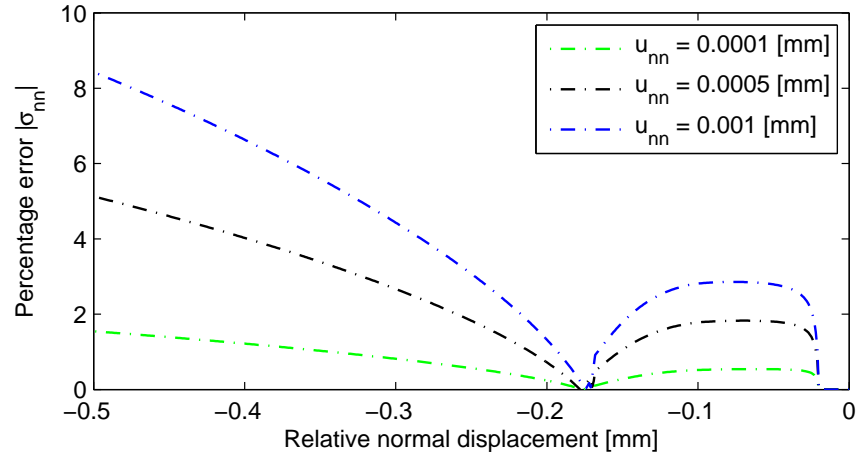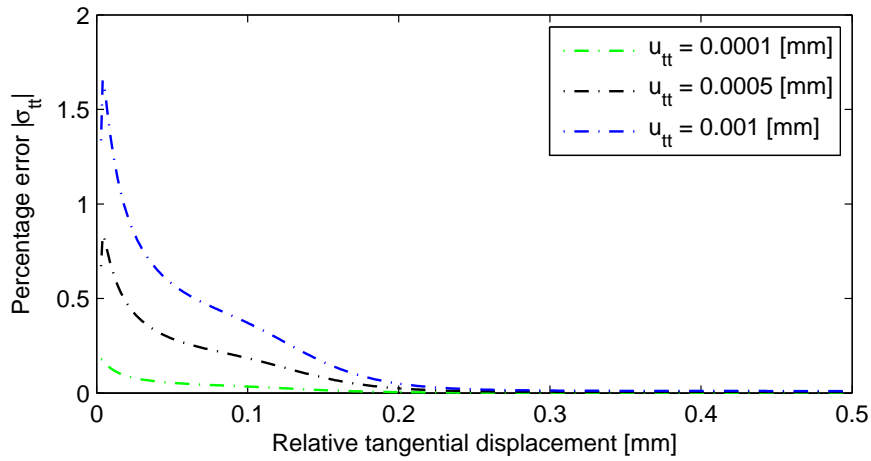
Figure 4.8: Plot for Error stress response along entire loading path: (a)tension; (b) compression; (c) shear.

The results are plotted in Figure 4.8. The result shows that

- the error of the solution increases as the load step size increases;

- the integration algorithm requires sub stepping not only to ensure convergence of the solution but also to ensure the accuracy of the final solution.

Non-associativity

The capacity of proposed algorithm for different non-associativity is cheeked here. A campaign of different dilatancy angle for a given load step is applied to 2D interface model. Seven dilatancy angle are considered $\psi = 0, 15, 30, 45, 60, 75, 90$. The displacement is applied in lateral direction at a different vertical pressure i.e. $p = 0, 0.1, 1, 10, 20, 22$. The result of these numerical example are summarized in Table 4.5 and 4.6, in term of no of iteration required for the convergence of algorithm with the tolerance of 1^{-10}.

Table 4.5: Convergence of algorithm without sub-stepping for different dilatency for load step = 0.005, at a Gauss point level

	$p = 0$	$p = 0.1$	$p = 1$	$p = 10$	$p = 20$	$p = 22$
$\psi = 0$	3	3	3	3	13	16
$\psi = 15$	7	7	7	8	24	16
$\psi = 30$	8	8	9	18	39	$Fail$
$\psi = 45$	10	10	11	$Fail$	$Fail$	$Fail$
$\psi = 60$	13	13	17	$Fail$	$Fail$	$Fail$
$\psi = 75$	41	67	83	$Fail$	$Fail$	$Fail$
$\psi = 90$	$Fail$	$Fail$	$Fail$	$Fail$	$Fail$	$Fail$

Table 4.6: Convergence of algorithm without sub-stepping for different dilatency for load step = 0.00001, at a Gauss point level

	$p = 0$	$p = 0.1$	$p = 1$	$p = 10$	$p = 20$	$p = 22$
$\psi = 0$	2	2	2	3	3	15
$\psi = 15$	2	2	2	3	3	15
$\psi = 30$	2	2	2	3	4	16
$\psi = 45$	2	2	3	3	4	16
$\psi = 60$	3	3	3	3	4	16
$\psi = 75$	4	4	4	6	6	25
$\psi = 90$	4	4	9	11	17	27

The result shows that for the higher dilatancy angle and load step, the algorithm does not converge. Thus sub steeping is also required for robust non-associativity. The same campaign of numerical test is repeated for the algorithm with sub stepping, and its results are summarized in Table 4.7. The number of iterations is augmented by the total number of sub increments (between parentheses) which are needed for convergence.

Table 4.7: Convergence of algorithm with sub-stepping for different dilatency for load step = 0.005, at a Gauss point level

	$p = 0$	$p = 0.1$	$p = 1$	$p = 10$	$p = 20$	$p = 22$
$\psi = 0$	3	3	3	3	13	16
$\psi = 15$	7	7	7	8	24	16
$P = 30$	8	8	9	18	39	59(6)
$\psi = 45$	10	10	11	39(3)	66(3)	66(3)
$\psi = 60$	13	13	17	116(9)	178(6)	220(5)
$\psi = 75$	21(2)	25(3)	75(10)	121(3)	138(26)	539(26)
$\psi = 90$	37(9)	41(9)	57(9)	390(75)	341(57)	942(57)

Algorithm with sub stepping

The algorithm requires sub-stepping not only to ensure convergence of the solution but also to ensure the accuracy of the final solution at both local and globe level. Fortunately, it is possible to integrate the constitutive equations by sub-dividing the load at the constitutive level [75–77]. Based on these considerations, an adaptive sub-stepping scheme has been developed for the present composite interface model. This technique starts with the previous system of Equation 4.33. The algebraic problem is modified significantly in order to obtain consistent tangent operator in the case of sub-stepping. It is assumed that any increment can be subdivided into N sub-increments, which could be of different sizes but the sum of all sub-increments always equals to the total displacement at the end of the increment

$$\Delta \epsilon = \sum_{i=0}^{N} \Delta \epsilon^i = \Delta \epsilon \left(\eta^i \right) \tag{4.46}$$

$$Where \ 0 < \eta^i < 1 \ and \ \sum_{i=0}^{N} \eta^i = 1$$

Hence rewriting the Equation 4.33, for sub-increment

$$\boldsymbol{r}(\boldsymbol{\sigma}^i, \boldsymbol{q}^i, \Delta\lambda^i) = \begin{cases} \boldsymbol{\sigma}^i - (\boldsymbol{\sigma}^{trial})^i + \Delta\lambda^i \boldsymbol{K}\boldsymbol{m}^i = 0 \\ \boldsymbol{q}^i - \boldsymbol{q}^{i-1} + \Delta\lambda^i \boldsymbol{\varpi}^i = 0 \\ F(\boldsymbol{\sigma}^i, \boldsymbol{q}^i) = 0 \end{cases} \tag{4.47}$$

Note that, now the independent variable of the system of equation are $\boldsymbol{\sigma}^i, \boldsymbol{q}^i, \Delta\lambda^i$ and the methodology for solving the equation is same as the one in previous section. For consistent tangent operator, taking the derivative of the equation with respect to $\Delta\epsilon$ and then apply the chain rule

$$\begin{bmatrix} \begin{bmatrix} \dfrac{\partial \boldsymbol{\sigma}^i}{\partial \boldsymbol{\epsilon}^i} \end{bmatrix}_{2x2} \\ \begin{bmatrix} \dfrac{\partial \boldsymbol{q}^i}{\partial \boldsymbol{\epsilon}^i} \end{bmatrix}_{6x2} \\ \begin{bmatrix} \dfrac{\partial \lambda^i}{\partial \boldsymbol{\epsilon}^i} \end{bmatrix}_{1x2} \end{bmatrix}_{9x2} = \boldsymbol{J}^{-1}(\boldsymbol{\sigma}_{n+1}^i, \boldsymbol{q}_{n+1}^i, \Delta\lambda_{n+1}^i)_{9x9} \begin{bmatrix} \eta^i \boldsymbol{K} \\ 0 \\ 0 \end{bmatrix}_{9x2} \tag{4.48}$$

The consistent tangent operator of a sub-increment can extracted from the preceding expression. The consistent tangent operator of the load step is obtained by linear combination of all sub-increments and can be written as

$$\begin{bmatrix} \dfrac{\partial \boldsymbol{\sigma}}{\partial \boldsymbol{\epsilon}} \end{bmatrix} = \sum_{i=0}^{N} \begin{bmatrix} \dfrac{\partial \boldsymbol{\sigma}^i}{\partial \boldsymbol{\epsilon}^i} \end{bmatrix} \tag{4.49}$$

Steps

1. Recover Solution Dependent Variables from the last converged iteration cycle
$$\boldsymbol{\sigma}_{n+1}, \boldsymbol{q}_n, \boldsymbol{W}_n^p, \boldsymbol{\epsilon}_n^p$$

2. Compute trial elastic stress
$$\boldsymbol{\sigma}_{n+1}^{trial} = \boldsymbol{\sigma}_n + \boldsymbol{K}\Delta\boldsymbol{\epsilon}$$

3. Compute the yield function $F^{trial}(\boldsymbol{\sigma}_{n+1}^{trial}, \boldsymbol{q}_n)$

4. Check for the yield condition

if $F^{trial}(\boldsymbol{\sigma}_{n+1}^{trial}, \boldsymbol{q}_n) < 0$ **then**

> **Elastic State**
> update $\boldsymbol{\sigma}_{n+1} = \boldsymbol{\sigma}_{n+1}^{trial}$;
> update $\boldsymbol{q}_{n+1} = \boldsymbol{q}_n$;
> update $\boldsymbol{W}_n^p = \boldsymbol{W}_n^p$;
> update $\boldsymbol{\epsilon}_n^p = \boldsymbol{\epsilon}_n^p$;

else

> **Plastic State**
> Compute the contact point $F(\boldsymbol{\sigma}_n + \gamma\Delta\boldsymbol{\sigma}, \boldsymbol{q}_n)$;
> Compute $(\boldsymbol{K}^{ep})^0 = \gamma\boldsymbol{K}$;
> **while** $i < n$ **do**
>> **while** $||\boldsymbol{r}(\boldsymbol{\sigma}_n, \boldsymbol{q}_n, \Delta\lambda_n)|| < tol$ **do**
>>> for simplicity superscript 'i' is not used ;
>>> Compute $\boldsymbol{n}_n^k, \boldsymbol{m}_n^k, \boldsymbol{\varpi}_n^k$;
>>> Compute $\boldsymbol{J}_n^k(\boldsymbol{\sigma}_n^k, \boldsymbol{q}_n^k, \Delta\lambda_n^k) = \dfrac{\boldsymbol{r}(\boldsymbol{\sigma}_n^k, \boldsymbol{q}_n^k, \Delta\lambda_n^k)}{\partial(\boldsymbol{\sigma}_n^k, \boldsymbol{q}_n^k, \lambda_n^k)}$;
>>> Compute $\delta(\boldsymbol{\sigma}_n, \boldsymbol{q}_n, \lambda_n)^{k+1} = -\boldsymbol{J}^{-1}(\boldsymbol{\sigma}_n^k, \boldsymbol{q}_n^k, \Delta\lambda_n^k)\boldsymbol{r}(\boldsymbol{\sigma}_n^k, \boldsymbol{q}_n^k, \Delta\lambda_n^k)$;
>>> Compute $[\boldsymbol{\sigma}_n, \boldsymbol{q}_n, \lambda_n]^{k+1} = [\boldsymbol{\sigma}_n, \boldsymbol{q}_n, \lambda_n]^k + \delta(\boldsymbol{\sigma}_n, \boldsymbol{q}_n, \lambda_n)^{k+1}$;
>> **end**
>> update $(\boldsymbol{\sigma}_{n+1})^i = (\boldsymbol{\sigma}_n^{k+1})^i$;
>> update $(\boldsymbol{q}_{n+1})^i = (\boldsymbol{q}_n^{k+1})^i$;
>> update $(\boldsymbol{W}_{n+1}^p)^i = ((\boldsymbol{W}_n^p)^{k+1})^i$;
>> Compute $(\boldsymbol{K}^{ep})^i$
> **end**
> update $\boldsymbol{\sigma}_{n+1} = (\boldsymbol{\sigma}_n^{k+1})^N$;
> update $\boldsymbol{q}_{n+1} = (\boldsymbol{q}_n^{k+1})^N$;
> update $\boldsymbol{W}_{n+1}^p = ((\boldsymbol{W}_n^p)^{k+1})^N$;
> Compute $\boldsymbol{K}^{ep} = \sum\limits_{i=0}^{N}(\boldsymbol{K}^{ep})^i$

end

Algorithm 2: Monolithic numerical integration algorithm with sub-stepping.

4.5 Conclusion

A plasticity based composite interface model is proposed, which is capable of simulating the initiation and propagation of crack under combined normal and shear stresses. Moreover, singularity at corner region is removed by using a single surface yield criteria. The yield function is capable of representing pressure-dependent friction shear failure, cracking by cut-off in tension and crushing by cap-off in compression. The model is developed by integrating the differential equation by fully implicit backward Euler method. The equation are solved by full Newton-Raphson technique in monolithic manner, which lead to combined local and global approach.

At last, the model is implemented in commercial finite element software ABAQUS. The three basic verification example are used to verify the implementation of algorithm. During the verification, it has been found that sub stepping is required to ensure the convergence and accuracy of the final solution at both local and global level. This Make the code to behaves well at even large load step.

Chapter 5

Validation of composite interface model

In the present chapter, the composite interface model proposed in previous chapter is validated, by comparing the numerical results with experimental results available in the literature. In this chapter first the micro-modelling strategy of masonry wall is discussed. Then, the strategy is successfully applied to the masonry shear walls. In the last, the applicability of model to simulate the direct cyclic behaviour is validated, by simulating the masonry bed joint.

5.1   Micro Modelling of Masonry

Micro-modelling approach includes distinct representations of units, mortar and the unit-mortar interface. The unit and mortar are represented by continuum elements and unit-mortar interface is represented discontinuous interface element. Elastic and inelastic properties of both unit and mortar are taken into account. This detailed micro-modelling procedure leads to very accurate results. However, it requires an intensive computational effort. This drawback is overcome by making an assumption that mortar and two unit-mortar interface is lumped into joint between expended units, see Figure 5.1. The units are expended in order to keep the geometry of structure unchanged. Thus, masonry is considered as a set of elastic blocks bonded by potential crack, potential slip and crushing plane at the joints.
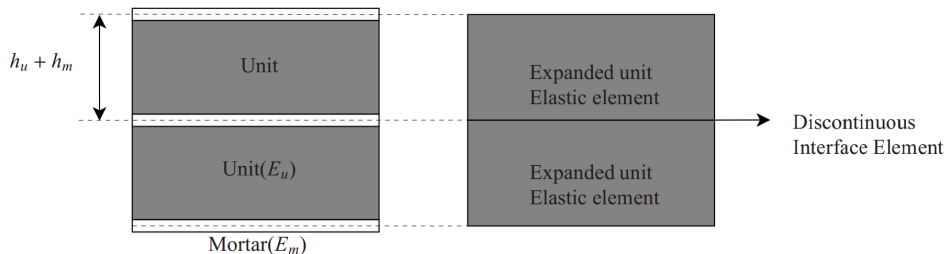
Figure 5.1: Simplified micro-modelling.

In the present section simplified micro modelling is adopted for the study of failure analysis of unreinforced masonry under plane stress condition. The joint interface is modelled with proposed composite interface model, which is capable of representing the potential crack, potential slip and crushing. Moreover, for modelling cracking of the bricks, a potential crack is placed vertically in the middle of each brick. Simple mode I crack model with exponential softening behaviour in tension is adopted for the potential crack. It is assumed that after initiation of the crack shear stress drops to zero. This assumption is made to overcome the bifurcation problem of shear tension regime, for detail see [12]. The modelling strategy is validated by comparing numerical results with the experimental results available in the literature. In this study, shear wall tests carried by the Vermeltfoort and Raijmakers [78, 79] is adopted for the further study.

5.2   Masonry shear wall

An experimental Study was carried out on masonry shear walls by Vermeltfoort and Raijmakers [78, 79]. The authors conducted the tests on two type of wall i.e. one without the opening and another with the opening. The authors used a set-up that consisted of a pier with a width to height ratio of one and with dimensions 990×1000 [mm^2]. It was built-up with 18 courses of which two courses were clamped in steel beam and only 16 courses were active. The wall was made up of wire cut solid clay [$210 \times 52 \times 100$ mm^3] and mortar [10 mm], prepared with a volumetric (cement : lime : sand) ratio of ($1 : 2 : 9$). The test involves a monotonically increasing horizontal load under different levels of uniformly distributed normal stress, keeping the bottom and top boundaries horizontally fixed. The material data is obtained from existing experimental results on tension, shear and compression from the sample collected for each wall and all other missing parameters are obtained from the calibration process.

From the present work both type of wall are presented their. The wall without opening is denoted by SW and wall with opening is denoted by SWO. The micro-properties of the shear wall material are obtained from [78, 79] and are given in Table 5.1, 5.2 and 5.3. The hardening/softening law for the compression cap is defined by the set $\{\zeta, w_4^p\} = \{(\zeta_p/3, 0.0); (\zeta_p, 0.09); (\zeta_p/2, 0.49); (\zeta_p/7, \infty)\}$. For the numerical analyses, units are represented by plane stress continuum elements (8-noded) while line interface elements (4-noded, with 2 integration point) are adopted for the joints and for the potential vertical cracks in the middle of the unit. Each unit is modelled with 4 x 2 elements. For the joints, the composite interface model described in previous chapter has been adopted.

Table 5.1: Properties for Potential Brick Cracks.

Elastic		Inelastic	
K_{nn} N/mm^3	K_{tt} N/mm^3	ξ_0 N/mm^2	G_f^I Nmm/mm^2
10^6	10^6	2.0	0.08

Table 5.2: Elastic material property.

Brick		Joint	
E N/mm^2	ν	K_{nn} N/mm^3	K_{tt} N/mm^3
16700	0.15	82;110;82	36;50;36

Table 5.3: Inelastic material property for the joints.

Tension	ξ_0 $[N/mm^2]$	$0.25; 0.16; 0.16$
	G_f^I $[Nmm/mm^2]$	$5\xi_0^2/2K_{nn}$
Shear	$C_0 \backslash C_r$ $[N/mm^2]$	$1.4\xi_0 \backslash 0.1C_Q$
	$C_{Q0} \backslash C_{Qr}$ $[N/mm^2]$	$1.1\xi_0 \backslash 0.1C_Q$
	$\phi_0 \backslash \phi_r$ $[radian]$	$0.65 \backslash 0.50$
	ψ $[radian]$	0
	G_f^{II} $[Nmm/mm^2]$	$10G_f^I$
Cap	ζ_p $[N/mm^2]$	$10.5; 11.5; 11.5$

Note: three different parameters are for three different initial vertical pressure.

5.2.1 Shear wall without opening (SW)

The experimental test was carried out successfully on the shear wall without opening (SW). These wall were tested for three different initial vertical pressure i.e. for wall SW-1a and SW-1b pressure equals 0.30 $[N/mm^2]$, for wall SW-2 pressure equals 1.21 $[N/mm^2]$ and for wall SW-3 pressure equals 2.12 $[N/mm^2]$. The experimental failure pattern for the different wall tested are shown in Figure 5.2. All the wall shows almost the similar behaviour. On applying the monotonically increasing horizontal load, first horizontal tensile cracks develop at the bottom and top of the wall particularly in the bed joint at an early loading stage and then, a diagonal stepped crack form. Finally, diagonal stepped cracked and crushing of the toes of the masonry leads to over all the failure of the masonry, simultaneously bricks gets cracked.

$P = 0.30$ $[N/mm^2]$

$P = 0.30$ $[N/mm^2]$

(a) SW-1a

(b) SW-1b

(c) SW-2

(d) SW-3
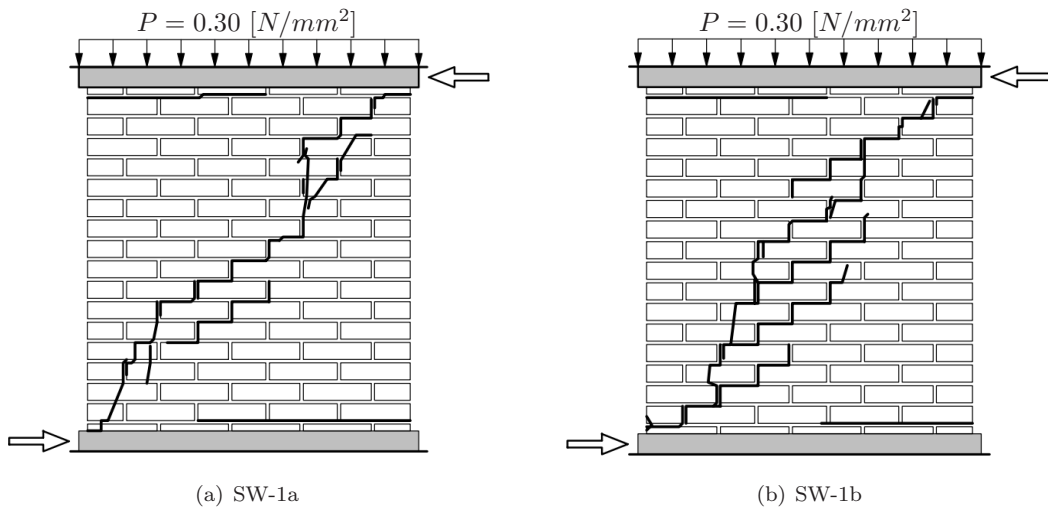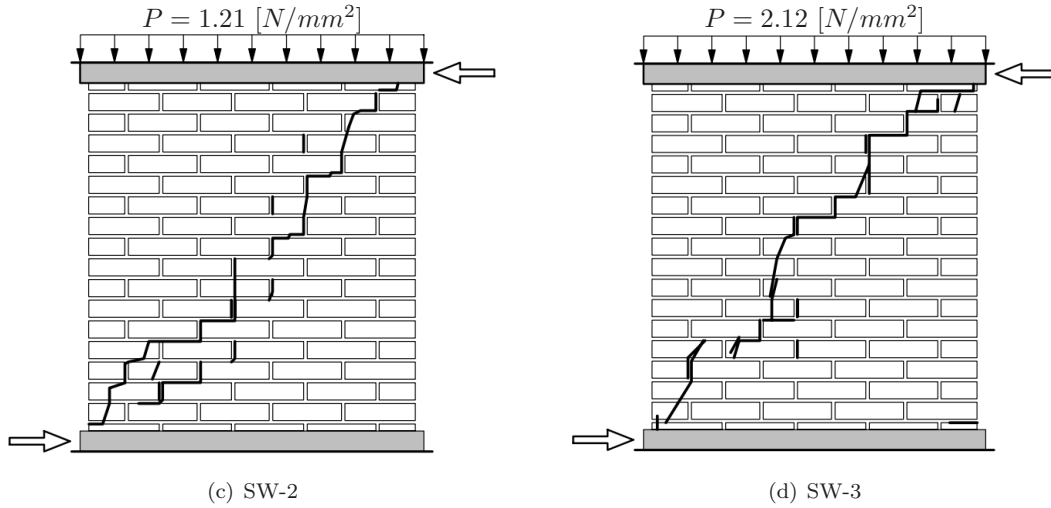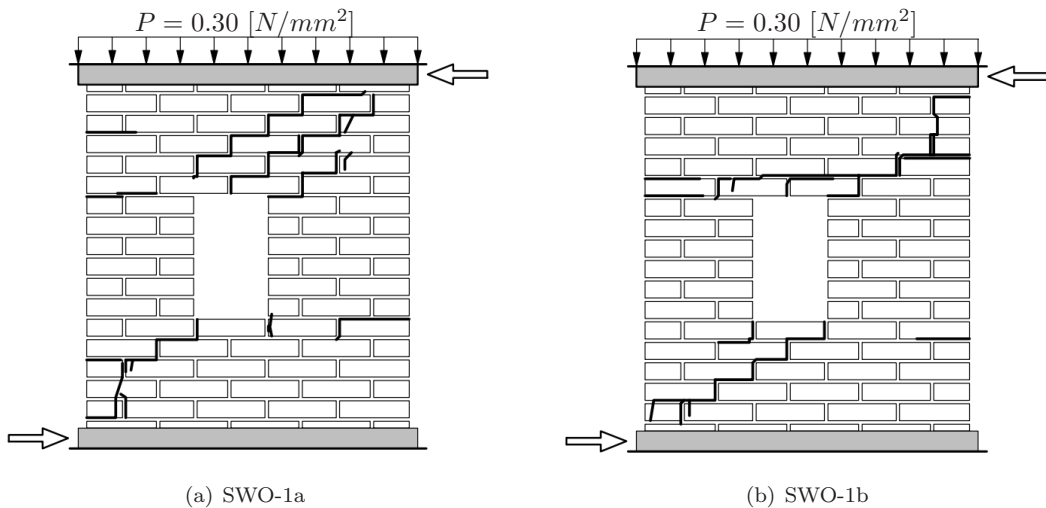
Figure 5.2: Experimental failure pattern for the different walls without opening [12, 78, 79].

The comparison between numerical and experimental load-displacement curves are shown in Figure 5.3. The experimental behaviour is satisfactorily reproduced by the proposed composite interface model. All the wall behaves in the same manner and confirms the idea that masonry can with-stand substantial post-peak deformation with reduced loss of strength. The masonry shear wall also shows that higher initial vertical loads lead to increase in it's strength, But, its ductility deceases. In case of shear wall softening region is govern by failure of compression toes of wall and material fail in out of plane direction. Higher initial vertical loads corresponds to higher failure loads, which leads to higher normal stresses. Thus, during crushing of the compressed toes higher normal stresses makes redistributions of stresses more and more difficult. This results in deceases in the ductility. This behaviour of shear wall also confirmed by the experimental result which also shows that higher initial vertical loads lead to increasing strength of the shear walls at the loss of its ductility.
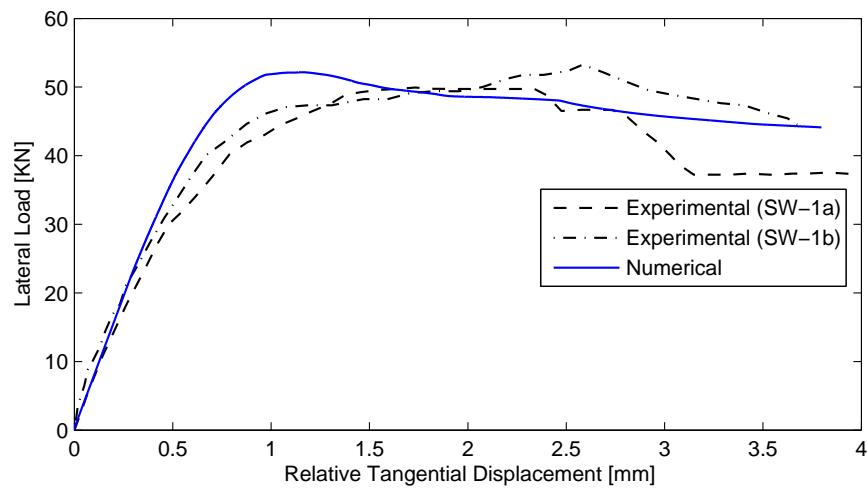
(a)
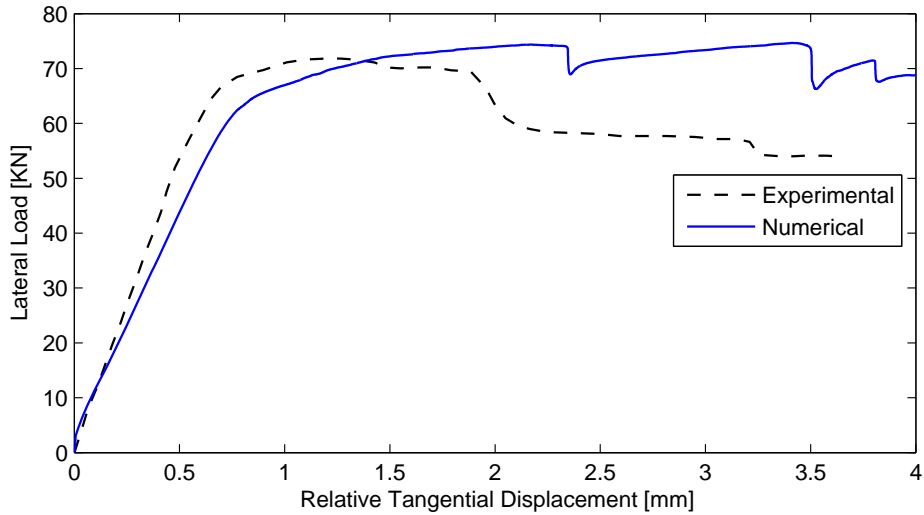
(b)
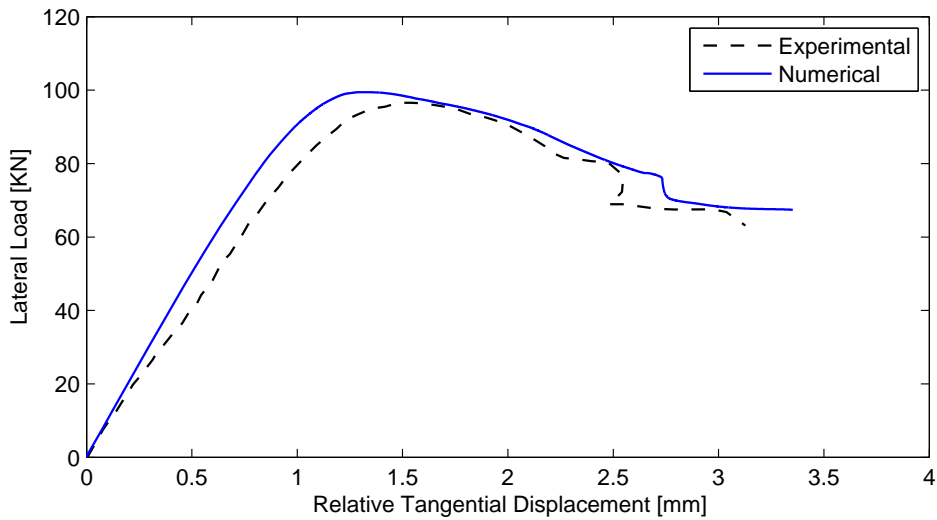
(c)

Figure 5.3: Comparison of experimental and numerical result obtained from the proposed model: (a) SW-1; ((b) SW-2; (c) SW-3.

The sharp load drops in Figure 5.3(b) is attributed to sudden drop of shear stress in single integration point of the potential crack, caused by cracking of a brick. The decision of setting the shear stress in potential crack of brick equal to zero upon initiation of the crack, causes the problem related to convergence. Thereby forcing the choice of load steps to be very very small and are impractical. This effects the numerical robustness of the model, due release of large amount of energy in single load step. However, if sufficiently fine meshes are adopted, the solution obtained is independent of the size of the load increments. The problem of large amount of energy release in single load step is over come by gradually decreasing the shear stress to zero in several load step rather than sudden drop to zero. This assumption allows us to overcome the problem and it is confirmed by the numerical example on the shear wall SW-1 and SW-3, Figure 5.3(a) and 5.3(c) .

$d = 1\ [mm]$ $d = 2\ [mm]$ $d = 4\ [mm]$

(a)

$d = 1\ [mm]$ $d = 2\ [mm]$ $d = 4\ [mm]$

(b)

$d = 1\ [mm]$ $d = 2\ [mm]$ $d = 4\ [mm]$
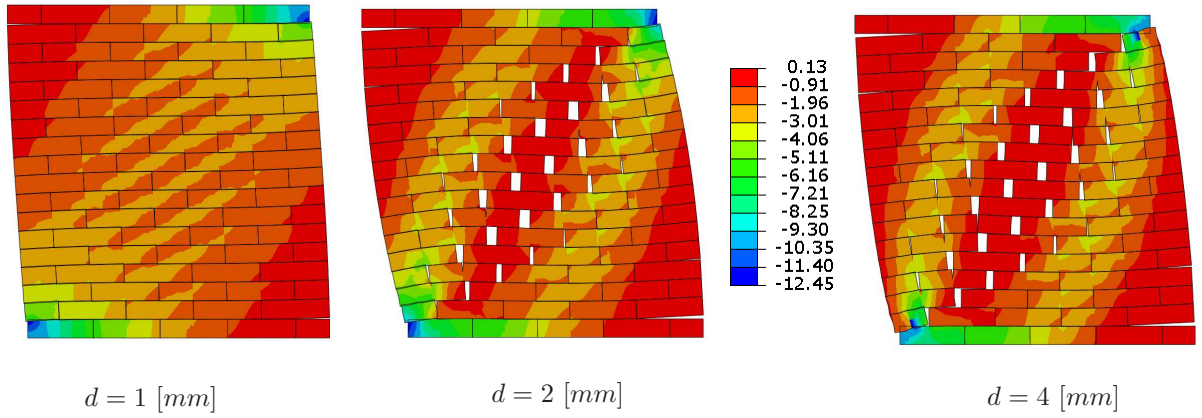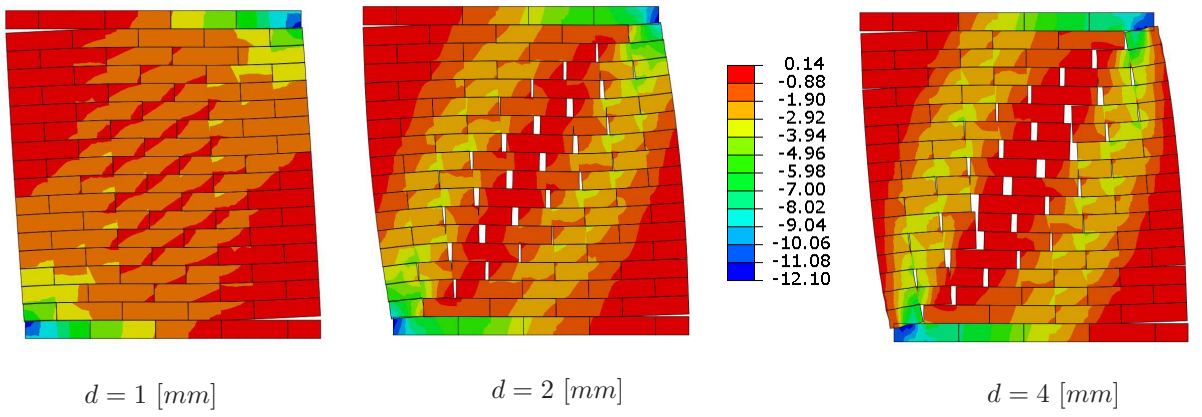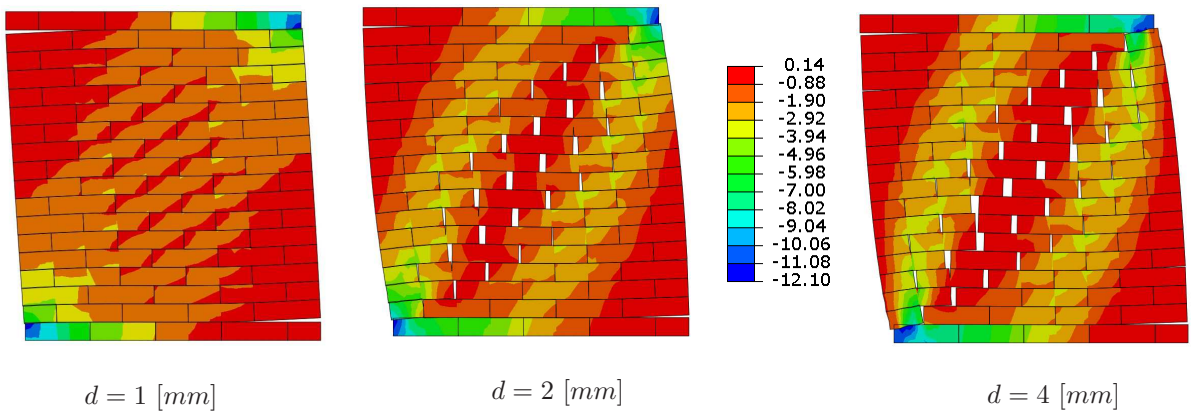
(c)

Figure 5.4: Minimum principal stress at different displacement (d) with deformed mesh for different shear wall without opening: (a) SW-1; ((b) SW-2; (c) SW-3.

The numerical crack pattern and minimum principle stress distribution for the different wall are presented in the Figure 5.4. The behaviour of shear wall can also be understood from the stress distribution plots. First, initial vertical loads are applied, which makes the stress distribution continuous. At early stages of horizontal displacement, small diagonal compression struts forms. These struts are defined by the center of the bricks due to the different stiffnesses of joints and bricks, see Figure 5.4. On further loading, a diagonal stepped crack opens and prevents the formation of compressive struts parallel to the diagonal line defined by the center of the bricks. Simultaneously, diagonal struts initiate the the splitting of bricks due to Possion's effect. When the diagonal cracks are fully open, two distinct struts are formed, one at each side of the diagonal crack. Finally, diagonal stepped crack and crushing of the toes in compression leads to collapse of shear wall, simultaneously with cracks in the brick.

Moreover, all the shear walls confirms ductile behaviour. However, for higher initial vertical load the shear transfer across the bed joints in the diagonal crack zone is higher, which reduced the opening of the diagonal crack. Therefore, a more continuous stress distribution is found with larger compression zones at the supports, which lead to reasonable ductility with delayed compressive failure at the toes.

5.2.2   Shear wall with opening (SWO)

In this section we present analysis the tests carried out on walls with a central opening. These walls are subjected to only one vertical normal pressure equals 0.30 N/mm^2. The material properties used in simulation are same as for the walls SW-1 (without opening). In these shear walls, opening creates two small weak piers on either sides of opening. Thus, two compressive strut develops under horizontal loading to spread the load around both sides of the opening. On applying the monotonically increasing horizontal load, first diagonal zigzag cracks arise from two corners of the opening. Than, a tensile cracks arise from the outside of the wall at the base and top of the small piers (in the bed joint). Finally, a collapse mechanism is formed by failure of the compressed toes, located at the bottom and top of the wall as well as the small piers.

(a) SWO-1a   (b) SWO-1b

Figure 5.5: Experimental failure pattern for the different walls with opening [12, 78, 79].
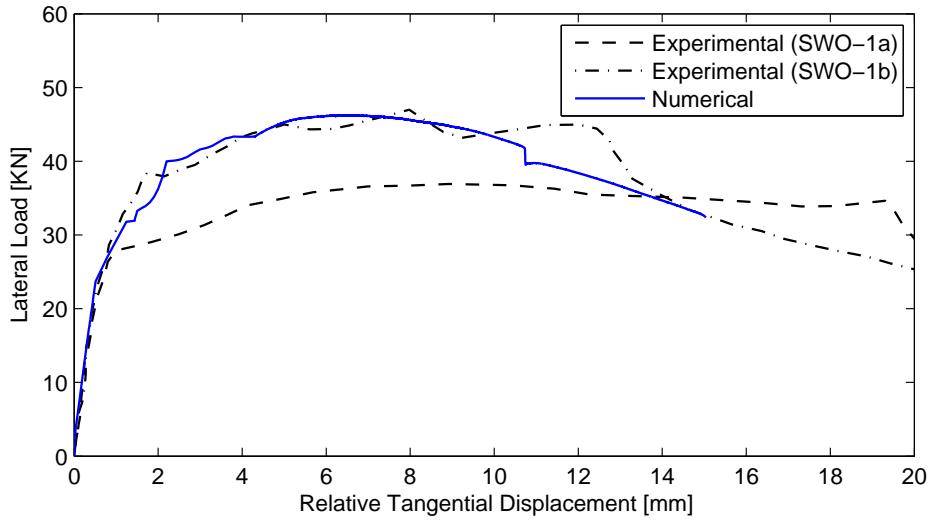
Figure 5.6: Comparison of experimental and numerical result obtained from the proposed model for SWO-1.

The comparison between numerical and experimental load-displacement curves are shown in Figure 5.6. The numerical result are very much in agreement with those obtained from the experiments. A good impression of the SWO-1a and numerical model is obtain because calculated stiffness of the numerical model matches with the experimental values. This indicates that the proposed model is able to predict correct failure mechanism.
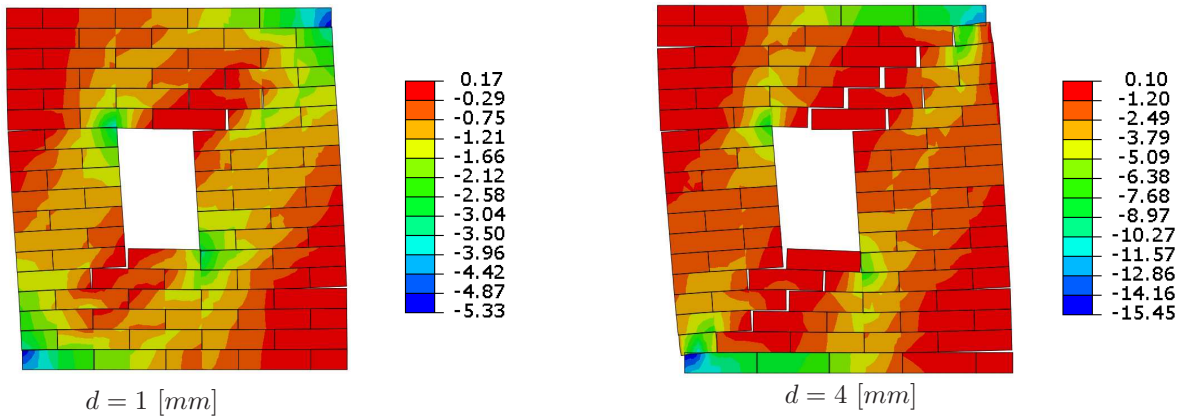
Figure 5.7: Minimum principal stress at different displacement (d) with deformed mesh for shear wall with opening (SWO-1).

The Numerical crack pattern and minimum principle stress distribution for the different wall are presented in the Figure 5.7. During the Initial horizontal loading, two diagonal crack that arise from the corners of the opening. simultaneously, horizontal crack in the top and bottom of the piers also arise, Figure 5.7 (first figure). The load is transfer by the two large compression struts on the both

side of opening. On further loading, the previous diagonal crack will stop and two new addition diagonal crack start to open, see Figure 5.7 (second figure). The two compression struts becomes narrower. Finally the diagonal crack progress toward the the supports and, then the compression toes at the top and bottom will crush. A complete collapse mechanism is formed with the failure of the smaller piers.

5.3   Masonry bed joints in direct cyclic shear loading

In the previous section 5.2 the proposed composite interface model has used for the monotonically increasing load. But, the propose model has more applicability. The experimental work [42, 63, 67, 80, 81] carried out to investigate cyclic behaviour of masonry interfaces has shown some important characteristics [1], summarized as

- stiffness degradation in both tension and compression regimes;

- residual relative normal displacements at zero stress;

- absence of stiffness degradation in direct shear;

- complete crack closing under compressive loading.

From the above summarized point, it becomes clear that the present formulation of composite interface model is unable to reproduce stiffness degradation in tension and compression unloading. But, the model can work for the cyclic behaviour for shear, where stiffness degradation is not required. Thus present model can only be used for the for analysis of masonry joint under direct cyclic shear loading. For the general cyclic loading kinematic hardening has to be include in the model for including the stiffness degradation in tension and compression unloading. It is not persuade in the present work and is suggested for the further work.
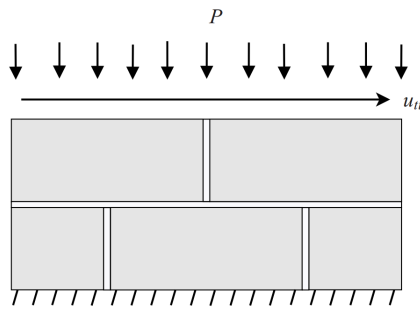
Figure 5.8: Direct shear test set-up as per Atkinson et al. [42]

Further in this section, the capability of the proposed composite interface model is validated by comparing the finite element results with experimental results obtained by Atkinson *et al.* [42], in representing the cyclic shear behaviour of masonry mortar joints under different load conditions. In [42] the authors conducted direct shear tests using a servo-controlled loading apparatus to examine

---

[1]Note: During unloading of the structure

the response of brick masonry bed joints under monotonic and cyclic shear loadings, see Figure 5.8. In each of these tests, first a uniformly distributed normal stress was applied ranging from $0.34 - 4.31 \, Mpa$, and then four cycles of shear reversals were imposed under displacement control. The authors used old and new bricks with low- and high-strength mortars. In the present study, new bricks specimens with high-strength mortar has been considered for the validation, under three different levels of compressive stress $(0.49, 1.34, 4.31 Mpa)$. The specimens consist of modern clay bricks $[193x55x92mm^3]$ and mortar joints $[7 \, mm]$, prepared with a volumetric cement : lime : sand ratio $(1 : 1.5 : 4.5)$. The bed joint area is equal to $92 \, x \, 398 \, mm^2 (0.037m^2)$. The values of the material parameters used in the simulations are summarized in Table 5.4 and 5.5. The stiffness of the brick is assumed to be 20 times the elastic normal stiffness of the mortar joint.

Table 5.4: Elastic material property for the brick and joints

Brick		Joint	
E N/mm^2	ν	K_{nn} N/mm^3	K_{tt} N/mm^3
220	0.15	3.8	11.5

Table 5.5: Inelastic material property for the joints

Tension	$\xi_0 \; [N/mm^2]$	0.65
	$G_f^I \; [Nmm/mm^2]$	$5\xi_0^2/2K_{nn}$
Shear	$C_0 \backslash C_r \; [N/mm^2]$	$1.4\xi_0 \backslash 0.1C_Q$
	$C_{Q0} \backslash C_{Qr} \; [N/mm^2]$	$1.1\xi_0 \backslash 0.1C_Q$
	$\phi_0 \backslash \phi_r \; [radian]$	$0.67 \backslash 0.57$
	$\psi \; [radian]$	$0.35 \backslash 0$
	$G_f^{II} \; [Nmm/mm^2]$	$10G_f^I$
Cap	$\zeta_p \; [N/mm^2]$	-16

The comparison between numerical and experimental load-displacement curves is shown in Figure 5.9, which shows that the proposed model is able to reproduce the shear behaviour of brick masonry bed joints not only in monotonic but also in cyclic loading. The experimental and numerical dilatancy curves show that, higher the compressive stress, smaller is the dilatancy and it is observed that the correlation of numerical and experimental results is good. The significant influence of dilatancy on the de-formability and strength of an interface can be demonstrated by this numerical example. When the interface between the elastic region (elastic brick) is subjected to shear deformations under a normal confinement, Initially the normal stress on the interface is zero. However, since the elastic boundary prevents the interface from dilating freely, a significant compressive stress develops on the interface during the application of relative tangential displacement. Depending on the amount of dilatancy, controlled by the dilatancy parameter, the shear response can change from softening to hardening, and the shear strength of the interface can change by an order of magnitude.

(a)

(b)

76
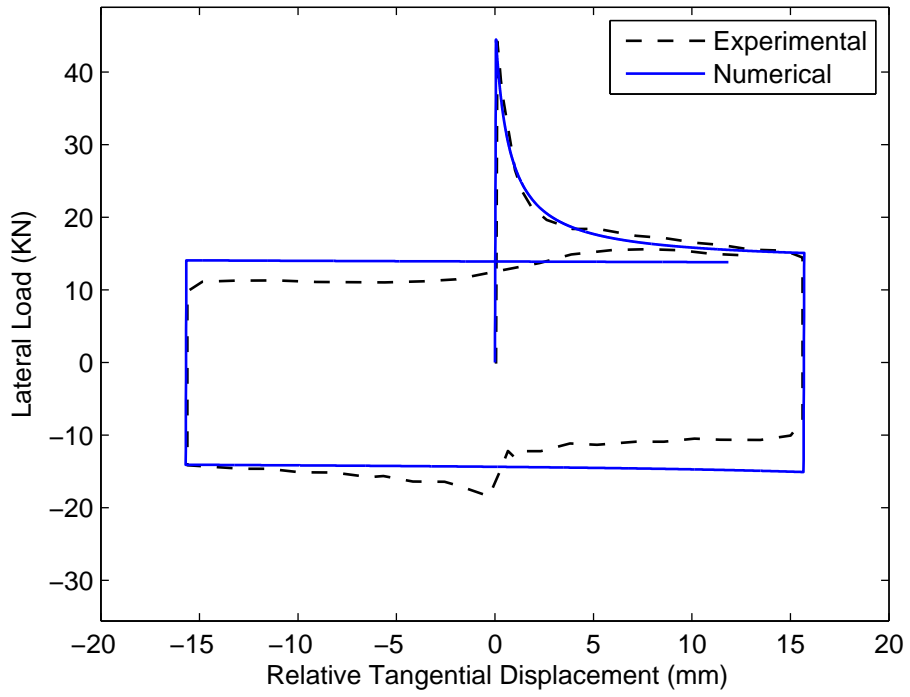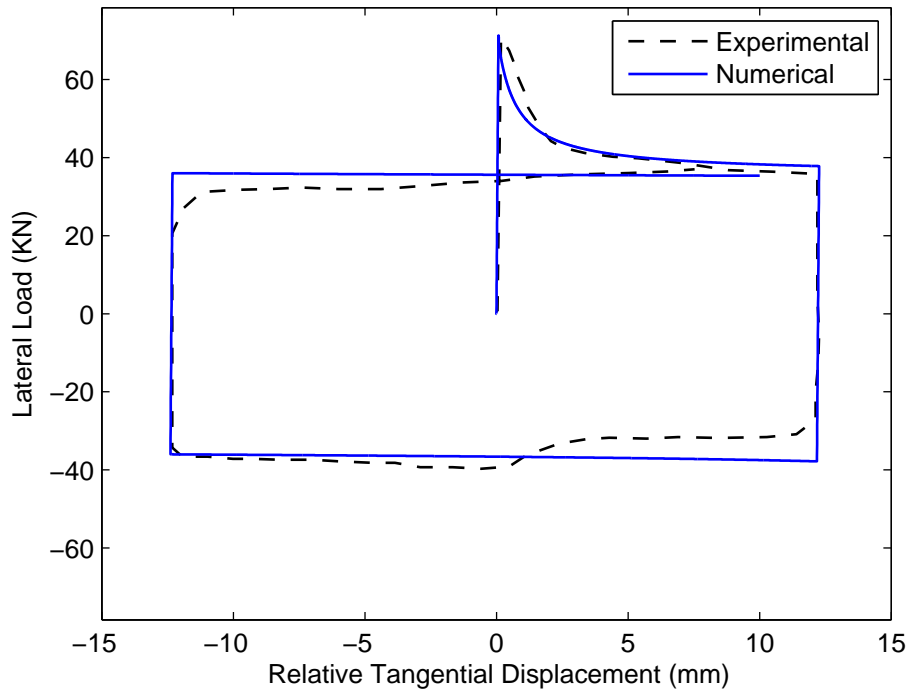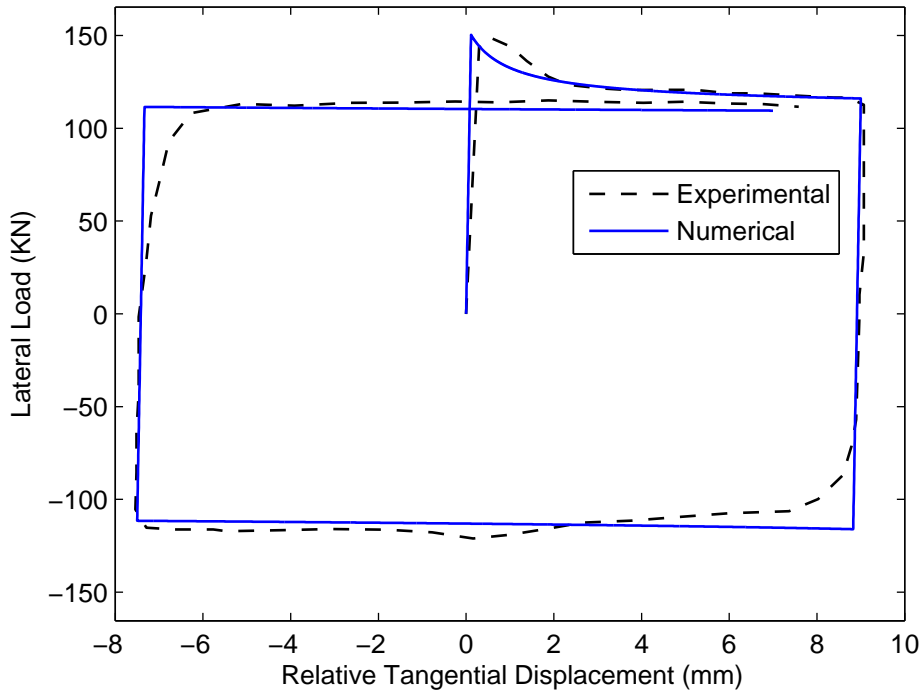
(c)
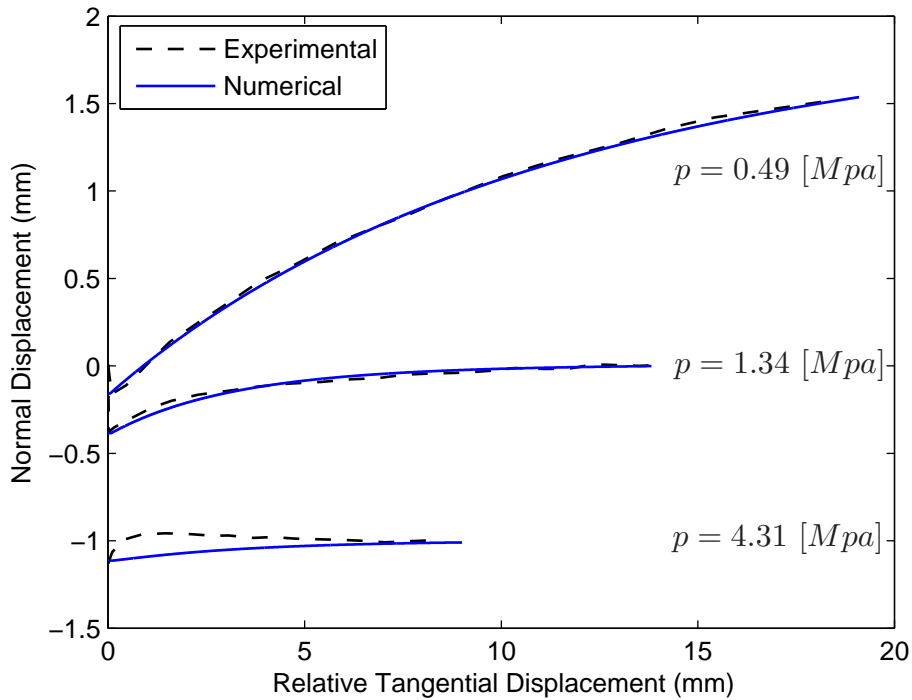
(d)

Figure 5.9: Comparison between experimental results from direct shear test [42] and Numerical results obtained from the present model (a) P = 0.49 MPa; (b) P = 1.34 MPa; (c) = 4.31 MPa; (d) distribution of normal displacements with relative tangential displacements for different pressure.

5.4   Conclusions

A simplified micro-modelling strategy for masonry has been presented for the validation of proposed model, in which the units are discretized with continuum elements and the joints are discretized with interface elements. Moreover, simple mode I potential crack is placed vertically in the middle of each brick, to model splitting of the brick. Validation of the model and the strategy against experiments carried out in shear walls. The numerical result shows that strategy is able to reproduce the complete path of the structures up to and beyond peak until total degradation of strength without numerical difficulties in the proposed model.

Finally, it has also been shown that the proposed model is able capture the cyclic effect in direct shear only. The numerical result on masonry bed joints in direct cyclic shear loading shows the good correlation with experimental result.

Chapter 6

Summary and conclusions

The main objective of work was to the development and use of reliable numerical tools. In particular, a tool which is able to describe the post-failure behaviour of masonry structures in order to assess the safety of architectural heritage. A Reliable tools is robust and provides accurate solution. In this study, an attempt has been made to provide tools for the analysis of unreinforced masonry structures at micro level in plane stress conditions. This research presents an original contribution to numerical strategies aimed at the analysis of structural.

Homogenization techniques

An aspect of the analysis of masonry structures, which has been discussed, is homogenization techniques. The importance of such techniques is that, it is possible to predict the behaviour of the different composites based on the micro-mechanical properties of its components. The main objective is to obtain a macro-properties of the composite. These macro-parameters can serve as input data for an independent macro-model based on plasticity or damage constitutive laws. In present study, homogenization theory for periodic media has been applied in a rigorous way for deriving the anisotropic elastic characteristic of masonry that is in one step. In particular, the real geometry has been taken into account (bond pattern and finite thickness of the wall). For the numerical example the two representative volume element having the same ratio of mortar and unit has been considered and their equivalent property has been found. Moreover, a careful examination for different stiffness ratio between mortar and unit has been done to assess the performance for inelastic behaviour.

Composite interface model

The mathematical theory of plasticity has been adopted for the representation of the quasi material behaviour. The yield function consists of a single surface yield criteria, which is capable of representing pressure-dependent friction shear failure, cracking of material by cut-off and crushing of plain by cap-off in compression. The proposed yield function is simple extension of Mohr-Coulomb criteria, which makes use of property of arc-tan for cut and cap-off. The algorithms have been developed by integrating the differential equation by fully implicit Euler backward method. These equations are solved by full Newton-Raphson technique in monolithic manner, which lead to combined local and global approach.

A careful and detailed investigation has been made to check robustness and accuracy of the algorithm for different load path and non associativity. It has been found that sub stepping is required to ensure convergence and accuracy of the final solution at both local and global level. Thus, Algorithm is combined with a sub stepping strategy. The adopted solution strategy has proven to be satisfactory because the loading paths could be traced completely, ranging from the elastic regime, pre-failure inelastic regime and post-failure inelastic regime until total degradation of strength.

Micro-modelling

For the micro-modelling strategy, mortar and unit-mortar interface is lumped into joint between expended units. The units are assumed to be linear-elastic and all inelastic phenomena are lumped in to the joints via a composite interface model. The composite interface model comprehends three different failure mechanisms. First, tension cut-off for mode I failure. Second, the Coulomb friction model for mode II failure. Third, cap for compression failure. It is assumed that the internal damage associated with each failure mechanism can be modelled using internal hardening/softening parameters which are related to a fracture energy in tension, shear and compression. Analyses of structures where all the modes of the composite interface model become active show that the strategy results in a stable and accurate algorithm.

Micro modelling of masonry provides a good understanding of the failure mechanisms involved in the analysed structures. However, this model is particularly suited for small structures. Particular for the structural where the interaction between units and mortar is of primary interest. It is noted that, for micro Modelling of large structures, the memory and time requirements become too large.

Scope for future work

In retrospect, the present study successfully achieved the objectives. In particular, robust and accurate numerical tools that can be offered to masonry analysts and designers have been developed at the micro-level. However, the proposed Composite interface model is restricted to masonry structure subjected to monotonic loading. In particular, kinematic hardening could be included in the model for the cyclic behaviour of masonry in the compression and tension region.

Moreover, for further application of the models to a wide range of masonry structures, it is emphasized that the experimental determination of material parameters is very important. In particular, information about the post-peak material behaviour is very rarely given in present literature.

In a more fundamental perspective for modelling the shear wall, an investigation of refined strategies to model cracks in the units is suggested.

List of Figures

List of Tables

Appendix-I

$$T_1 := [(C - \sigma_{nn} \tan(\phi))] \qquad T_2 := [C_Q - \sigma_{nn} \tan(\psi)]$$

$$f_t(\boldsymbol{\sigma}, \boldsymbol{q}) := \frac{2}{\pi} \arctan\left(\frac{\xi - \sigma_{nn}}{\alpha_t}\right) \qquad D_t := 1 + \left(\frac{\sigma_{nn} - \xi}{\alpha_t}\right)^2$$

$$f_c(\boldsymbol{\sigma}, \boldsymbol{q}) := \frac{2}{\pi} \arctan\left(\frac{\sigma_{nn} - \zeta}{\alpha_c}\right) \qquad D_c := 1 + \left(\frac{\sigma_{nn} - \zeta}{\alpha_t}\right)^2$$

$$F(\boldsymbol{\sigma}, \boldsymbol{q}) := -[(C - \sigma_{nn} \tan(\phi))]^2 f_c f_t + \sigma_{tt}^2$$

$$Q(\boldsymbol{\sigma}, \boldsymbol{q}) := -[C_Q - \sigma_{nn} \tan(\psi)]^2 f_c f_t + \sigma_{tt}^2$$

$$\boldsymbol{n} = \left[\begin{array}{cc} 2T_1 \tan\phi F_c F_t - T_1^2 \left(\frac{2F_c}{\pi\alpha_t D_t} + \frac{2F_t}{\pi\alpha_c D_c}\right) & 2\sigma_{tt} \end{array} \right]$$

$$\boldsymbol{m} = \left[\begin{array}{cc} 2T_2 \tan\psi F_c F_t - T_2^2 \left(\frac{2F_c}{\pi\alpha_t D_t} + \frac{2F_t}{\pi\alpha_c D_c}\right) & 2\sigma_{tt} \end{array} \right]$$

Derivative of $\boldsymbol{m}$

$$T_3 = \frac{F_c}{\pi\alpha_t^3 D_t^2} + \frac{F_t}{\pi\alpha_c^3 D_c^2} + \frac{4}{\pi^2\alpha_t D_t\alpha_c D_c}$$

$$\frac{\partial\mathbf{m}}{\partial\boldsymbol{\sigma}} = \left[\begin{array}{cc} -2\tan^2\psi F_c F_t + 8T_2 \tan\psi\left(\frac{F_c}{\pi\alpha_t D_t} + \frac{F_t}{\pi\alpha_c D_c}\right) + 2T_2^2 T_3 & 0 \\ 0 & 2 \end{array} \right]$$

$$\frac{\partial m_1}{\partial\boldsymbol{q}} = \left[\begin{array}{c} 0 \\ 2\tan\psi F_c F_t - 4T_2\left(\frac{F_c}{\pi\alpha_t D_t} + \frac{F_t}{\pi\alpha_c D_c}\right) \\ 0 \\ 2\sec^2\psi F_c F_t(T_2 - \sigma_{nn} \tan\psi) - 2(\sigma_{nn} \sec^2\psi - 2T_2)\left(\frac{F_c}{\pi\alpha_t D_t} + \frac{F_t}{\pi\alpha_c D_c}\right) \\ \frac{-4\tan\psi T_2 F_c}{\pi\alpha_t D_t} + 4T_2\left(\frac{1}{\pi^2\alpha_c D_c\alpha_t D_t} - \frac{F_c(\sigma - \xi)}{\pi\alpha_t^3 D_t^2}\right) \\ \frac{-4\tan\psi T_2 F_t}{\pi\alpha_c D_c} + 4T_2\left(\frac{1}{\pi^2\alpha_c D_c\alpha_t D_t} - \frac{F_c(\sigma - \xi)}{\pi\alpha_c^3 D_c^2}\right) \end{array} \right]$$

$$\boldsymbol{H} = \left[\begin{array}{cc} \langle\sigma_{nn}\rangle & 0 \\ 0 & \sigma_{tt} - \sigma_{t_{r1}} sign(\sigma_{tt}) \\ 0 & (\sigma_{tt_{r1}} - \sigma_{tt_{r2}}) sign(\sigma_{tt}) \\ \langle\langle\sigma_{nn}\rangle\rangle & 0 \end{array} \right]$$

$$
\boldsymbol{\varpi} = \begin{bmatrix}
\left(-m_1 \boldsymbol{H}(1,1)\dfrac{\beta_C}{G_f^I} - m_2 \boldsymbol{H}(2,2)\dfrac{\beta_C}{G_f^{II}} \right)(C_0 - C_r)\exp^{-\beta_C\left(\frac{w_1^p}{G_f^I} + \frac{w_2^p}{G_f^{II}} \right)} \\[2em]
\left(-m_1 \boldsymbol{H}(1,1)\dfrac{\beta_{C_Q}}{G_f^I} - m_2 \boldsymbol{H}(2,2)\dfrac{\beta_{C_Q}}{G_f^{II}} \right)(C_{Q_0} - C_{Q_r})\exp^{-\beta_{C_Q}\left(\frac{w_1^p}{G_f^I} + \frac{w_2^p}{G_f^{II}} \right)} \\[2em]
-m_2 \boldsymbol{H}(3,2)\beta_\phi (\phi_0 - \phi_r)\exp^{-\beta_\phi w_3^p} \\[1em]
-m_2 \boldsymbol{H}(3,2)\beta_\psi (\psi_0 - \psi_r)\exp^{-\beta_\psi w_3^p} \\[1em]
\left(-m_1 \boldsymbol{H}(1,1)\dfrac{\beta_\xi}{G_f^I} - m_2 \boldsymbol{H}(2,2)\dfrac{\beta_\xi}{G_f^{II}} \right)\xi_0 \exp^{-\beta_\xi\left(\frac{w_1^p}{G_f^I} + \frac{w_2^p}{G_f^{II}} \right)} \\[2em]
-m_1 \boldsymbol{H}(4,1)\dfrac{\partial \zeta}{\partial w_4}
\end{bmatrix}
$$

$$
\frac{\partial \zeta}{\partial w_4} = \begin{cases}
2(\zeta_p - \zeta_0)\left(\left(\dfrac{2w_4^p}{w_p} \right) - \left(\dfrac{w_4^p}{w_p} \right)^2 \right)^{-\frac{1}{2}}\left(\dfrac{2}{w_p} + \dfrac{2w_4}{w_p^2} \right) & \text{if} \quad w_4^p \le w_p \\[2em]
2(\zeta_m - \zeta_p)\left(\dfrac{w_4^p - w_p}{(w_m - w_p)^2} \right) & \text{if} \quad w_p \le w_4^p \le w_m \\[2em]
\beta_\zeta \exp^{\beta_\zeta \left(\frac{w_4^p - w_p}{\zeta_m - \zeta_r} \right)} & \text{if} \quad w_4^p > w_m
\end{cases}
$$

References

[1] L. Pelà, *Continuum damage model for nonlinear analysis of masonry structures*. PhD thesis, Università degli studi di Ferrara, 2009.

[2] R. E. Goodman, R. L. Taylor, and T. L. Brekke, "A model for the mechanics of jointed rock," *Journal of Soil Mechanics & Foundations Div*, 1968.

[3] J. G. Rots, *Computational modeling of concrete fracture*. PhD thesis, Technische Hogeschool Delft, 1988.

[4] A. Zubelewicz and Z. P. Bazant, "Interface element modeling of fracture in aggregate composites," *Journal of engineering mechanics*, vol. 113, no. 11, pp. 1619–1630, 1987.

[5] I. Carol, P. C. Prat, and C. M. López, "Normal/shear cracking model: application to discrete crack analysis," *Journal of engineering mechanics*, vol. 123, no. 8, pp. 765–773, 1997.

[6] A. Caballero, I. Carol, and C. López, "A meso-level approach to the 3d numerical analysis of cracking and fracture of concrete materials," *Fatigue & Fracture of Engineering Materials & Structures*, vol. 29, no. 12, pp. 979–991, 2006.

[7] R. G. Drysdale, A. A. Hamid, and L. R. Baker, *Masonry structures: Behavior and design*. Englewood Cliffs, NJ, 1994.

[8] A. W. Hendry, *Reinforced and prestressed masonry*. Longman Scientific & Technical, 1991.

[9] A. Brencich, L. Gambarotta, and S. Lagomarsino, "A macroelement approach to the three-dimensional seismic analysis of masonry buildings," in *11th European Conference on Earthquake Engineering*, pp. 6–11, 1998.

[10] G. Magenes and A. Fontana, "Simplified non-linear seismic analysis of masonry buildings," in *Proc. Br. Masonry Soc. No. 8*, pp. 190–195, 1998.

[11] P. Roca, C. Molins, and A. R. Marí, "Strength capacity of masonry wall structures by the equivalent frame method," *Journal of structural engineering*, vol. 131, no. 10, pp. 1601–1610, 2005.

[12] P. Lourenço, "Computational strategies for masonry structures," 1996.

[13] H. R. Lotfi and P. B. Shing, "Interface model applied to fracture of masonry structures," *Journal of structural engineering*, vol. 120, no. 1, pp. 63–80, 1994.

[14] A. Tzamtzis, *Dynamic finite element analysis of complex discontinuous and jointed structural systems using interface elements.* PhD thesis, PhD Thesis, Department of Civil Engineering, QMWC, University of London, 1994.

[15] P. B. Lourenço and J. G. Rots, "Multisurface interface model for analysis of masonry structures," *Journal of engineering mechanics*, vol. 123, no. 7, pp. 660–668, 1997.

[16] L. Gambarotta and S. Lagomarsino, "Damage models for the seismic response of brick masonry shear walls. part i: the mortar joint model and its applications," *Earthquake engineering & structural dynamics*, vol. 26, no. 4, pp. 423–439, 1997.

[17] L. Gambarotta and S. Lagomarsino, "Damage models for the seismic response of brick masonry shear walls. part ii: the continuum model and its applications," *Earthquake engineering & structural dynamics*, vol. 26, no. 4, pp. 441–462, 1997.

[18] K. M. Dolatshahi and A. J. Aref, "Two-dimensional computational framework of meso-scale rigid and line interface elements for masonry structures," *Engineering Structures*, vol. 33, no. 12, pp. 3657–3667, 2011.

[19] A. Page, "The biaxial compressive strength of brick masonry.," in *ICE Proceedings*, vol. 71, pp. 893–906, Ice Virtual Library, 1981.

[20] A. Page, "The strength of brick masonry under biaxial compression-tension," *International Journal of Masonry Construction*, vol. 3, no. 1, pp. 26–31, 1983.

[21] M. Dhanasekar, P. W. Kleeman, and A. W. Page, "Biaxial stress-strain relations for brick masonry," *Journal of Structural Engineering*, vol. 111, no. 5, pp. 1085–1100, 1985.

[22] A. Benedetti, L. Pelà, and A. Aprile, "Masonry properties determination via splitting tests on cores with a rotated mortar layer–8th international seminar on structural masonry (issm 08), istanbul 5-7 novembre 2008," tech. rep., ISBN 978-975-561-342-0.

[23] A. Zucchini and P. Lourenço, "A micro-mechanical model for the homogenisation of masonry," *International Journal of Solids and Structures*, vol. 39, no. 12, pp. 3233–3255, 2002.

[24] A. Anthoine, "Derivation of the in-plane elastic characteristics of masonry through homogenization theory," *International Journal of Solids and Structures*, vol. 32, no. 2, pp. 137–163, 1995.

[25] R. Luciano and E. Sacco, "Homogenization technique and damage model for old masonry material," *International Journal of Solids and Structures*, vol. 34, no. 24, pp. 3191–3208, 1997.

[26] P. B. Lourenco, G. Milani, A. Tralli, and A. Zucchini, "Analysis of masonry structures: review of and recent trends in homogenization techniques this article is one of a selection of papers published in this special issue on masonry.," *Canadian Journal of Civil Engineering*, vol. 34, no. 11, pp. 1443–1457, 2007.

[27] A. Urbanski, J. Szarlinski, and Z. Kordecki, "Finite element modeling of the behavior of the masonry walls and columns by homogenization approach," *Computer methods in structural masonry*, vol. 3, pp. 32–41, 1995.

[28] A. Zucchini and P. B. Lourenço, "A micro-mechanical homogenisation model for masonry: Application to shear walls," *International Journal of Solids and Structures*, vol. 46, no. 3, pp. 871–886, 2009.

[29] H. Lotfi and P. Shing, "An appraisal of smeared crack models for masonry shear wall analysis," *Computers & structures*, vol. 41, no. 3, pp. 413–425, 1991.

[30] E. Papa, "A unilateral damage model for masonry based on a homogenisation procedure," *Mechanics of Cohesive-frictional Materials*, vol. 1, no. 4, pp. 349–366, 1996.

[31] L. Berto, A. Saetta, R. Scotta, and R. Vitaliani, "An orthotropic damage model for masonry structures," *International Journal for Numerical Methods in Engineering*, vol. 55, no. 2, pp. 127–157, 2002.

[32] L. Pelà, M. Cervera, and P. Roca, "Continuum damage model for orthotropic materials: application to masonry," *Computer Methods in Applied Mechanics and Engineering*, vol. 200, no. 9, pp. 917–930, 2011.

[33] M. Massanas, P. Roca, M. Cervera, and G. Arun, "Structural analysis of küçük ayasofya mosque in ístanbul," *Structural Analysis of Historical Constructions IV, Padova, Italy*, 2004.

[34] L. Pelà, A. Aprile, and A. Benedetti, "Seismic assessment of masonry arch bridges," *Engineering Structures*, vol. 31, no. 8, pp. 1777–1788, 2009.

[35] V. Mallardo, R. Malvezzi, E. Milani, and G. Milani, "Seismic vulnerability of historical masonry buildings: A case study in ferrara," *Engineering Structures*, vol. 30, no. 8, pp. 2223–2241, 2008.

[36] G. Martínez, P. Roca, O. Caselles, and J. Clapés, "Characterization of the dynamic response for the structure of mallorca cathedral," *Structural analysis of historical constructions, New Delhi, India*, 2006.

[37] J. Murcia Delso *et al.*, "Seismic analysis of santa maria del mar church in barcelona," 2009.

[38] R. A. Vonk, "Softening of concrete loaded in compression," 1992.

[39] P. Schubert, "Tensile and flexural strength of masonry: influences, test methods, test results," in *Proc. 10th Int. Brick and Block Masonry Conf*, pp. 895–907, 1994.

[40] R. Van der Pluijm, "Material properties of masonry and its components under tension and shear," in *Proceedings of the 6 th Canadian Masonry Symposium. Saskatoon, Saskatchevan: University of Saskatchevan*, 1992.

[41] R. Pluijm, "van der.(1993). shear behaviour of bed joints," in *Proc. 6th North American Masonry Conf., Drexel University, Philadelphia, Pennsylvania, USA*.

[42] R. Atkinson, B. Amadei, S. Saeb, and S. Sture, "Response of masonry bed joints in direct shear," *Journal of Structural Engineering*, vol. 115, no. 9, pp. 2276–2296, 1989.

[43] H. K. Hilsdorf, "Investigation into the failure mechanism of brick masonry loaded in axial compression," in *Proceedings of International Conference on Mansory Structural Systems*, pp. 34–41, 1969.

[44] L. Binda, A. Fontana, and G. Frigerio, "Mechanical behaviour of brick masonries derived from unit and mortar characteristics," *Brick and Block Masonry(8 th IBMAC) London, Elsevier Applied Science,*, vol. 1, pp. 205–216, 1988.

[45] W. Mann and M. Betzler, "Investigations on the effect of different forms of test samples to test the compressive strength of masonry," in *Proc. 10th. Brick and block Masonry Conf., eds. NG Shrive and A. Huizer, University of Calgary, Calgary, Alberta, Canada*, pp. 1305–1313, 1994.

[46] W. Samarasinghe and A. Hendry, "The strength of brickwork under biaxial tensile and compressive stress," in *Proc. Br. Ceram. Soc.*, no. 30, p. 129, 1982.

[47] H. Backes, "On the behaviour of masonry under tension in the direction of the bed joints," *Dissert., Aachen Univ. of Tech., Aachen, Germany*, 1985.

[48] H. Ganz and B. Thürlimann, "Tests on the biaxial strength of masonry," *Rep. No. 7502*, vol. 3, 1982.

[49] R. Guggisberg and B. Thürlimann, "Experimental determination of masonry strength parameters," tech. rep., Report, 1987.

[50] F. Lurati and B. Thürlimann, "Tests in concrete masonry walls," tech. rep., Report, 1990.

[51] G. Pande, J. Liang, and J. Middleton, "Equivalent elastic moduli for brick masonry," *Computers and Geotechnics*, vol. 8, no. 3, pp. 243–265, 1989.

[52] G. Maier, A. Nappi, and E. Papa, "Damage models for masonry as a composite material: a numerical and experimental analysis," *Constitutive laws for engineering material: Theory and application*, pp. 427–432, 1991.

[53] S. Pietruszczak and X. Niu, "A mathematical description of macroscopic behaviour of brick masonry," *International Journal of Solids and Structures*, vol. 29, no. 5, pp. 531–546, 1992.

[54] G. Geymonat, F. Krasucki, and J.-J. Marigo, "Sur la commutativité des passages à la limite en théorie asymptotique des poutres composites," *Comptes rendus de l'Académie des sciences. Série 2, Mécanique, Physique, Chimie, Sciences de l'univers, Sciences de la Terre*, vol. 305, no. 4, pp. 225–228, 1987.

[55] M. Mistler, A. Anthoine, and C. Butenweg, "In-plane and out-of-plane homogenisation of masonry," *Computers & Structures*, vol. 85, no. 17, pp. 1321–1330, 2007.

[56] I. Gitman, H. Askes, and L. Sluys, "Representative volume: existence and size determination," *Engineering Fracture Mechanics*, vol. 74, no. 16, pp. 2518–2534, 2007.

[57] C. K. Yan, *On homogenization and de-homogenization of composite materials.* PhD thesis, Drexel University, 2003.

[58] E. Sacco, "A nonlinear homogenization procedure for periodic masonry," *European Journal of Mechanics-A/Solids*, vol. 28, no. 2, pp. 209–222, 2009.

[59] D. Addessi, E. Sacco, and A. Paolone, "Cosserat model for periodic masonry deduced by non-linear homogenization," *European Journal of Mechanics-A/Solids*, vol. 29, no. 4, pp. 724–737, 2010.

[60] S. Arya and G. Hegemier, "On non-linear response prediction of concrete masonry assemblies," in *Proc. North Am. Masonry Conf, Masonry Society, Boulder, Colorado*, pp. 19.1–19.24, 1978.

[61] A. Page, "Finite element model for masonry," *Journal of the Structural Division*, vol. 104, no. 8, pp. 1267–1285, 1978.

[62] T. Stankowski, *Numerical simulation of progressive failure in particle composites*. PhD thesis, Ph. D. Thesis, Technical. University of Colorado, Boulder, Colorado, 1990.[Links], 1990.

[63] T. Stankowski, K. Runesson, and S. Sture, "Fracture and slip of interfaces in cementitious composites. i: Characteristics," *Journal of engineering mechanics*, vol. 119, no. 2, pp. 292–314, 1993.

[64] H. R. Lotfi, *Finite element analysis of fracture of concrete and masonry structures*. PhD thesis, University of Colorado, 1992.

[65] P. Lourenço, "Analysis of masonry structures with interface elements," *TNO Building and Construction Research*, 1994.

[66] G. Giambanco, S. Rizzo, and R. Spallino, "Numerical analysis of masonry structures via interface models," *Computer methods in applied mechanics and engineering*, vol. 190, no. 49, pp. 6493–6511, 2001.

[67] D. V. de Castro Oliveira, *experimental and numerical analysis of blocky masonry structures under cyclic loading*. PhD thesis, Universidade do Minho, 2003.

[68] D. V. Oliveira and P. B. Lourenço, "Implementation and validation of a constitutive model for the cyclic behaviour of interface elements," *Computers & structures*, vol. 82, no. 17, pp. 1451–1461, 2004.

[69] U. Andreaus, "Failure criteria for masonry panels under in-plane loading," *Journal of structural engineering*, vol. 122, no. 1, pp. 37–46, 1996.

[70] R. Van der Pluijm, H. Rutten, and M. Ceelen, "Shear behaviour of bed joints," in *12 th Int. Brick/Block Masonry Conf. Proc.*, vol. 3, pp. 1849–1862, 2000.

[71] J. Simo and T. Hughes, "Computational inelasticity. 1998," *Springer, New York. Local iteration at Global iteration Max. Ave. Max. Ave. Unified Non-unified*, vol. 6, no. 4.5, p. 3.

[72] O. C. Zienkiewicz, R. L. Taylor, and J. Z. Zhu, *The finite element method: its basis and fundamentals*, vol. 1. Butterworth-Heinemann, 2005.

[73] S. O. Niels and R. Matti, "The mechanics of constitutive modeling," 2005.

[74] V. ABAQUS, "6.9 online documentation," *SIMULIA Inc.*

[75] A. Pérez-Foguet, A. Rodrıguez-Ferran, and A. Huerta, "Consistent tangent matrices for sub-stepping schemes," *Computer methods in applied mechanics and engineering*, vol. 190, no. 35, pp. 4627–4647, 2001.

[76] W. Wang, M. Datcheva, T. Schanz, and O. Kolditz, "A sub-stepping approach for elasto-plasticity with rotational hardening," *Computational Mechanics*, vol. 37, no. 3, pp. 266–278, 2006.

[77] A. Caballero, K. Willam, and I. Carol, "Consistent tangent formulation for 3d interface modeling of cracking/fracture in quasi-brittle materials," *Computer Methods in Applied Mechanics and Engineering*, vol. 197, no. 33, pp. 2804–2822, 2008.

[78] T. Raijmakers and A. T. Vermeltfoort, "Deformation controlled tests in masonry shear walls," *Report Ba*, vol. 1156, 1992.

[79] A. T. Vermeltfoort and T. Raijmakers, "Deformation controlled tests in masonry shear walls, part 2," tech. rep., Report TUE/BKO/93.08, Eindhoven University of Technology, Eindhoven, The Netherlands, 1993.

[80] A. Jefferson and N. Mills, "Fracture and shear properties of concrete construction joints from core samples," *Materials and Structures*, vol. 31, no. 9, pp. 595–601, 1998.

[81] P. B. Lourenço and L. ı. s. F. Ramos, "Characterization of cyclic behavior of dry masonry joints," *Journal of Structural Engineering*, vol. 130, no. 5, pp. 779–786, 2004.